Martin Andreas Solbakken Løvaas

Management of a High Arctic River

Erosion and Sediment Transport in Longyearelva, Svalbard

Master's thesis in Arctic Geology
Supervisor: Bjørn Frengstad
Co-supervisor: Aga Nowak and Lena Rubensdotter
May 2021

Master's thesis

NTNU
Norwegian University of Science and Technology
Faculty of Engineering
Department of Geoscience and Petroleum

Photo: Arne T. Pedersen (Svalbard Museum)

NTNU
Kunnskap for en bedre verden

UNIS
The University Centre in Svalbard

Martin Andreas Solbakken Løvaas

Management of a High Arctic River

Erosion and Sediment Transport in Longyearelva, Svalbard

Master's thesis in Arctic Geology
Supervisor: Bjørn Frengstad
Co-supervisor: Aga Nowak and Lena Rubensdotter
May 2021

Norwegian University of Science and Technology
Faculty of Engineering
Department of Geoscience and Petroleum

NTNU
Kunnskap for en bedre verden

Abstract

The High Arctic town, Longyearbyen (78º13'N, 15º38'E), is rearranging its infrastructure as a consequence of increasing geohazards and awareness. After establishing permanent scour and flooding mitigation (sills and riprap) in Longyearelva, several institutions found it interesting to enhance the understanding of the local glaciofluvial system draining the 22.2km^2 catchment. Therefore, the objectives for this thesis were to; - Assess the scour and flooding mitigation over the first ablation season since completion. - Quantify discharge, erosion, sediment transport and investigate the associated sources. - Contribute to the long-term monitoring in Longyearelva.

Fieldwork was conducted from June 5th to September 15th, covering most of the 2020 ablation season in Longyearelva. Water-stage and discharge rating curves were established from a water pressure transducer and point measurements of discharge from slug injection of diluted salt. Water samples were acquired using an automatic ISCO-pump, and suspended sediment concentration (SSC) was determined gravimetrically and used to calculate suspended sediment yield (SSY). Bedload transport was monitored using coloured passive tracers (pebble to large cobble). Geomorphological mapping of the moraines and the fluvial system was based on remote sensing data with relatively high spatial- and temporal resolution combined with field observations.

The hourly hydrograph illustrates an average discharge of 1.5m^3/s and peaks up to 8.6m^3/s. The peaks correlate with the record high air temperatures in late July. The highest recorded SSC at 24.1g/l coincides with the rising limb of the hydrograph on July 25th and indicates flushing of easily available sediments. The specific SSY was 1866t/km^2/yr, and both SSC and SSY were considerably higher than in comparative catchments - erosion and active layer detachments in the moraine could have increased the sediment input combined with construction work. Bedload transport capacity is at least large cobbles, as transport of the largest passive tracers was documented. The sedimentation dam with an initial volume of 30 000m^3 had to be excavated to increase the capacity after the late July Flooding. The riprap remained intact with only minor damages downstream Sill 8. Several sills collapsed or subsided, some developed scour holes, and a few remained intact. Lithology, construction work, and channelized water arguably affect the ground thermal regime and thus the mechanical strength of the ground around the sills – which could explain the subsidence and collapse. The scour mitigation limited a general channel degradation despite some scouring holes and transport of passive tracers over Sill 3 and 18.

Baseline data for further studies were acquired as planned and contributed to the established monitoring program (RIS ID 11641). It is believed that the system needs time to achieve an equilibrium between capacity and available sediments before the full effect of the scour mitigation can be revealed. An analysis of thermal data in the fluvial channel and the moraines are considered highly interesting for further research.

Sammendrag

Som en konsekvens av økende fokus på geofarer gjennomføres en storstilt omstilling av infrastruktur og boligmasser i Longyearbyen, Svalbard (78º13'N, 15º38'E). Permanent erosjon- og flomsikring av Longyearelva ble ferdigstilt høsten 2019, etter en fireårig byggeperiode. Flere organer viste interesse for å igangsette et forskningsprosjekt som kunne resultere i en bedre forståelse av de rådende forholdene i det 22,2km^2 store nedbørsfeltet rundt Longyearbyen. Denne masteroppgaven har dermed følgende problemstillinger; - Evaluere det nylig ferdigstilte erosjon og flomvernet. - Bidra til langsiktige observasjoner i Longyearelva, der vannføring, erosjon og sedimenttransport skal kvantifiseres og de respektive kildene skal identifiseres.

Feltarbeidet ble gjennomført i perioden fra 5. juni til 15. september og dekket det meste av smeltesesongen i 2020. Vannstand og vannføring ble målt med henholdsvis en vanntrykksensor og punktmålinger med injeksjon av oppløst salt, før forholdet ble uttrykt i likninger. Vannprøver for kvantifisering av transport av suspendert materiale ble innhentet med hjelp av en automatisk ISCO-pumpe mens bunntransport ble overvåket med bruk av fargede markører (kornstørrelsene grus – blokk). Geomorfologisk kartlegging av morenene og det fluviale systemet ble basert på fjernanalyse og feltobservasjoner, med god oppløsning både romlig og tidsmessig.

Kalkulering av kontinuering vannføring ga et gjennomsnitt på 1,5m^3/s i 2020, der toppene i hydrografen på 8,6m^3/s korrelerer med de rekordhøye temperaturene i den siste uken av juni. Høyeste målte konsentrasjon av suspendert materiale (KSM) var 24,1g/l (25.juni) og det spesifikke resultatet for transport av suspendert materiale (TSM) var 1866t/km^2/yr. Ekstremverdiene for KSM samsvarer med de første oppsvingene i hydrografen, noe som indikerer en utvasking av lett tilgjengelig sediment. Både KSM og TSM er betydelig høyere enn i relativt tilsvarende nedbørsfelt - betydelig erosjon i morene kan ha økt tilførselen av materiale i tillegg til bygningsarbeid i kanalen. Kapasiteten for bunntransport i Longyearelva er små blokker eller større, ettersom selv de største markørene ble transportert 80m. Sedimentasjonsdammen som hadde kapasitet til 30 000m^3 ble fylt og måtte tømmes i etterkant av flommen sent i juli. Plastringen av elvevollene viste bare tegn til skade nedstrøms Bunnbånd 8, som ellers viser tegn til kollaps og store setningsskader, noe som også ble dokumentert på andre bunnbånd. Litologi, byggeprosessen og kanalisering av vannet er elementer som antas å øke temperaturen i permafrosten og dermed redusere den mekaniske styrken i grunnen rundt bunnbåndene - en mulig forklaring på de skadene som har oppstått. Bunnbåndene har til en viss grad oppnådd målet om å hindre bunnsenkning, til tross for utbredte erosjonsgroper og transport av passive markører over bunnbånd 3 og 18.

Resultatet av målingene fra 2020 bidrar som planlagt til datagrunnlaget for videre arbeid i et langtidsperspektiv (RIS ID 11641). Den fulle effekten av flomvernet ligger noen sesonger frem i tid, ettersom det antas at systemet trenger tid til å oppnå likevekt mellom transportkapasitet og tilgjengelig materiale. Analyse av termisk data fra elvekanalen og morene er anbefalt for videre forskning.

Preface

After five years at NTNU, the journey has come to an end and is expressed in the following 100 pages or so. This 60 ECTS Master Thesis within Arctic Geology at NTNU and UNIS is the outcome of 16 weeks of fieldwork in the Longyearbyen area during the summer and autumn of 2020. It is now more or less one year since the first run along the Longyearelva at the beginning of my field season, and the final deadline approaches. I was fortunate to be one of the few Guest Master Students at UNIS during the challenges caused by Covid-19, and I am genuinely grateful for the opportunity.

I would like to thank those who have contributed during the process. My supervisor, Bjørn Frengstad (NTNU), for guidance and discussion. My co-supervisor Aga Nowak (UNIS) and Lena Rubensdotter (UNIS/NGU) for involving me in the project, encouragement during fieldwork and valuable input during the process of writing these pages. Anders Bjordal from NVE, for help during fieldwork and discussion of the scour and flooding mitigation and Longyearbyen Lokalstyre (w/Kjersti Olsen Ingerø) for letting me tag along on inspections. The Logistical Department at UNIS provided equipment and expertise for effective fieldwork, an essential factor for the successful outcome of the fieldwork. Spending three months in Longyearbyen to gather data was possible thanks to the financial support from both the Research Council of Norway (Arctic Field Grant) and UNIS (funds for Guest Master Students, Arctic Geology).

Thanks to friends and family in Trondheim, Svalbard, and at home for offering mental diversions. Thanks to SvalbardButikken for selling the world's most fantastic chocolate, my go-to companion for fieldwork and coffee breaks; Marabou Apelsin Krokant. SteinKubben and Kaffidrekkarlauget made my time as a student in Trondheim memorable. Although, the coffee breaks lasted longer than they should, and the amount of chocolate consumed would frighten any diet expert out there.

Martin Solbakken Løvaas

Trondheim, 15.05.2021

Cover Photo

The cover photo is provided by Svalbard Museum (historical photograph library) and Arne T. Pedersen (photo). Bulldozers at work in Longyearelva around 1950-60, making a deeper thalweg to control the water and sediment transport away from infrastructure. The location is approximately where Veg 501 is today.

Contents

List of figures

Chapter 1

Chapter 2

Chapter 3

Chapter 4

Chapter 5

List of tables

List of Equations

Abbreviations and dictionary

Abbreviations	**Meaning**
CTB	Central Tertiary Basin
DEM	Digital Elevation Model
DTM	Digital Terrain Model
EC	Electrical conductivity
GIS	Geographic Information System
LL	Longyearbyen Lokalstyre (Longyearbyen Community Council)
MET	Norwegian Meteorological Institute
NCCS	Norwegian Centre for Climate Services
NGU	Geological Survey of Norway
NPI	Norwegian Polar Institute
NTNU	Norwegian University of Science and Technology
NVE	Norwegian Water Resources and Energy Directorate
RIS	Research in Svalbard
SDM	Salt Dilution Method
SfM	Structure-from-Motion
SNSK	Store Norske Spitsbergen Kulkompani
SSC	Suspended Sediment Concentration
SSY	Suspended Sediment Yield
UNIS	University Centre in Svalbard
xx-PT	(Location) - Passive Tracer
g/l	Gram/liter
m^3/s	Cubic meter/second
Q	Discharge
t	Tons
yr	Year
^oC	Degree Celsius (temperature)
Dictionary	
Bre	Glacier
By	Town
Dal	Valley
Elv	River
Fjell / Berg	Mountain
Fjord	Fjord
Gruve	Coal mine
Veg	Road

1 Introduction

1.1 Motivation and objectives

Erosion and sediment transport in a fluvial system is closely linked to the discharge and the force of the water flowing through a channel (Fergus et al., 2010). The establishment of permanent scour- and flooding mitigation is recently completed in Longyearbyen, and the small town is rearranging its infrastructure in the light of increased geohazard awareness. Long term data-series of erosion and discharge is sparse on Svalbard (Nowak et al., 2021; Sund, 2008), and it is a crucial need for an up-to-date and representative dataset for the Longyeaelva river. A collaboration between Longyearbyen Lokalstyre (LL), the Norwegian Water- and Energy Directorate (NVE), and the University Centre in Svalbard (UNIS) were therefore initiated. This thesis is an outcome of the collaboration and will during the 2020 ablation season focus on the following objectives:

- *Quantify the discharge and sediment yield from the Longyearelva catchment.*
- *Investigate the sources for discharge and sediment input.*
- *Assess the adequacy and limitations of the recently established scour- and flooding mitigation.*
- *Contribute to the long-term monitoring in the catchment and identify additional topics to address over the coming years.*

The tasks were tackled with comprehensive fieldwork from early June to mid-September. Fieldwork involved establishing a hydrological monitoring station, measurements of sediment transport, and geomorphological mapping of the moraines and the constructed channel. See Chapter 3 Methodology for further description.

The next subsections introduce the historical and present social situation in Longyearbyen, followed by a description of the Svalbard climate, Longyearelva catchment and a summary of the continuous attempts at managing the local river.

1.2 Historical background and present situation

Longyearbyen is located in the middle of Spitsbergen (78º13'N, 15º38'E), the largest island in the Svalbard archipelago (NPI, 2020b) see *Figure* 1. Longyearbyen is the main settlement on Svalbard with 2400 inhabitants (SSB, 2020), including infrastructure expected in modern society (SSB, 2016). Longyearbyen was founded in the early 20th century as a small coal mining community (Arlov, 1994), and the remnants of the first infrastructure are still a part of the local scenery. For instance, a couple of the old cableway ramps can be recognized along Longyearelva (*Figure 7* and *Figure 8).* Coal mining was the primary industry for several decades. However, the demand for coal began to decrease in the second half on the century (Arlov, 2020) and tourism is now the number one source of income for the community (Elliassen, 2020; SSB, 2016). As of 2021, the only active coal

mines are Gruve 7 and one mine in Barentsburg, a Russian mining settlement. Gruve 7, operated by Store Norske Spitsbergen Kulkompani (SNSK), provides coal for the local power plant (SNSK, 2020).

The social development from mine workers living in barracks to a fully developed family society led to an increasing need for residential areas in the 1980s (SSB, 2016; Arlov, 2020). A new residential area called Lia developed to meet the rising number of families, in contrast to the barracks in Nybyen and Sverdrupbyen (Arlov, 2020). Elvesletta was also of interest for building purposes in the 1990s (Sværd, 1996).

SNSK had responsibility for everything in Longyearbyen during the middle of the 20th century, but responsibilities for infrastructure such as roads, pipelines and buildings were gradually transferred to the Norwegian Government and Longyearbyen Community Council (Longyearbyen Lokalstyre, LL). LL was aligned as a local democracy in 2002 (SSB, 2016). The transition from a coal mining society to the present Longyearbyen was enhanced when The University Center in Svalbard (UNIS) was established in 1993 (UNIS, 2020). Research and education are now one of the cornerstones in the economy (SSB, 2016).

The infrastructural planning and housing situation took a dramatic turn during Christmas in 2015. A snowstorm on the 19th of December triggered a snow avalanche that crushed eleven houses in Lia, caused several injuries and the loss of two lives (DSB, 2016). SvalbardPosten (the local newspaper) posted an article from the one-year memorial that emphasizes the social scar made by the avalanche in such a small community (Røsvik, 2016). In February 2017, another avalanche was triggered in the same area, hitting two houses, but it caused only material damages (Landrø et al., 2017). The remaining houses in Lia were decided to be demolished in the following years. The need for safe housing facilities became precarious, and the Elvesletta area was again in focus as a potential site for establishing residential areas (LL, 2019). The river needed, therefore, to be permanently controlled to prevent erosion and flooding.

Figure 1: Overview map of Longyearbyen and the Svalbard archipelago. Detailed Longyeardalen area with relevant labeling based on location mentioned in the text. Annotated from TopoSvalbard, NPI (2020).

1.3 Geological setting

1.3.1 Bedrock lithologies

Tectonic plate movement caused a collision of Svalbard (Eurasian) and Greenland, a foreland basin developed as the tectonic plates diverged after the collision of Svalbard (Eurasian) and (Müller and Spielhagen, 1990). The foreland basin is now known as The Central Spitsbergen Tertiary Basin (CTB) and accumulated sediments in the Paleogene period (Dallmann, 2015). The Longyeardalen stratigraphy consists of horizontal, slightly southward dipping, sedimentary rocks from the CTB (Major and Nagy, 1972), see *Figure 2*. The overall trend in the sedimentary lithostratigraphy is a general regression, with several trans- and regressions during Paleocene and Eocene. The bottom units in the area marine sand- and siltstone with beds of shales from the Cretaceous, whereas the top units are mostly terrestrial sandstone (Dallmann, 2015; Müller and Spielhagen, 1990).

The Carolinefjellet Formation (Cretaceous) holds alternating marine sand and mudstones but is only exposed in some road cuts and mostly covered with sediments from the younger stratigraphy (Dallmann, 2015). The Firkanten Formation, with sandstones, conglomerates, and a coal seam, marks the transition (hiatus) from the underlying Carolinefjellet Formation to the Paleocene epoch (Major and Nagy, 1972; Müller and Spielhagen, 1990). Steel et al. (1981) further describe the Firkanten Formation, divided into Todalen- and Endalen Member as followed. The foremost holds the rich and easily accessible coal layers, the very reason for the Longyearbyen settlement. The latter makes out the first pronounced cliff-forming sandstone bodies in the valley sides, see *Figure 2* and *Figure 3*.

Grumantbyen and Hollendardalen Formation are described by Dallmann (2015) as strongly bioturbated sandstone, visible as the uppermost cliff-forming unit and form the flat plateaus, Sverdruphammeren and Gruvefjellet, see *Figure 2*. Steel et al. (1981) differentiates the two Formations and describes the Hollendardalen Formation as sandstone, wedge-shaped, which disappears towards the northeast in the CTB with beds of shale. It is, therefore, likely that it is the Grumantbyen Formation that is exposed Longyeardalen, even though the geological map from the Norwegian Polar Institute (NPI, 2020a) displays them as one. Steel et al. (1981) further describes the Grumantbyen Formation as strongly bioturbated greenish sandstone.

Helland-Hansen (1990) described the alternating silt and sandstones in the Battfjellet Formation, based on outcrops in the cliffs south in the Longyeardalen. The underlying dark shales belong to the Frysjaodden Formation. On top of the Battfjellet Formation lays the thick, terrestrial sand and siltstone-rich Aspelintoppen Formation (Helland-Hansen, 1990). The formation can be found in the uppermost parts of the area, such as in the vertical cliffs in the south-western corner of Longyearbreen, see *Figure 2* (Helland-Hansen, 1990; Müller and Spielhagen, 1990). Etzelmüller et al. (2000) characterize the clastic sedimentary rocks in the area as mechanically soft, easily eroded, and fine-grained, factors that are crucial for grain size distribution and further sediment transport.

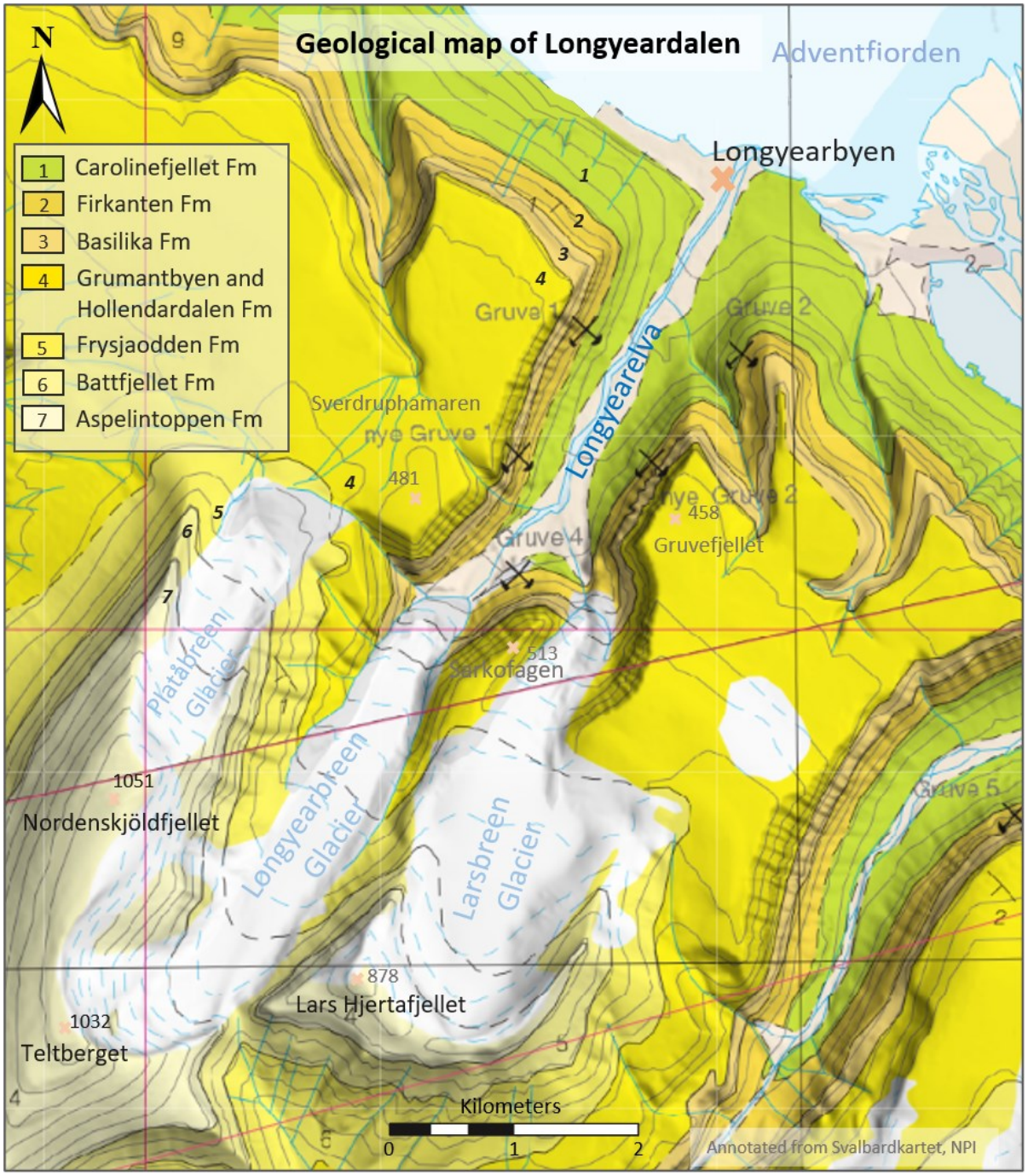

Figure 2: Geological map annotated from NPI (2020a), illustrating the geological units around Longyearbyen. The lithology is in general, mechanically weak sedimentary rocks. The ''pickaxe and shovel'' indicate the old coal mines and the Todalen Member.

1.3.2 Quaternary geology and geomorphology

Glaciers are a typical feature of Svalbard due to the high latitude and Arctic climate. The glacier inventory is versatile, with large ice caps and smaller valley glaciers (Dallmann, 2015). Hagen et al. (1993) reveal that glaciers covered more than 60% of the land area. However, relatively recent research by Nuth et al. (2013) indicates a 57% glacier coverage and claims that a general negative glacier mass balance caused the decrease. With the NCCS (2019) climate report in mind, it is expected that the glaciated area today is even lower than the findings in Nuth et al. (2013). The glacier inventory in the surroundings of Longyearbyen consists of an abundance of relative small valley- and cirque glaciers (Hagen et al., 1993).

Humlum et al. (2003) define the Longyearbyen area as a zone with continuous permafrost (see chapter *2.2.1 Permafrost and ground thermal regime*). Glaciers in a zone of continuous permafrost will, according to Ødegård et al. (1992), cause the small glaciers to be cold-based, meaning that they are frozen to the ground, relatively immobile and less abrasive. The fact that Humlum et al. (2005) documented in situ vegetation at the base of Longyearbreen illustrates that at least it is immobile, which also concurs with the findings in Etzelmüller et al. (2000). The permafrost thickness around Longyearbyen has not been studied in detail. Still, Humlum et al. (2003) describe thicknesses around 100m along the coast and 4-500m further inland for the area in general. The permafrost in Longyeardalen is described by Gilbert et al. (2019) as saline with high ice content.

The landscape around Longyearbyen (see *Figure 3*) consists of wide U-shaped valleys, with braided rivers draining the glaciers. Plateau mountains flank the valleys, influenced and controlled by the horizontal stratigraphy, and the steep mountainsides are covered with landslide deposits (Lied and Hestnes, 1986). The harder quartz-rich sandstone withstands the physical erosion better than the softer shales and therefore stand out as pronounced cliffs (Lied and Hestnes, 1986), see *Figure 3*. The area has minimal vegetation and an absence of plants with considerable rooting systems (Lied and Hestnes, 1986).

The sediment thickness in the Longyeardalen varies, although the different boreholes provide only point data, and the complete picture is uncertain (Instanes and Rongved, 2017). Investigations by Gilbert et al. (2018) in the northern part of Longyeardalen show marine clays and a gradually coarsening upward into deltaic deposits. The marine limit is around 70m above the current sea level due to isostatic lifting (Gilbert et al., 2018; Instanes and Rongved, 2017). The fact that a marine shell found at 3.8m depth in a borehole in Lia by Berggren and Finseth (2019) supports the conclusion of isostatic lifting and change in sea level. The high salinity can consequently originate from the influence of seawater and marine sediments.

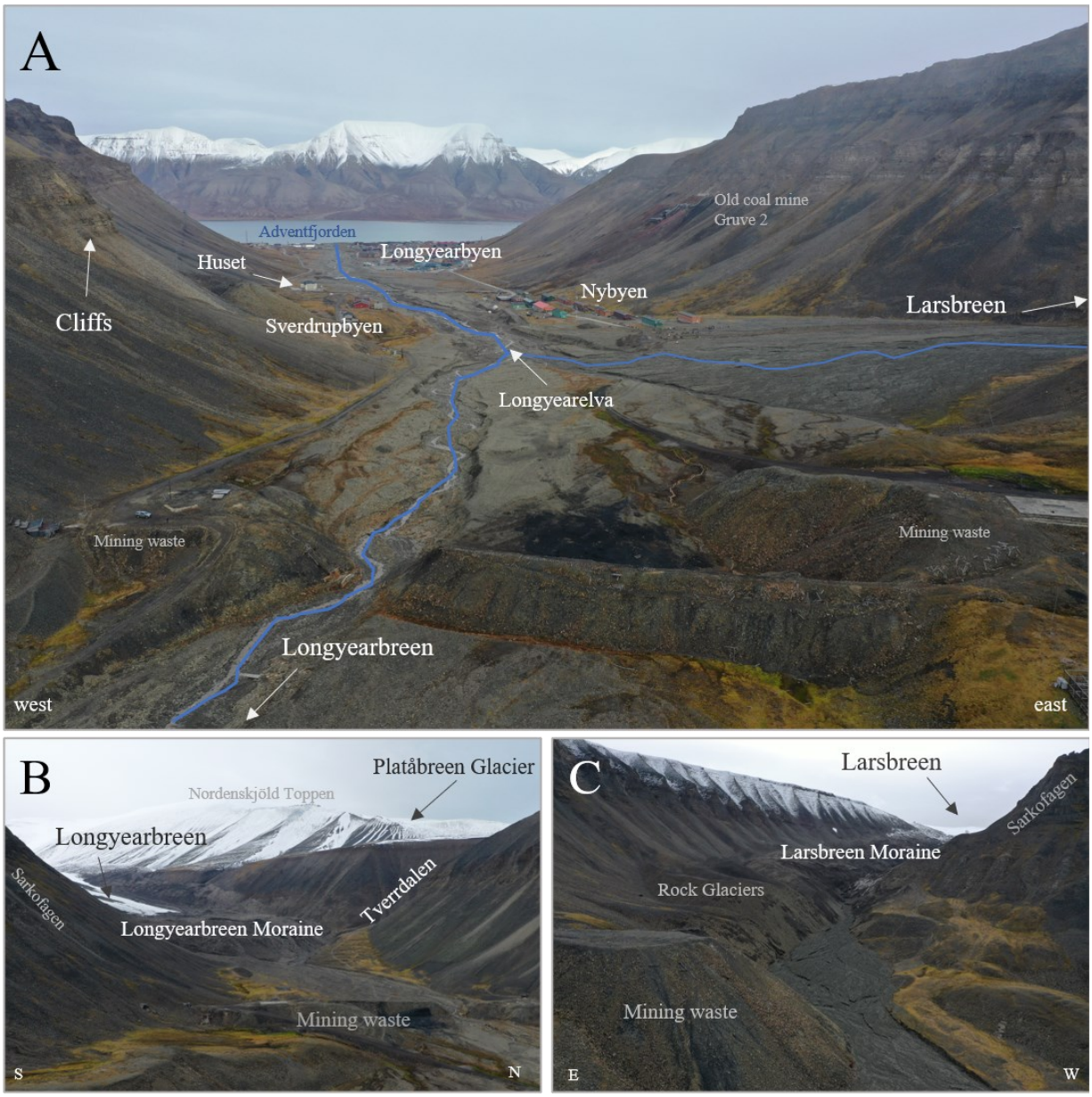

Figure 3: Annotated drone pictures to illustrate the landscape around Longyearbyen. **A)** An overview looking northwards, downstream the Longyearelva. **B)** looking westward at Longyearbreen and the moraine. **C)** Looking southwards at Larsbreen and the moraine.

An increasing sediment thickness is to be expected towards the centre of the valley, although local variations may be caused by jagged bedrock morphology (Instanes and Rongved, 2017). Gregersen (1995) conducted a series of drillings along Longyearelva (from Veg 501 to the outlet, see *Figure 1*) and concluded that spatial variation of sediment thickness could be the result of shifts in the erosional- and depositional environment over time, a plausible explanation which also was discussed by Lied and Hestnes (1986). The uppermost 2-3m alongside the Gregersen (1995) drilling profile consists of coarse gravel. Underneath is a 3-4m thick, wedge-shaped layer of sand, which thins out and disappears halfway downstream the profile. Below this sand layer was a laterally persisting layer of clay, 3-8 m thick, inter-bedded with layers of silt. In the outer edge of the drilling profile, another layer of sand was documented in the deepest part of the sediment sequence.

Gregersen (1995) also detected high salinity with an increasing concentration towards the outlet in Adventfjorden. Lied and Hestnes (1986) conducted a series of sieving tests to investigate the geotechnical properties of the sediments. However, the material in the fluvial channel was only briefly described, as it was believed to be unproblematic for engineering properties due to the low content of fines (clay, silt, and fine sand). A single sieving test resulted in 95% sand, gravel, and cobble while the remaining 5% were fine sediments.

Nårstad et al. (2018) described a 24m deep borehole east of Elvesletta as a coarser top layer of gravel, followed by alternating sand and clay and clay with layers of silty sand towards the bottom, without reaching bedrock. Pedersen (2018) described sediment thickness of 20-28m down to bedrock at another borehole at Elvesletta, with similar stratigraphic content as Nårstad et al. (2018). However, even courser sediments in the top layer were described, possibly due to the closer proximity, and thus influence, of the glaciofluvial system.

Geotechnical investigations down to 15m around the UNIS building (see *Figure 1*) did not reach the bedrock. Investigations by Gregersen and Tuft (1994) and Gilbert et al. (2019) documented a consolidated top layer of coarse gravel, followed by more silty sand and clay with some coarser sections towards the bottom of the drillings. In contrast, LNS Spitsbergen reached bedrock at 11-13m in Sjøområdet, after drilling through nothing but clay (LNSS, 2016). Drilling at the more elevated area at Skjeringa (*Figure 1*) shows relatively coarse material (sand and gravel) with only 8m of sediment above the bedrock (Instanes and Rongved, 2017).

Sediment thickness and origin change from the central valley towards the steep mountainsides, with more input from mass movement events and less fluvial sedimentation (Lied and Hestnes, 1986). Eckerstorfer et al. (2013) describe the slope the morphology and sediments as snow avalanche colluvial fans, with sediment material reflecting weathering of the local lithostratigraphy, a description similar to the findings in Lied and Hestnes (1986). The more low-angled alluvial fan at the mouth of the small side-valley Vannledingsdalen reaches far out on the valley floor and is related to repeated slush-avalanche activity at Haugen, see *Figure 1*.

The periglacial areas in front of the Longyearbreen and Larsbreen glaciers are described by Etzelmüller et al. (2000) as ice-cored moraines with a 0.5-1.5m surface layer of mixed sediment, see *Figure 3*. The eastern margin of the Larsbreen moraine complex has later been categorized as avalanche-derived rock glaciers, see *Figure 3* (Humlum et al., 2007). The till in the Larsbreen moraine is considerably more fine-grained than the till at the Longyearbreen moraine. Etzelmüller et al. (2000) argue that this is due to the higher topographic position of Larsbreen, which results in sediment input from mechanically weaker lithological units, such as the shales from the Frysjaodden Formation (see *Figure 2*). In contrast, the lower situated Longyearbreen has eroded into coarser lithologies and more resistant lithologies, such as Firkanten- and Battfjellet Formation. Longyearbreen and thus the moraine receive additionally input through rockfall and snow avalanches from the Aspelintoppen Formation (see *Figure 2*). The moraines described above are constantly eroded by the glacier meltwater streams from the glaciers and are thus directly connected with the Longyeardalen glaciofluvial system. A simplified summary of the sediment distribution in Longyeardalen is illustrated in *Figure 4.*

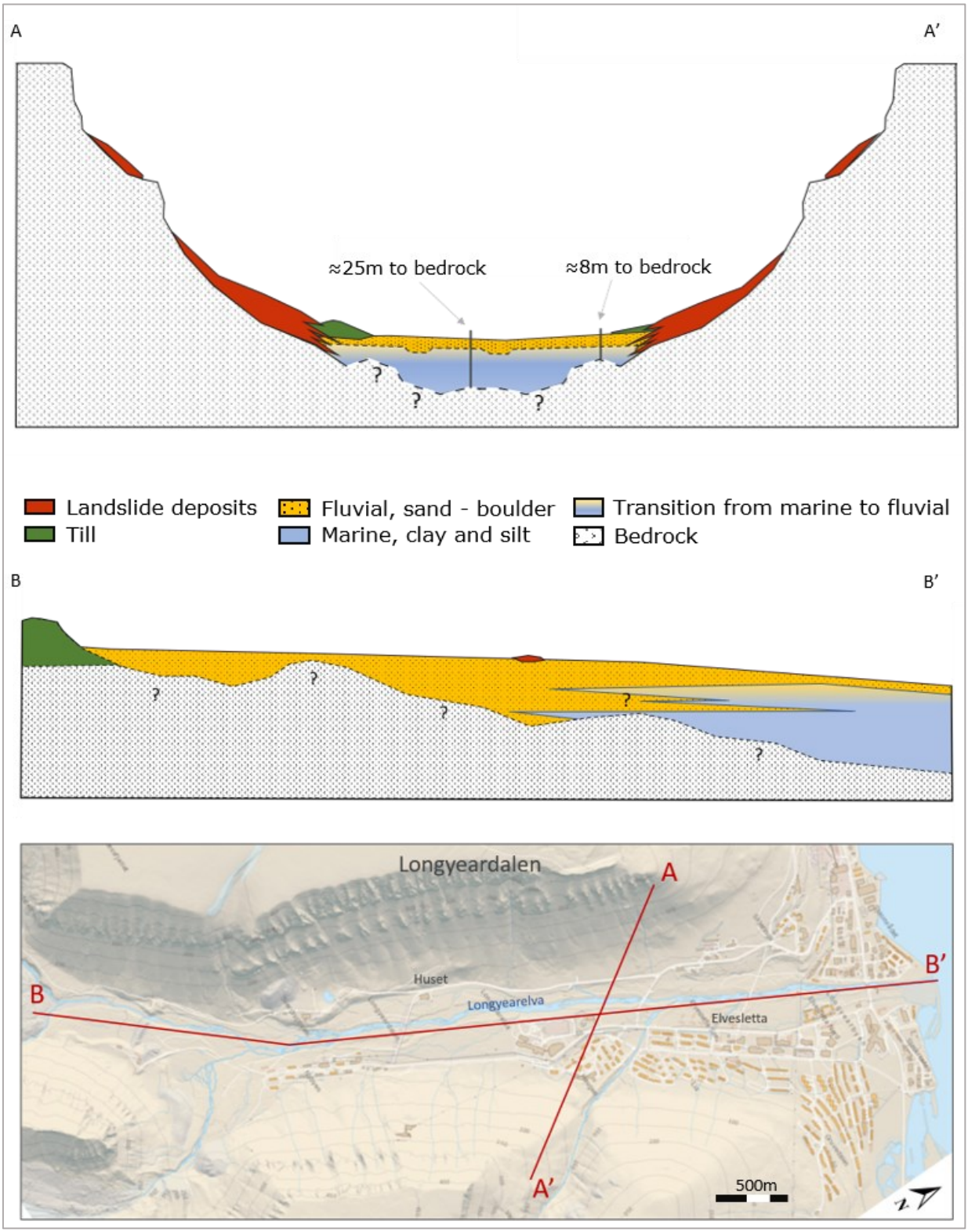

Figure 4: Schematic illustration of the general deposits and sediment thicknesses in Longyeardalen based on a basic interpretation of the data presented in the text.

1.4 Hydrological conditions

1.4.1 Svalbard weather and climate

The Norwegian Centre for Climate Services (NCCS, 2019) report clarifies that climate changes are pronounced in the High Arctic. Svalbard and the surrounding ocean show the most extensive temperature increase and loss of sea because of the climate changes (Isaksen et al., 2017; NCCS, 2019). The rise in air temperature is most noticeable during the winter months (Isaksen et al., 2017; Wawrzyniak and Osuch, 2020).

Isfjorden, a massive fjord in the middle of the Spitsbergen island (see *Figure 1*), allows ocean currents to bring warm ocean water inland from the west coast, resulting in a warmer climate than expected so close to the North Pole (Walczowski and Piechura, 2011). Eckerstorfer and Christiansen (2011) suggest a 'High Arctic maritime Snow Climate' to best describe the climate in the vicinity to Longyearbyen, and a long-term dataset from Hornsund documents how the ocean currents contribute to relative humid conditions along the west-coast (Wawrzyniak and Osuch, 2020). Precipitation on Svalbard is historically sparse with large spatial variations (Førland and Hanssen-Bauer, 2003; Isaksen et al., 2017) and Wawrzyniak and Osuch (2020) demonstrate how late autumn precipitation events are common. However, a warmer climate alters the precipitation patterns, e.g., increasing volumes and rain during the winter is more frequent (NCCS, 2019). Strong winds cause snowdrift, and the measured precipitation might not reflect the actual snow coverage in the catchment, as large cornices and uneven spatial distribution of the snow have been documented by Hancock et al. (2018)

The nearest weather station is located at Svalbard Airport (28 m.a.s.l) 4km northwest of the Longyearbyen city centre, see *Figure 1*. The monitoring station has been functional since 1976, operated by the Norwegian Metrological Institute, MET Norway, and precipitation and temperature data is displayed in *Figure 5*. The mean annual air temperature over the last 30 years (1991-2020) is -4.7ºC, and the average yearly precipitation over the same period is 202mm (MET, 2021).

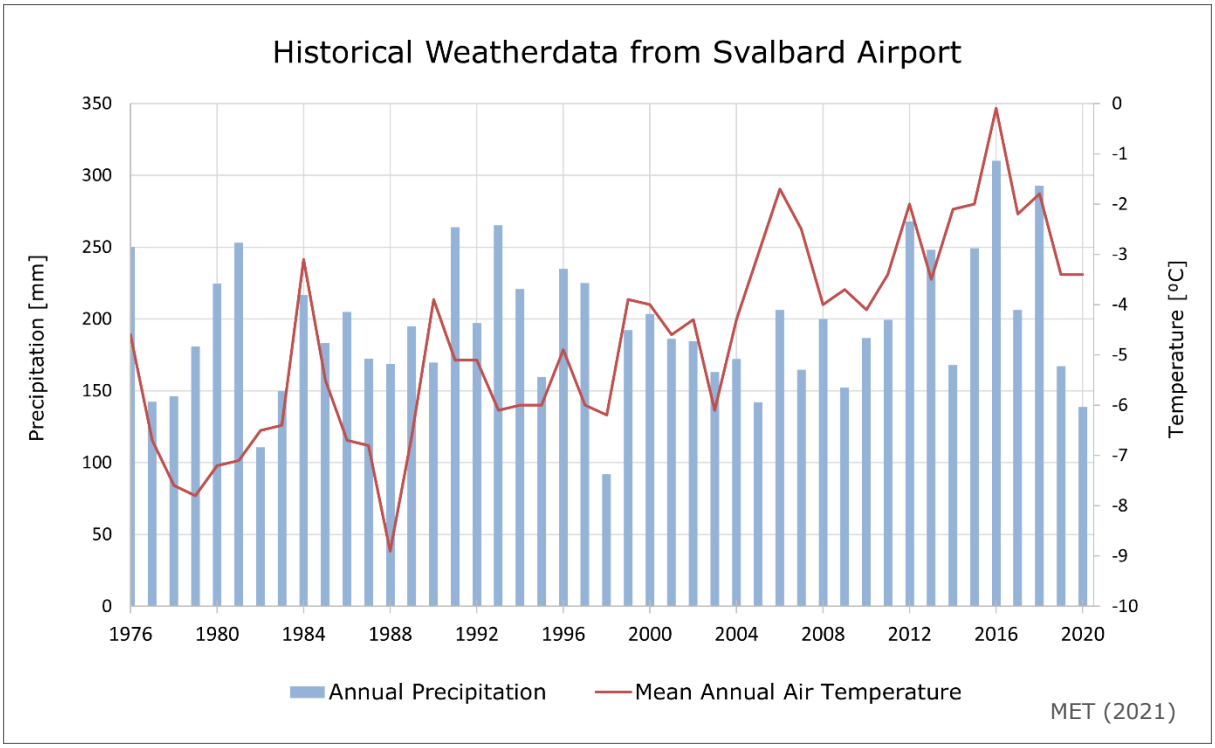

Figure 5: Historical weather data from the meteorological station at Longyearbyen Airport, data from Norwegian Metrological Institute (MET, 2021).

1.4.2 Longyearelva catchment description

The Longyearelva catchment consists of glaciers, mountains, and infrastructure, unlike most of the catchments on Svalbard, see *Figure 6*. The total catchment area is 22.2km^2, including two glaciers covering 5.7km^2. Etzelmüller et al. (2000) mapped Longyearbreen and Larsbreen to be 2.7km^2 and 3.0km^2, respectively, and described them as cold-based, although a small patch of temperate ice was discovered in the uppermost western corner of Longyearbreen. However, considered the climate situation described in NCCS (2019) and the effect on small valley glaciers, the thickness and area of the glaciers are likely to have decreased. Longyearbreen meltwater stream receives a limited contribution from Platåbreen, which drains partly through Tverrdalen. The meltwater streams from Larsbreen and Longyearbreen glaciers confluence near Nybyen and forms Longyearelva, 3.3km from the outlet in Adventfjorden.

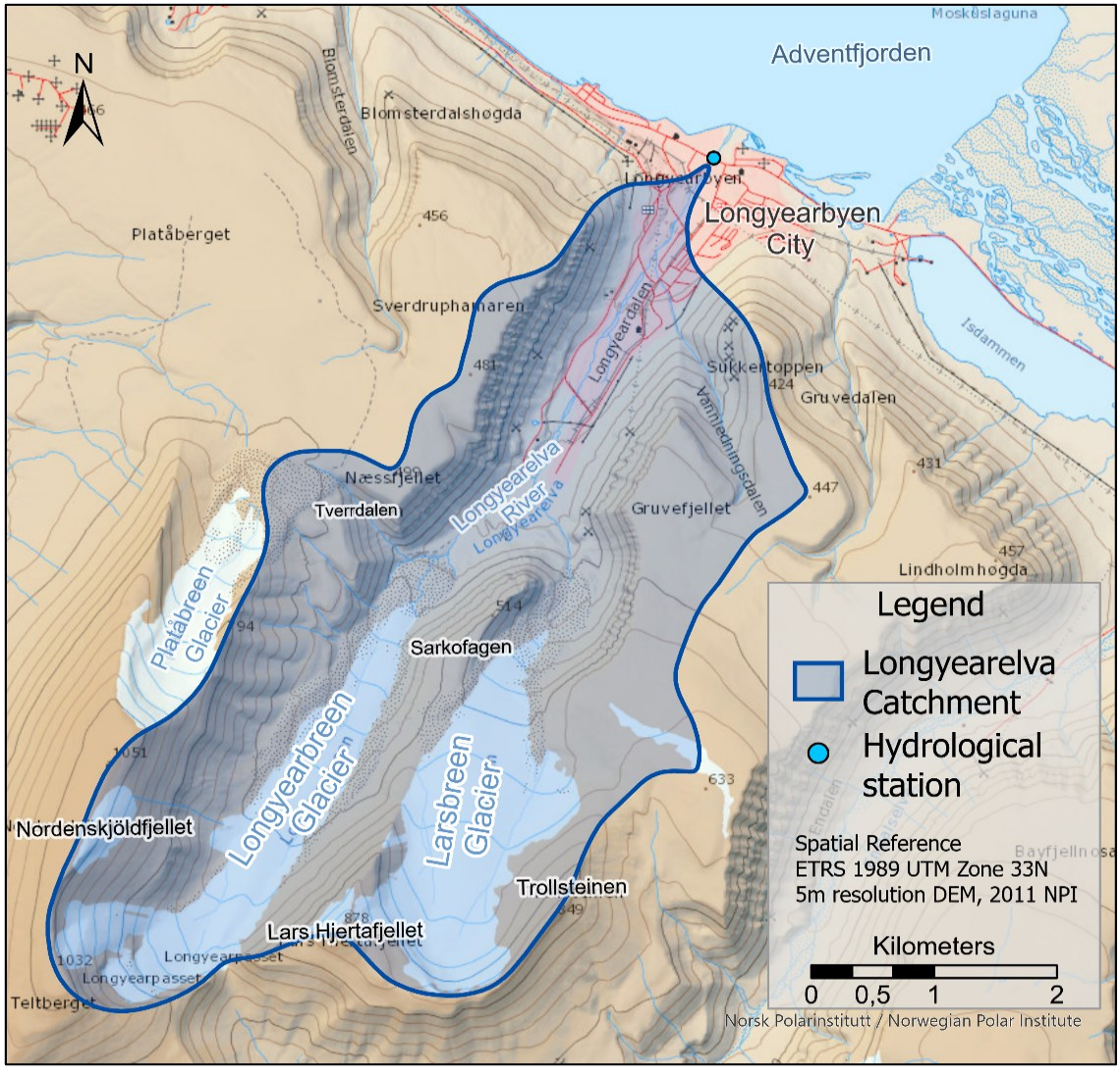

Figure 6: Longyearelva catchment covering 22.2km^2, ranging from above 1000 m.a.s.l to the outlet in Adventfjorden, including two glaciers and Longyearbyen. The watershed is calculated using a 5x5m DTM and adequate hydrology modelling-tools.

The gradual expansion of Longyearbyen has restricted the river into an artificial channel in the middle of the valley. The old aerial photographs by the Norwegian Polar Institute (NPI, 1936) (*Figure 7A*) show the natural state of Longyearelva as it filled the whole valley floor back in 1936. Reconstruction of the historical photograph illustrates the current situation in 2020, demonstrated in *Figure 7B.*

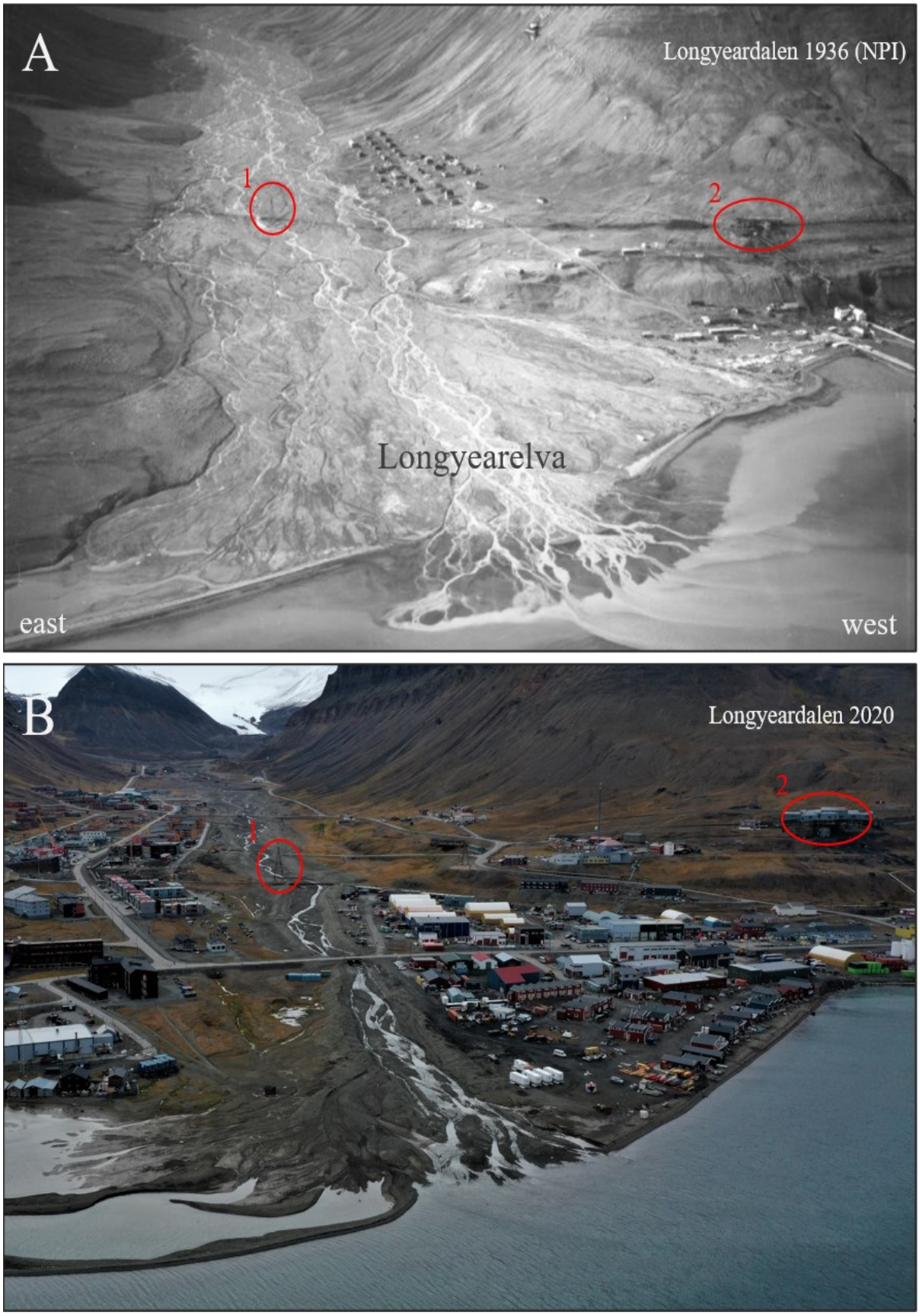

Figure 7: Illustrating changes in Longyeardalen over the last 90 years. **A**) Aerial oblique photo from NPI (1936), showing the natural state of Longyearelva and the early settlement. **B)** Drone photo from 2020, replicating the photo in A. Note the cableway ramp (1) and the cableway station (2) marked with red circles for reference points.

1.4.3 Previous research in Longyearelva catchment

Discharge and sediment transport in the catchment has previously been the topic in several research projects; Etzelmüller et al. (2000) investigated glacier characteristics and sediment transport in the catchment over two seasons, 1993-94, and Yde et al. (2008) studied the hydrochemistry in the meltwater from Longyearbreen. Furthermore, two master projects, Grønsten (1998) and Riger-Kusk (2006), have covered discharge and fluvial sediment transport over one or two seasons. The neighbouring catchment towards the east, Endalen catchment, drains into Isdammen (the water reservoir for Longyearbyen). NVE has monitored discharge and sediment transport in Endalselva over several years during the 1990s (Bogen and Bønsnes, 2003; Sund, 2008).

1.5 Measurements and previous initiatives

The white paper ''Svalbard'' from the Solberg Government in 2016 states that extensive funding for permanent geohazard mitigation measures in Longyearbyen is a part of the national budget (St.meld 32 (2015-2016), 2016). The white paper further states that NVE has the responsibility to evaluate geohazards on behalf of the Department of Justice and Public security, and LL will be responsible for maintenance. Geohazard mitigations must now meet the strict regulations on the Norwegian mainland. A more long-term perspective regarding geohazard mitigation was therefore needed.

1.5.1 Development of geohazard mitigation

Geohazard mitigation has been an ongoing process since the establishment of the town. Although previous initiatives seem to be short-termed, and more permanent measures tend to follow dramatic events. A deadly slush avalanche hit the residential area at Haugen in 1953 (Larsen, 2016) (see Figure 1). Despite countermeasures such as reinforced embankment and extensive usage of bulldozers to clear the narrow Vannledningsdalen, the area was struck once again in 1989 (Larsen, 2016). Snow cornices breaking and triggering snow avalanches a real danger in Longyeardalen (Vogel et al., 2012). SNSK used explosives to remove the cornices when coal miners lived in barracks in Nybyen (Larsen, 2016). However, evacuation of the residents is now preferred, as the snow avalanches are still a hazard (Bårdseth, 2021).

1.5.2 Mitigation measurements in Longyearelva

The gradual expansion of infrastructure on the valley floor required extensive usage of bulldozers to control the river and protect infrastructure, such as the cableway-ramps, see *Figure 8* (Pedersen and Svalbard Museum, 1960; Hoseth and Daae, 1996; Bjordal and Hoseth, 2017). SNSK increased the usage of bulldozers following a large flood in 1964 and planned a sedimentation dam next to Nybyen after consultations from NVE over the following years; however, the plans were never commenced (Hoseth and Daae, 1996). SNSK and NVE considered more permanent solutions for flooding mitigation again in 1989, but the usage of bulldozers continued (Øvereng, 1989; Hoseth and Daae, 1996). Elvesletta area was investigated for the development of residential and commercial buildings as early as the 1980 and '90s (Lied and Hestnes, 1986; Gregersen, 1995; Hoseth and Daae, 1996). Preliminary flooding calculations and plans for controlling the river were initiated in the mid-90s (Hoseth and Daae, 1996; Sværd, 1996). However, it would take another 20 years before the plans were put into action.

Extensive usage of bulldozers continued until NVE initiated the construction of more permanent erosion and flooding measures in 2016. The action plan by Bjordal and Hoseth (2017) states that the levees needed scour-protection once the water was channelized,

and a sedimentation dam should be built between Huset and the school (*Figure 1*) to control the sediment supply (see *Figure 9*). Shutting off the sediment supply could lead to channel degradation, and sills were therefore built. Construction work was completed in 2019, and the assessment of the mitigation is hence an essential part of this thesis. The different measurements and specific constructions are further explained in Chapter *2.6 Hydrological engineering and scour protection.*

Critical infrastructure, such as bridges and culverts, has also been reinforced. Old culverts have been replaced with bigger weirs and spillways, such as around Veg106, Veg501, and Veg600 (Larsen, 2016; Bjordal and Hoseth, 2017). The bridge at Veg503 is missing, however, extra scour protection is already in place (Bjordal and Hoseth, 2017). Larsen (2016) illustrates how the new bridges have been built with reinforced fundaments, scour protection and are designed to withstand a 200year-flood event while limiting the influence on the ground thermal regime by allowing natural heat flux between the ground and the air.

Figure 8: Crucial use of bulldozers to protect infrastructure along Longyearelva river dates to the 1950's (Pedersen and Svalbard Museum 1960). In this case is a bulldozer is used to keep the river from eroding the fundaments of the cableway ramps used for transportding coal from the mines to the harbour.

Figure 9: Timeline for construction work (building sills and riprap) in the river by NVE since 2016 and placements of all the sills and the sedimentation dam. Riprap is continuous on both sides from the sedimentation dam to Veg 600.

2 Theoretical background

2.1 Arctic conditions

The arctic conditions influence the geological processes and features in the morphology. Catchments with glaciers are normal on Svalbard (Hagen et al., 1993), but Longyearelva, strongly influenced by human activity, is one of a kind on the archipelago. Thus, a combination of literature and technics from a global and local perspective is needed to cover all relevant theoretical aspects.

2.2 Heat flow and thermodynamics

Some basic terms must be defined to understand the heat flow through the sediments in Longyeardalen and the coupling between water, air, and thawing of the uppermost section of sediments.

2.2.1 Permafrost and ground thermal regime

Svalbard and, therefore Longyearelva, are in a zone of continuous permafrost (Humlum et al., 2003), which has important implications for both hydrology and engineering. Permafrost is defined based on the ground temperature, which cannot exceed 0ºC for two consecutive years (Andersland et al., 2003). The perennially frozen ground holds distinct mechanical properties compared to the thawed counterpart, as the mechanical strength increases with a frozen soil-skeleton and permeability will be limited or absent (Andersland et al., 2003).

An important aspect is the yearly fluctuating air temperature and the response in the ground thermal regime, illustrated with the trumpet curve, see *Figure 10*. The uppermost section of the ground where temperatures rise above 0ºC for a period of the year is defined as the active layer, illustrated in *Figure 10*. The air temperature affects the ground temperature even deeper than the active layer, known as the depth of zero annual amplitude. Instanes and Rongved (2017) show active layer thickness at 1.5m in Longyearbyen city centre and depth of zero annual amplitude at 5-10m in several boreholes around the area, whereas Bjordal and Hoseth (2017) documented active layer thickness in Longyearelva at 2.5m. The active layer reaches a maximum depth late in the ablation season (September) (Andersland et al., 2003).

The permafrost depth is controlled by the geothermal gradient, historical climate conditions, thermal properties in the ground. Temperature readings from a borehole close to the Longyearbyen airport document permafrost thickness at 22-39m (NGU, 2007), in contrast to the general 100m thickness in coastal areas (Humlum et al., 2003). The active layer thickness is controlled by the heat exchange between the ground and the air. Increased insulation from, e.g., snow or infrastructure can hence slow down the refreezing, while infrastructure or vegetation can provide shadow and reduce the warming during the summer. The temperature in the active layer can further change the depth of zero annual amplitude and thus affect the properties of the permafrost (Andersland et al., 2003). Buildings in Longyearbyen are built on stakes to allow natural air circulation and heat exchange or with artificial cooling in the foundation, both to limit the effect on the ground thermal regime (Hestnes et al., 2016; Larsen, 2016). Increased permafrost temperature and a thicker active layer decrease the strength of the foundations and can cause settling damage (Andersland et al., 2003). Reestablishing permafrost after construction work and thus achieve the intended foundation has been a problem for the Svalbard Global Seed Vault (Statsbygg, 2019).

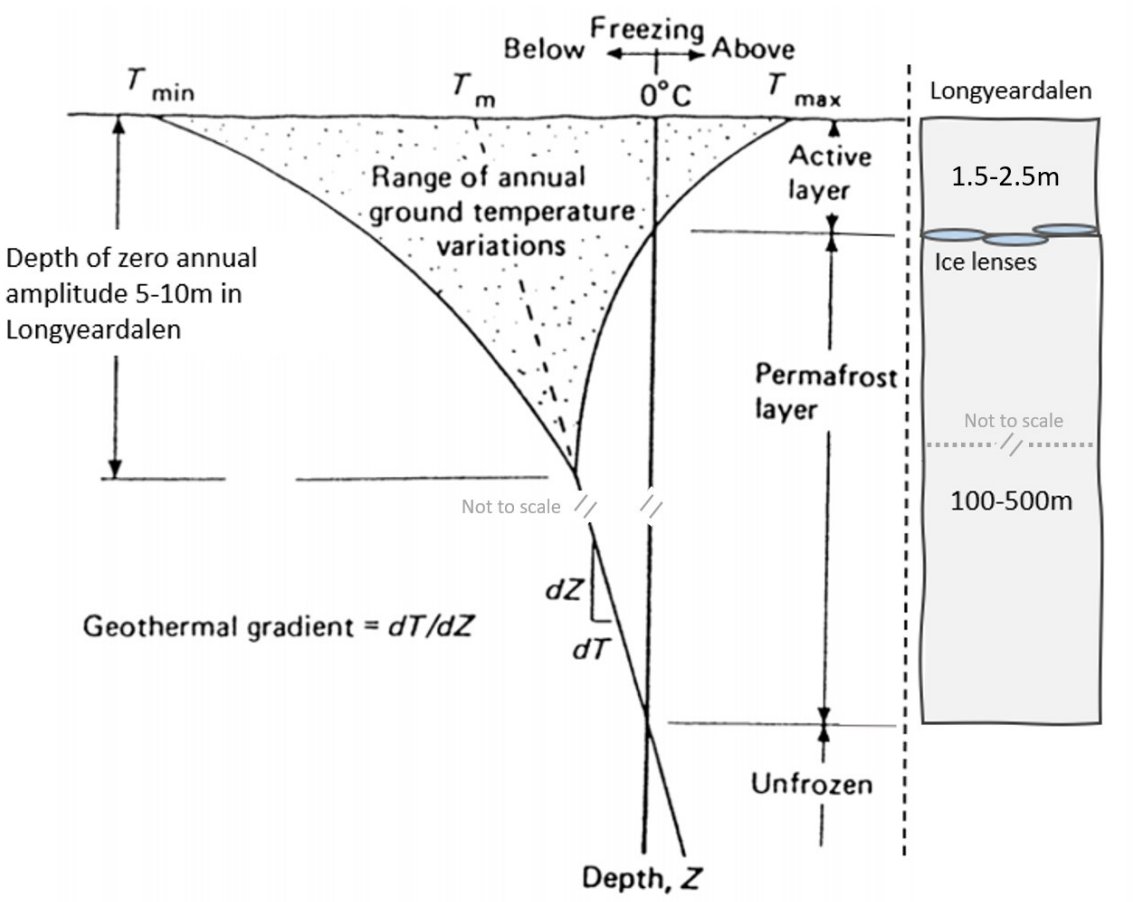

Figure 10: Trumpet curve annotated from Andersland and Ladanyi (2003) to fit the conditions in Longyearelva catchment. Illustrating the thermal regime in the ground with the annual variation based on surface temperature. Cite specific considerations are based on Instanes and Rongved (2017) and Humlum et al (2003).

2.2.2 Thermal conductivity

Thermal conduction is the transfer of kinetic energy from an area of high energy to an area of low energy (Andersland et al., 2003). Thermal conductivity is further described as how efficiently a material transmits energy - the ability to transfer heat increases with the dry density and saturation of soils. Materials have various conductivity, e.g., the mineralogy of soils or bedrock will affect the thermal characteristics. Water has a high conductivity compared to air and, likewise, with metamorphic rocks compared to sedimentary rocks (Labus and Labus, 2018). The relative conductivity (C) between material represented in Longyeardalen: $C_{mineral} > C_{ice} > C_{water} > C_{air}$ (Woo and Xia, 1996). Subsequently, the heat transfer efficiency decreases over the ablation season as the ground ice starts to melt, water drains, and the pores are filled with air. Andersland et al. (2003) define the ratio of thermal conductivity and density of soil as the thermal diffusivity, in other words, how fast heat is transferred through a material. Frozen soil will have a higher diffusivity compared with a thawed sample of the same soil. The above will influence the heat transfer through the soil as the uppermost layer start to thaw, and the active layer thickens (Andersland et al., 2003).

2.2.3 Heat capacity

Heat capacity is the amount of energy (heat) needed to raise the temperature in a given sample by 1º. Different components in soils, e.g., water, mineralogy, and air, will have different heat capacities. Adding the specific values from each material determines the net heat capacity of a given soil or deposits (Andersland et al., 2003).

2.2.4 Heat flow in soils

The general heat flow in sediments depends on the thermal conductivity and the temperature differences. The energy exchange between the atmosphere and the ground can be expressed through the energy balance. The penetration of surface energy will gradually decrease with increasing depth until a point where the temperature in the ground is stable all year round (dept of zero annual amplitude, see *Figure 10*).

2.3 Hydrology in the Arctic

Discharge in Arctic rivers is typically limited to the ablation season, May to September (Killingtveit, 2004), and is generally frozen during the remaining months of the hydrological year (October 1st to 30th of September). However, as a result of a warmer and wetter climate, the timing of initial discharge and freeze-up is changing. (NCCS, 2019; Hestnes et al., 2016).

Snowmelt occurs early in the ablation period, typically May-June, leading to the first peak in discharge. The accumulation of snow in the catchment is therefore important as water is temporarily stored during winter. Less snow means less insulation for the permafrost and glaciers, hence will the glacial melt start earlier in the summer if the snow cover already is gone. For the rest of the ablation season (June-September), discharge and glacial coverage in the watershed are closely coupled through air temperature and glacial melt (van Pelt et al., 2019). Minor floods late in the ablation season tend to correspond with precipitation (Killingtveit, 2004; Nowak and Hodson, 2013). However, snowmelt-induced floods are not the most prominent hazard, according to Hoseth and Daae (1996), but it is instead the high temperatures and precipitation during July-September that cause the most severe floods and related engineering difficulties.

Water percolating through the active layer can pick up solutes from the sediments and increases electrical conductivity (EC). Groundwater has, therefore, a higher EC compared to meltwater from clean snow and clean ice (Yde et al., 2008). The EC in Arctic rivers increases late in the ablation season as the meltwater contribution declines and the active layer thickens (Yde et al., 2008) – which illustrates the coupling of ground thermal regime and the hydrological conditions in a catchment.

2.3.1 Water balance in Longyearelva

As described above, several factors influence the discharge in a catchment, and the water balance can be expressed with *Equation 1* (Killingtveit, 2004).

Equation 1

$$P_A - Q_S - Q_G - E_A \pm \Delta M = \varepsilon$$

Where P_A is the input through precipitation measured in mm, Q_S refers to the surface discharge and Q_G to the groundwater flow, both measured in cubic meters per second

(m^3/s). E_A is the actual evaporation, and ΔM is water storage. ε is the error term and should ideally be zero based on the accuracy of the other parameters (Killingtveit, 2004).

An important factor regarding precipitation described in Killingtveit (2004) and Nowak and Hodson (2013) is the elevation distribution in a catchment (which can be illustrated by a hypsographic curve). Precipitation can change from rain to snow with increasing elevation due to decreasing temperatures. Strong winds can cause under-catchment in gauging stations, and snow depth in a catchment may not correlate with the recoded precipitation due to redistribution (Dingman, 2015). Observations from, e.g., Wawrzyniak and Osuch (2020) document increased precipitation, and climate models (e.g., Hansen et al., 2014; Bintanja and Andry, 2017; NCCS, 2019) show a continuing increase in precipitation and a warmer and wetter Arctic in the future, especially during winter months.

Q_S, hereafter called discharge, is measured or computed, e.g. based on the water stage-discharge relationship (Dingman, 2015). Groundwater flow or seepage can be more challenging to measure. Groundwater flow in permafrost areas is relatively poorly understood (Neilson et al., 2018), however as stated by Nowak et al. (2021), the topic has received increased attention. The investigations of pingos in the Adventdalen valley illustrate sub-permafrost groundwater flow in the area (Hodson et al., 2020), and the understanding of permafrost groundwater is improving. Groundwater flow will increase due to a warmer climate and permafrost degradation across the Arctic, according to models from Bense et al. (2009). The fact that geotechnical investigation by Pedersen (2017) documented water seepage at a depth of 4-7m at Elvesletta indicates some groundwater in the catchment, although the exact contribution is yet to be investigated in detail.

As discussed in Killingtveit (2004) and Dingman (2015), the potential evaporation may be significantly higher than the actual evaporation given the midnight sun. Despite this, the actual evaporation on Svalbard is considered to be minimal due to the geology, sparse vegetation, low precipitation, and cold temperatures (Killingtveit, 2004). Evaporation can potentially increase and thus also precipitation due to the observed increased temperatures and less sea ice (Bintanja and Andry, 2017).

Water storage (ΔM) is a vital part of the water balance in glaciated catchments on Svalbard as the air temperature and glacier ablation control discharge (van Pelt et al., 2019). Both snow accumulation and ground ice contribute to the total water storage in a catchment. However, van Pelt et al. (2019) show that the contribution from snowmelt and groundwater is limited compared to the glacier melt. Accumulation of snow and ice could keep the glacier mass balance in equilibrium, and change in storage could be neglected. However, the glaciers on Svalbard are shrinking in time with a warmer climate, and ΔM is hence positive (NCCS, 2019; Nowak et al., 2021).

2.3.2 Glacial hydrology

The high proportion of glacial coverage on Svalbard constitutes most of the water storage across the archipelago and is thus highly relevant for the water balance in glaciated catchments (van Pelt et al., 2019). The thermal regimes of glaciers are of high importance for seasonal trends, glacial runoff, and sediment yield (Hodson et al., 1997; Hodson and Ferguson, 1999). Previous literature concludes that the combination of small, thin glaciers and continuous permafrost makes a typical Svalbard polythermal or cold-based as size decreases (Ødegård et al., 1992; Björnsson et al., 1996; Hodson et al., 1997). The glaciers on Svalbard are generally shirking (NCCS, 2019), and a shift from polythermal to cold-based is documented, e.g., at Austre Brøggerbreen (Nowak and Hodson, 2014). In cold-based glaciers, like the ones in Longyearelva catchments, supra-glacial drainage is more

important than subglacial drainage (Etzelmüller et al., 2000). The linkage between the thermal regime in glaciers and sediment transport has been widely investigated (e.g., Hodson et al., 1997; Etzelmüller et al., 2000; Bogen and Bønsnes, 2003; Hodgkins et al., 2003), and temperate or polythermal glaciers tend to produce both higher discharge and sediment transport rates compared to the cold-based counterparts.

2.4 Erosion

Charlton (2007) defines fluvial erosion or scouring as the relationship of transport capacity and sediment supply in a stream. Erosion can be understood as a loss of material and channel degradation. Erosive forces and flow regimes are further described.

2.4.1 Gravel- and cobble bed rivers

The term ''gravel-bed river'' is a collective term used in literature for describing rivers where gravel is the median grain size, e.g., in Kociuba (2014) and Laronne and Carson (1976). A combination of the grain size classes defined in Wentworth (1922) and the typical Norwegian grain size chart presented in Fergus et al. (2010) is shown in *Figure 11*. Bunte and Abt (2001) presents principles for the classification of rivers with different dominating grain sizes. Classification of sediments is typically based on a sieving test and plotted in a logarithmic grain size distribution curve. The mechanical strength of the local lithology is crucial as it will reflect the grain size distribution, based on how easy sediments are weathered and crushed during transport. However, the term gravel-bed river seems to be widely used in the literature regarding high Arctic rivers. Sediment sizes referred to in this thesis are based on the classification presented below.

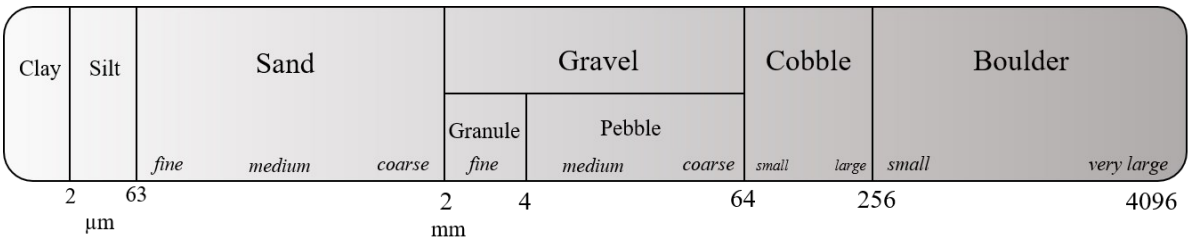

Figure 11: Grain size chart for classification of mineral sediments based on Wentworth (1922) and Fergus et al. (2010). The Norwegian chart disregards granule and pebble and categorizes gravel from fine to coarse. The transition from cobble to boulder is at 200mm in the Norwegian system, not 256mm as it is in the Wentworth (1992) chart.

2.4.2 Fluvial morphology

The valley floors on Svalbard are typically covered by glaciofluvial outwash plains (Dallmann, 2015) or sandar (sandur in singular), where the shape and size of the valley influence the morphology (Boothroyd and Ashley, 1975; Rudberg, 1988).

Braided rivers are recognized by the numerous bars and channels, which are repeatedly flooded and migrating laterally. The bars tend to be longitudinal and with imbrication, special within larger clasts (Nichols, 2009). Braided channels in a sandur are common due to high bedload transport, channel aggregation, and ever-changing discharge (Krigström, 1962; Boothroyd and Ashley, 1975). Krigström (1962) further describes the change in morphology as the distance from the glacier snout increases. Forking, or braiding, becomes more frequent further downstream. Boothroyd and Ashley (1975) highlight the effect of

the surrounding topography as length, width, and gradient of the available area will control the fluvial morphology.

Anastomosing rivers are distinguished by interfingering channels with bars or flood plains in between (Nichols, 2009). Both channels and bars are more stable than in braided river systems, with less channel aggradation and lateral migration.

Arctic rivers remain frozen for most of the year, given the cold climate and can thus be defined as ephemeral rivers. Ephemeral rivers are characterized by how discharge is limited to events, such as rain and snow or glacier melt (Nichols, 2009; Dingman, 2015).

2.4.3 Flow regimes

Specific flow regimes in a stream control the erosive forces and thus effects the mitigation measurements needed. Firstly, flow regimes are divided between laminar or turbulent flow. The former is defined based on the parallel movement of water molecules and no mixing within the water column (Charlton, 2007; Nichols, 2009). The latter is defined based on water particles move in all three dimensions with a net downstream movement, resulting in a highly efficient mixing within the water column (Charlton, 2007; Brooks et al., 2012). Grain size, relief, geology, and human activity affect the channel characteristics and hence the flow regime in the river. A laminar flow interacting with an obstacle in the channel will result in a turbulent flow, or eddies, downstream of the obstacle. Turbulent flow causes more uplift and thus higher stress on the bed material (Charlton, 2007; Brooks et al., 2012) see *Figure 12*. Kay (2008) differentiates between subcritical- and supercritical flows based on the Froude number. A Froude number greater than 1 refers to a supercritical flow and subcritical when the number is below 1. A supercritical flow has high energy and can be very erosive (Charlton, 2007; Kay, 2008). A breaking wave develops directly in transition between sub- and supercritical flow, known as a hydraulic jump. Given a supercritical flow, the speed of the water will be greater than the wave speed.

2.4.4 Erosive forces

Water moves due to gravity and shifts from potential energy to kinetic energy. Kinetic energy allows the water to perform work and apply shear stress on the wetting perimeter

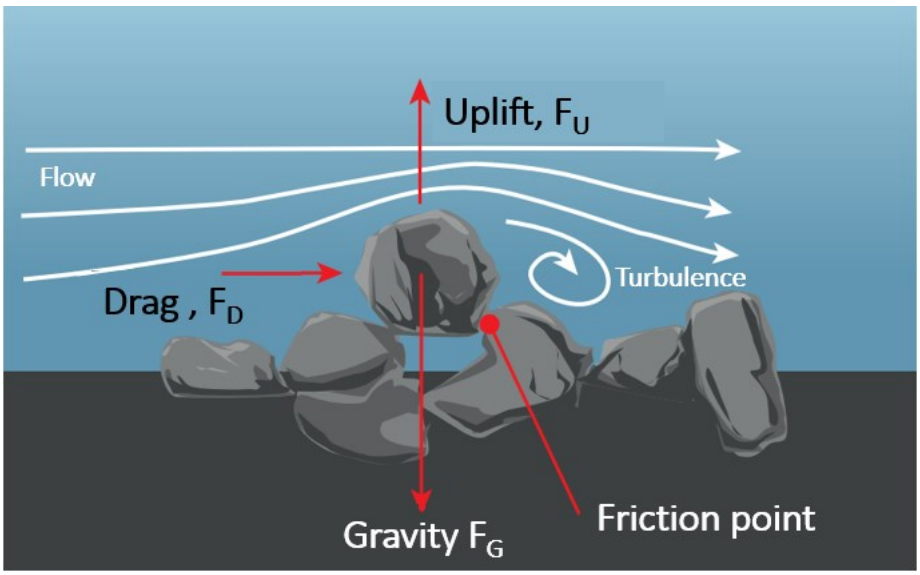

Figure 12: Illustration of the forces working on the riverbed, annotated from Fergus et al., (2010). The flow is laminar until the roughness of the bed causes disturbance and thus a turbulent flow. The flow can turn supercritical as the water velocity increases as the white flow-arrows are closing in over the grains.

(Charlton, 2007). The wetting perimeter is known as the zone where water interacts with the channel. Charlton (2007) further presents the Du Boys Equation, see *Equation 2*, and defines the shear stress [N/m] in a fluvial channel.

Equation 2

$$\tau_0 = \rho g h S$$

Where τ_0 is the average shear stress applied on the channel, (ρ) is the density of the water, (g) acceleration due to gravity, (h) refers to water depth and (S) is the gradient of the channel. The shear stress will increase with an increasing inclination (S) and water depth (h). A steeper channel will thus produce higher shear stress and potentially more erosion than its counterpart. Increasing the wetting perimeter and thereby decrease the depth (h), will reduce the shear stress.

The Shield parameter is utilized to calculate the threshold shear stress for initiating movement on a particle with a given dimension (Charlton, 2007). The Shield parameter is expressed with *Equation 3.*

Equation 3

$$\theta_{cr} = \frac{\tau_{cr}}{g(\rho_s - \rho)D}$$

Where θ_{cr} is the critical bed shear stress or Shield parameter, τ_{cr} is the shear stress. Acceleration due to gravity (g), density of the sediment (ρ_s), density of water (ρ), and D refers to the grain size dimensions. A small particle with low density will be more exposed to erosion and transport than the opposite particles, based on the Shield parameter. The shape and orientation of each grain in relation to the flow direction are critical, in addition to size and density (Self et al., 1989).

2.5 Sediment transport

Flowing water is the prominent transport medium for sediment through the Longyearelva catchment (Lied and Hestnes, 1986). Sediment transport in a fluvial system is divided into two main patterns of movement: in suspension or as bedload, based on the interaction of water, sediment, and channel bed (Nichols, 2009). Hjulström (1935) illustrated the relationship between water velocity and grain size for erosion, transport, and deposition with the Hjulstrøm Curve, see *Figure 13*.

Sediment transport will mirror sediment sources in the fluvial system. Bank erosion can cause undercutting, potentially collapse, and consequently increased sediment input. The mechanical strength of local lithology is important for the capability to resist erosion (Brooks et al., 2012). Factors such as permafrost and glacial characteristics are also contributing under Arctic conditions. Glaciers that abrade the bedrock can induce considerably higher erosive forces than flowing water. The active layer thickness is of high interest concerning sediment supply, as frozen sediments are more stable and harder to erode (Andersland et al., 2003; Instanes and Rongved, 2017).

2.5.1 Suspended sediment transport

Based on the Hjulstrøm curve (see *Figure 13*), fine particles (<63µm) will be transported even on low flow velocities and are typically kept in suspension in the water column (Hjulström, 1935). Suspended transport is caused by turbulent forces exceeding the gravity working on the grain (Brooks et al., 2012). In highly turbulent and powerful water, even fine sand can be transported in suspension (Kay, 2008). Threshold values for entrainment of fine-grained sediments can be relatively high due to cohesive forces (Brooks et al., 2012). Particularly when compared to the forces needed for transporting the grains once suspended. Suspended sediment can be transported over long distances, depending on the flow regime.

2.5.2 Bedload sediment transport

Courser sediments, e.g., sand, pebbles, and cobbles, are transported as bedload as the uplift from turbulent waters does not exceed the gravitational force on the grains. Bedload is characterized by rolling and saltation along the channel floor (Nichols, 2009). Larger grains will require more energy for initiation motion based on the Shield parameter and the Hjulström Curve. A pebble in motion can collide with other particles and thus increase the stress and further increase the bedload. Pitlick et al. (2008) discuss the effect of larger particles protecting the underlying fines in a channel, creating an armouring layer. Coarse sediment (>sand) can occur in imbrication patterns, increasing the anchoring effect leading to higher critical shear stress for entrainment.

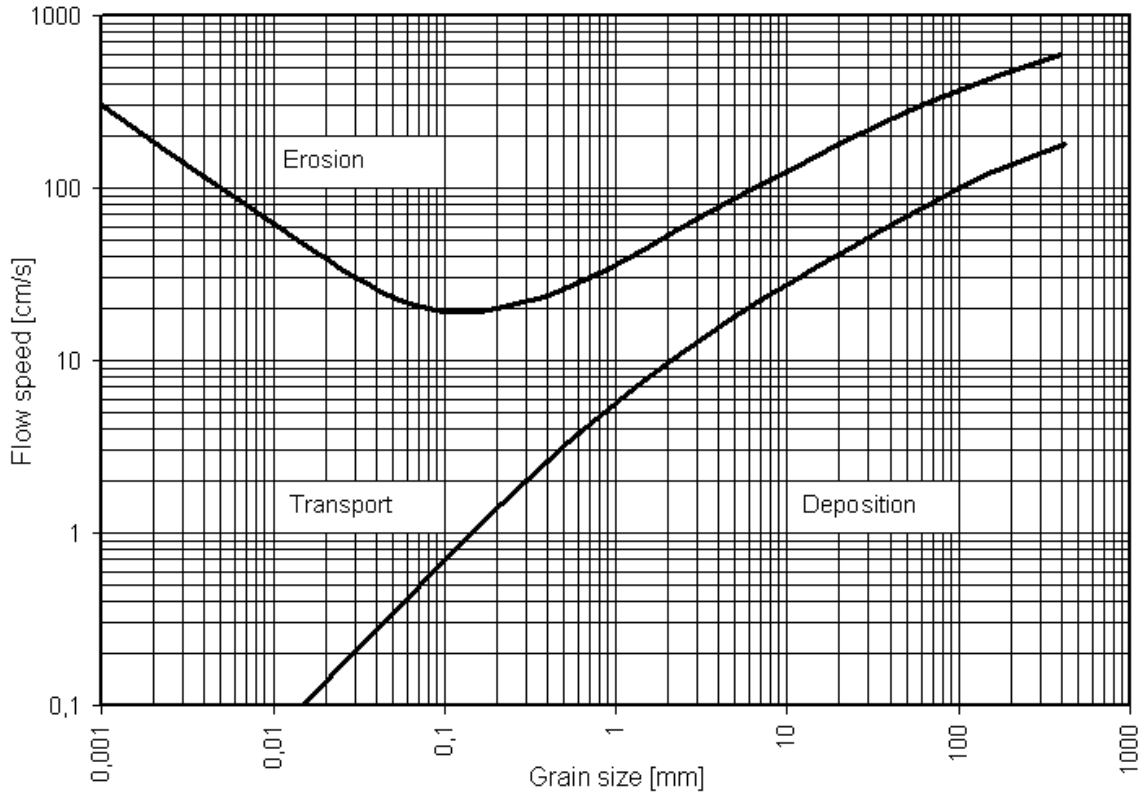

Figure 13: The Hjulstrøm Curve, logarithmic curve for illustrating the relation of water speed and erosion-transport-deposition regime in the fluvial channel with respect to the grain size (Hjulström, 1935).

2.6 Hydrological engineering and scour protection

Constructions and engineering in conjunction with waterways aim to protect infrastructure from potential hazards. Mitigation measures will minimize the effect of an event, whereas preventional measurements reduce the chance for a hazard to occur. The NVE has developed detailed guidelines for waterway constructions on mainland Norway, described in detail by Fergus et al. (2010). Building material is typically blasted or quarry rock, but due to the poor quality of the local lithology, granitic gneiss had to be shipped from mainland Norway (Bjordal and Hoseth, 2017). Alternative methods to blasted rock is to use gabions (Hoseth and Daae, 1996) or concrete blocks (Reid and Church, 2015). A gabion is a cube or a mat of wire net, holding rocks in place and can be used in the same ways as building bricks. A gabion does not require the same rock strength and size as riprap, and Sværd (1996) mentioned the opportunity to utilize local resources in gabions. Still, it was not recommended due to challenging maintenance.

2.6.1 Sedimentation dam

A sedimentation dam or pool aims to obstruct further bedload in the channel (Fergus et al., 2010). By constructing a dam and thereby decrease the energy of the water, bedload will start to accumulate. The capacity of the dam will inevitably decline, and maintenance (excavation) depends on the accumulation rate (Fergus et al., 2010). Maintenance is mentioned in the building plan by Bjordal and Hoseth (2017), although a detailed schedule is missing due to uncertain accumulation rates.

Based on the building plans from NVE (Bjordal and Hoseth, 2017), the sedimentation dam was built as follows (see *Figure 14* for illustration). The barrier is made up of a 2m high weir across the channel, with large boulders (100-150cm) facing upstream. Smaller boulders (50-100cm) were used for the apron downstream the crest. The apron aims to reduce the energy of the water flowing over the crest and thus avoid scouring holes. The large boulders allow water to percolate through while sufficiently decreased the energy to allowing bedload to settle. The levees directly upstream were reinforced and riprapped to avoid undercutting and collapse. The dam has an initial capacity of thirty thousand cubic meters of sediments.

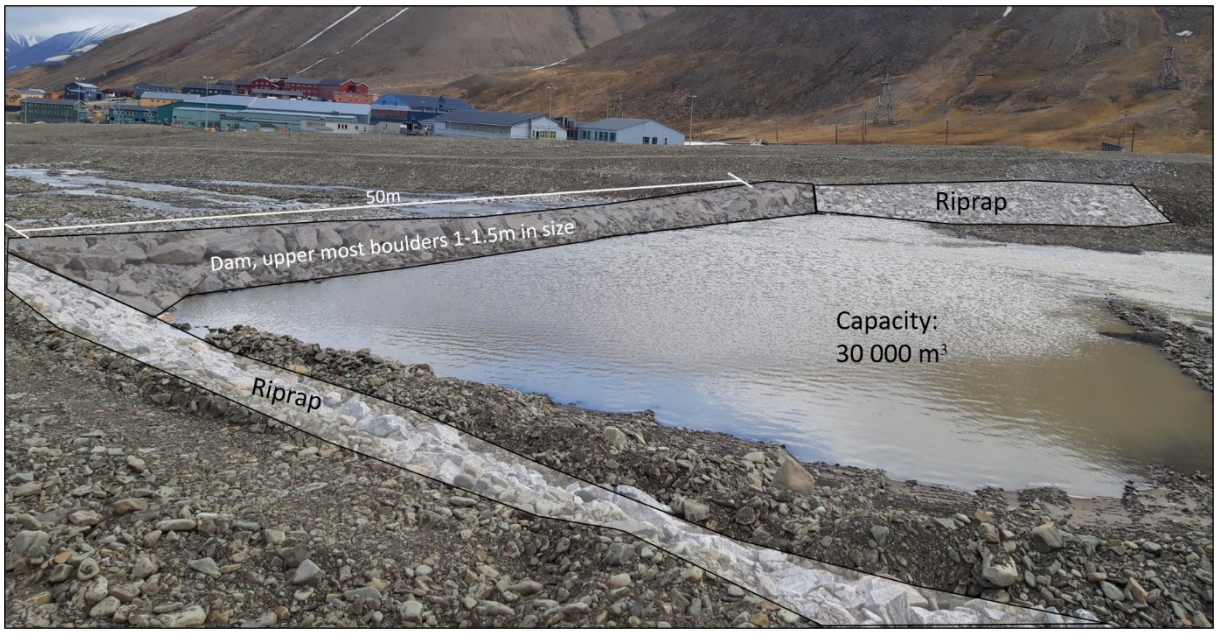

Figure 14: Annotated picture of the Sedimentation dam, riprap on both flanks to avoid undercutting. The dam consists of large boulders of blasted granitic gneiss, with an apron of smaller boulders downstream. The large boulders allow water to percolate through, while reducing the energy and allow bedload to settle.

2.6.2 Riprap

Riprap is defined by Fergus et al. (2010) as scour protection, based on large angular rocks (boulder size) placed in the river or on the levees as an armouring layer, resisting the erosive forces from the flowing water. Reid and Church (2015) state that riprap is frequently used to avoid scouring, stabilize, and prevent lateral migration in fluvial systems.

The riprap in Longyearelva was placed on the existing levees, on both sides of the channel from the sedimentation dam down to the hydrological station (see *Figure 15*). Fergus et al. (2010) emphasize that the riprap-rocks must be larger than the transport capacity of the river to avoid erosion. A 0.7m thick layer of angular granitic gneiss at a 1:2.5 inclination on the levees, down to a 1m depth relative to the channel floor to prevent undercutting (Bjordal and Hoseth, 2017), see *Figure 15*. The boulders must be positioned in a precise pattern to protect the underlying finer sediments to prevent flushing (Bjordal and Hoseth, 2017). The levees in Longyearelva are 2m high and constructed to withstand a bank-full stage of flooding with a 200-year return period. The criteria for bank-full capacity in Fergus et al. (2010) is thereby met.

2.6.3 Placement and construction of sills

The construction of riprapped levees constrains the river to a channelized flow. Shear stress on the channel bed will increase as the water depth increases because of decreasing channel width, given the parameters in the Shield parameter. The consequences can be increased erosion, bedload, and potentially channel degradation.

Fergus et al. (2010) suggest sills across the channel to decrease bedload and prevent channel degradation. A sill is a barrier built across the channel to avoid bedload and scouring on the channel floor by holding the channel bed in place. Sills can be assembled in a variety of geometries, straight across perpendicular to the flow direction or V-shaped facing both upstream and downstream. Placement should be in areas where increased erosion is expected, such as under bridges or other sections where the channel width is decreasing. The placement of each boulder is critical to ensure effective interlocking and to avoid scouring of the foundation.

The sills in Longyearelva were based on a 1m deep, 3m wide ditch, dug out straight across the channel, and filled with blasted granitic gneiss. The grain size used for construction to be 0mm<d<800mm, and d_{mean} 400mm. An excavator placed the larger blocks upstream in the ditch, with the sill crest in flush with the channel bed and connected with the riprapped levees, as illustrated in *Figure 15*.

Fergus et al. (2010) recommend avoiding building in frozen ground and at high discharge. The sills in Longyearelva were built in September-October over four years, and the discharge in September should be at a minimum. Still, the frozen ground is close to inevitable on Svalbard, and the construction work was conducted during the time of the year when the active layer is at a maximum and when refreezing normally starts.

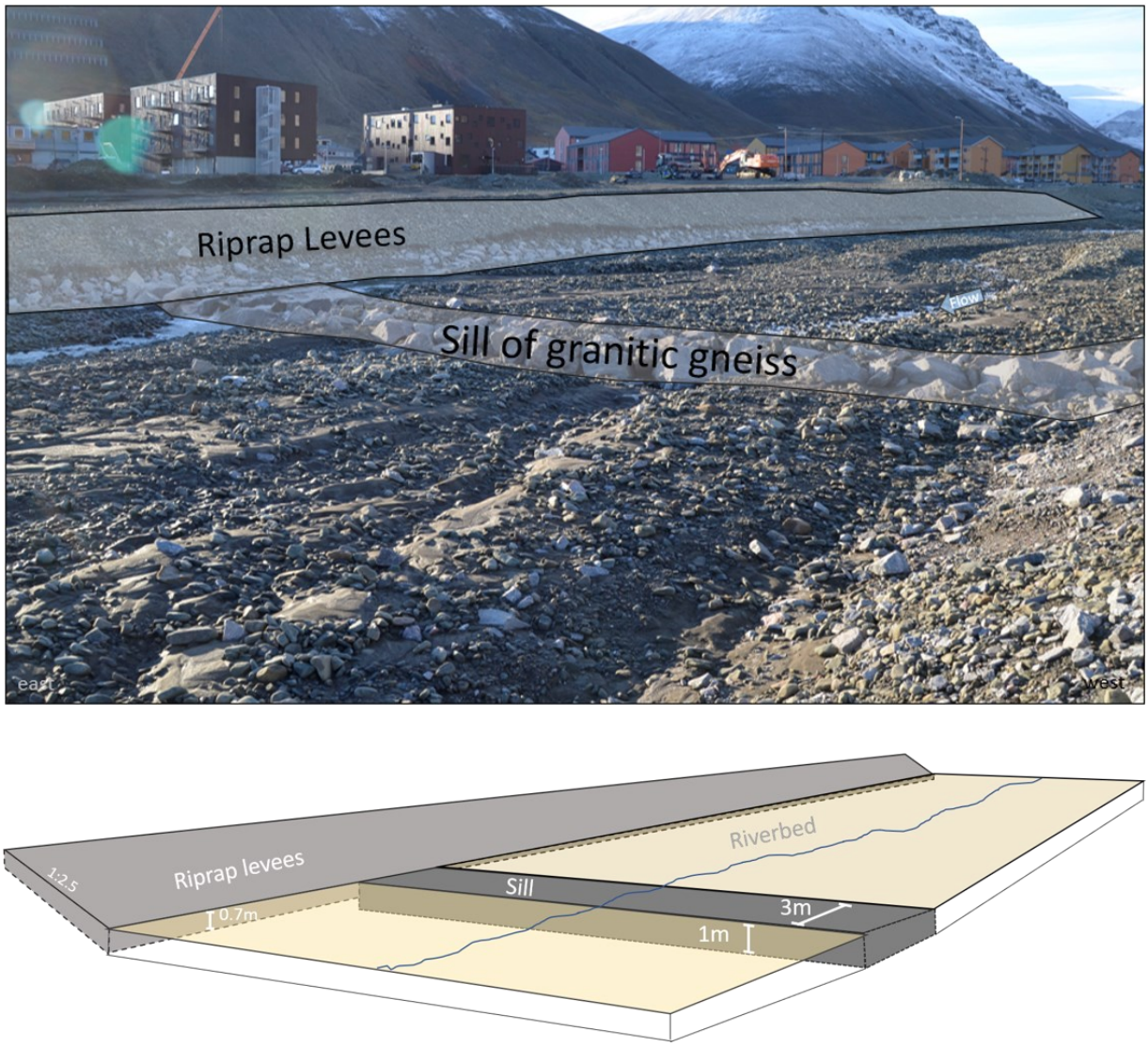

Figure 15: Annotated picture of a section of Longyearelva, illustrating riprap and one of many sills across the channel to prevent channel degradation. The sill is constructed of blaster granitic gneiss, placed in a 1m deep and 3m wide ditch, as shown in the schematic illustration. Tote that the riprapped levees are on both sides of the riverbed from the sedimentation dam to Veg 600.

3 Methodology

Fieldwork in Arctic conditions requires a special skill set and the ability to improvise. The combination of thorough planning, specific experience, and practical support from the Logistical Department at UNIS provided a background for executing fieldwork safely and effectively.

As this project intends to contribute to long-term monitoring, a description of the methods was given special attention. Specifications of monitoring installations and detailed descriptions fieldwork will make it easier for the successor to both compare data and potentially improve the processes.

Continuous water-stage measurements combined with point measuring of discharge enabled the computation of an hourly hydrograph. Bedload- and suspended sediment transport was monitored using passive tracers and water samples, respectively, and enabled quantification of the sediment yield in Longyearelva. Mapping geomorphology and fluvial sediments proved valuable for detecting sediment sources. An assessment of the scour- and flooding mitigation was done with remote sensing and field observations. During the fieldwork period, ideas for possible improvements of the techniques developed, which were both directly applied and beneficial for the successor.

3.1 Hydrological monitoring

A persistent problem with hydrological measurements in the Arctic is the rapidly changing condition and migrating channels. The polar hydrological monitoring program by NVE illustrates the difficulties (Sund, 2008). The method for obtaining discharge data used in this project relies on continuous water stage records, combined with point measurements of discharge to produce stage-discharge relation curves. This method has been used in multiple scientific campaigns on the archipelago (e.g., Grønsten, 1998; Etzelmüller et al., 2000; Bogen and Bønsnes, 2003; Hodgkins et al., 2003; Riger-Kusk, 2006).

3.1.1 Measuring water stage

A Cambell Scientific (CR800 CX10) data logger was utilized to obtain a continuous water stage dataset from June 11th to September 15th, see *Figure 16.* A Cambell pressure transducer was placed in the stream to measure water depth and wired to the data logger. Another sensor was floating in the main current measuring electric conductivity (EC) and temperature. Both sensors were connected to the data logger and secured. The logger was programmed to perform a reading every twenty seconds and store the hourly average. Regular maintenance was crucial to detect and solve potential problems that could cause data deterioration.

The ever-changing nature of channels through sandar obscures the stage-discharge relation. The NVE hydrological monitoring program illustrates ways to overcome the problem by utilizing sections where the stream flows through bedrock or stable sections (Sund, 2008). The monitoring station in Longyearelva was therefore placed on the stable, concrete pier beneath the bridge at Veg 600, see *Figure 16.*

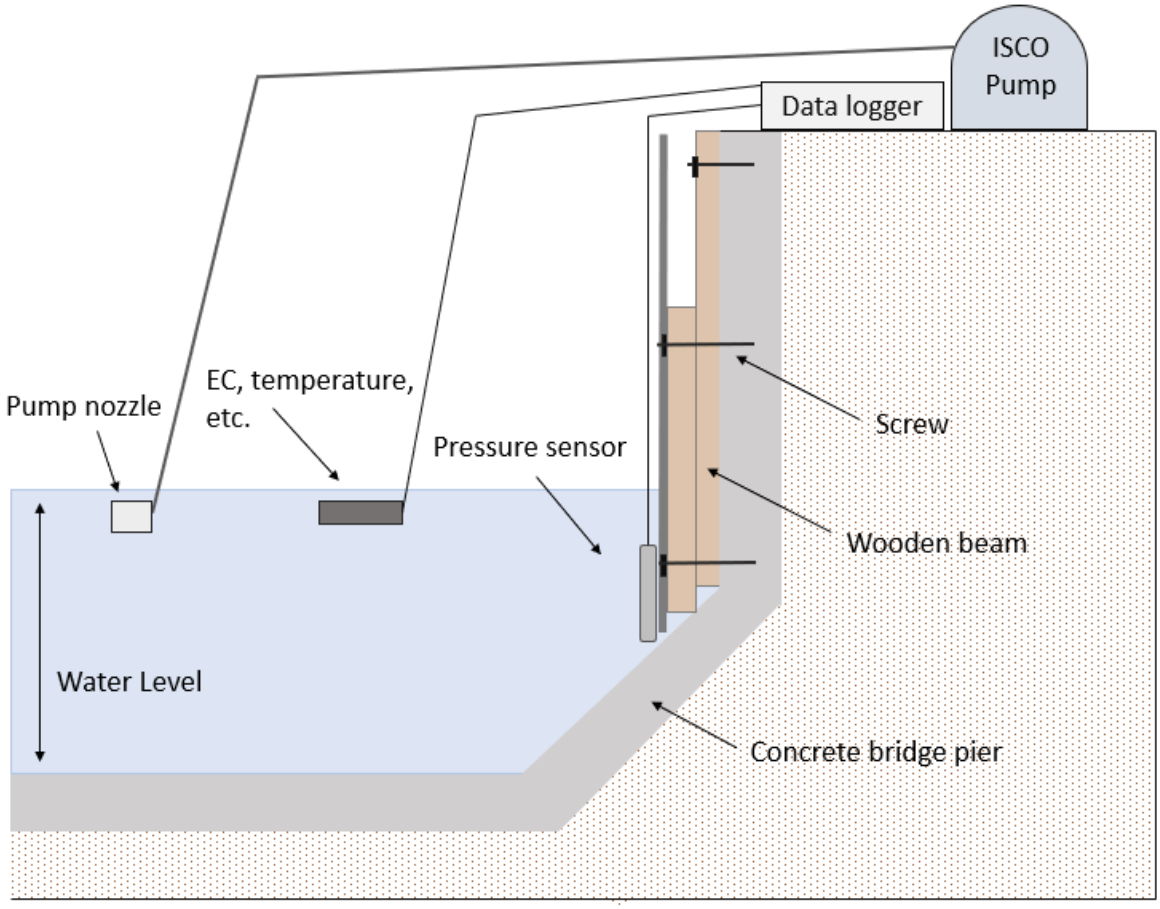

Figure 16: Schematic illustration of the hydrological station with a Cambell Scientific pressure transducer, a CR800 CX10 data logger and a Sigma 900 automatic water sampler (ISCO pump).

3.1.2 Discharge measurements

Point measurements of discharge (Q) were computed with *Equation 4,* based on the salt dilution method (SDM) with slug injection according to Moore (2005). Moore (2005) further describes the technique as highly suitable in changing conditions as it requires minimal equipment and is relatively accurate, according to Day (1976).

Equation 4

$$Q = \frac{kM}{(T_2 - T_1)(\overline{EC} - EC_b)}$$

Q being discharge measured in m^3/s. M refers to the mass of diluted salt, T_1 is the time at first observed increase in background electrical conductivity, EC_b. T_2 is the time when the electrical conductivity has returned to the EC_b. $\overline{EC}$ being the average electrical conductivity during T_1-T_2. The constant, k, was calibrated by measuring known concentrations of diluted salt at the same water temperature as the river.

A known amount of regular coarse-grained salt was diluted in a 15liter bucket with water from the river and injected into the main current with one swift motion. Downstream in the same, confined channel, an operator makes readings of the EC (µS/cm) in the stream with an EC-meter. Once the 'cloud' of diluted salt passes by, the EC in the river increases, and the operator notes the concentration at a given time interval (5 sec). The operator recorded the EC-meter and plotted the data directly from the video and calculated discharge in the lab, see *Figure 17*.

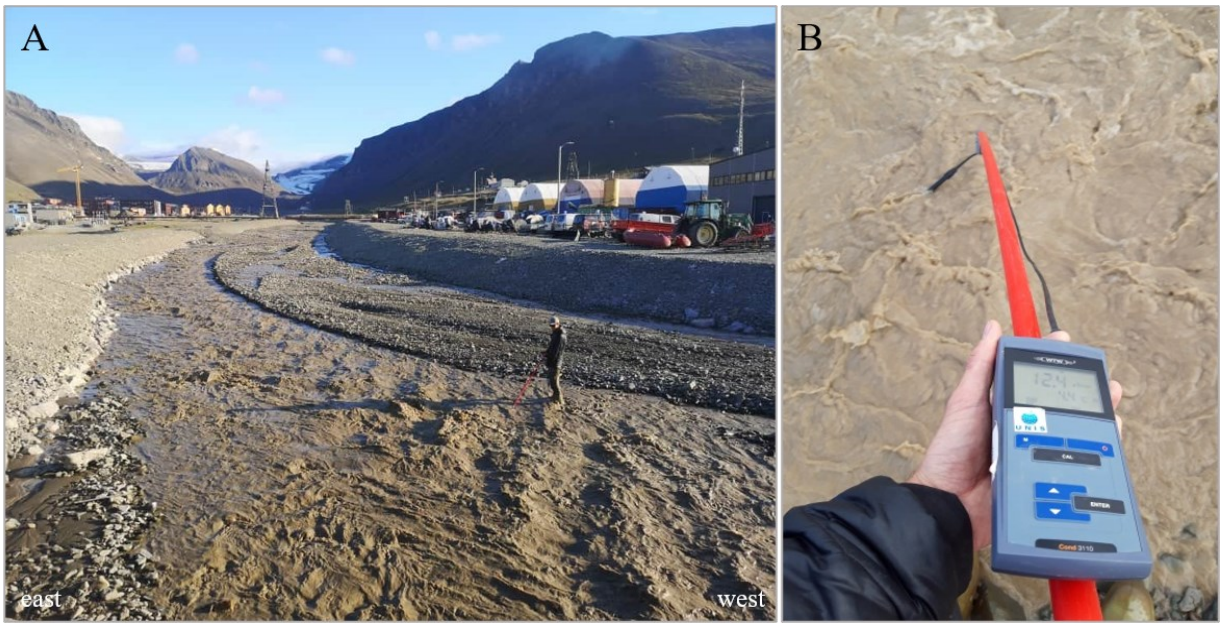

Figure 17: Measuring discharge. **A**) The writer recording electrical conductivity (EC) in the river after a slug injection of diluted salt. **B)** To avoid the EC-meter from flapping and catching air in turbulent water, it was attached to a plastic rod and securely submerged.

3.1.3 Stage-discharge rating curve

The discharges recorded with the SDM were be plotted against the water level at the specific time of the measurement. The discharge-water stage plots established a linear stage-discharge rating curve similar to the methodology in Stott and Mount (2007). Despite the location at the stable concrete bridge pier, changes to the channel geometry occurred, and the pressure sensor had to be adjusted. The water stage was plotted in different segments based on how the pressure sensor was adjusted, thus overcoming the inconsistency problem. Each plotted segment with corresponding levels and discharge values produced a standard linear equation, see *Equation 5* (Stott and Mount, 2007).

Equation 5

$$Q = aL + b$$

Where discharge, Q, can be calculated from the variable L, water stage, and the constants *a* and *b* retrieved from the equation based on the plotted data.

3.2 Suspended sediment transport monitoring

Suspended sediment yield (SSY) from a catchment can be calculated based on the suspended sediment concentration (SSC) in combination with the corresponding discharge at the time (Bogen and Bønsnes, 2003). The method is widely used within the field of Arctic hydrology and glaciology on Svalbard (e.g., Hodson et al., 1997; Hodson et al., 1998; Hodson and Ferguson, 1999; Etzelmüller et al., 2000; Bogen and Bønsnes, 2003; Hodgkins et al., 2003).

3.2.1 Suspended sediment sampling

Østrem (1975) describes manually sampling by submerging bottles in the channel, but typically an automatic sampling pump, ISCO-pump, is used (Bogen and Bønsnes, 2003; Sund, 2008). The manually sampling may be the optimal solution in remote field areas, as in the case of Hodgkins et al. (2003). Easy access to the field area in Longyeardalen made an automatic sampling pump the obvious choice for this project. A Sigma 900 automatic water sampler (ISCO pump) running on a 12V battery was placed by the bridge pier at Veg600, see *Figure 16* and *Figure 1.*

The ISCO-pump is based on a hose running from the ISCO-pump to the stream for collecting water samples and a controller for programming sampling parameters. The pump will firstly flush the hose to remove any remaining sediments, before collecting a sample (500ml in this case) and store it in one of the 24 sampling bottles inside the canister. Comparable studies have used sampling volumes between 750ml (Sund, 2008) and 3-400ml (Hodson and Ferguson, 1999). Since the SSC is determined gravimetrically, minor changes in the volume can be neglected as long as the sample is representative of the stream. In high turbulent waters, the suspended sediment is expected to be distributed throughout the water coulomb (Hjulström, 1939; Østrem, 1975).

The sampling frequency is inconsistent between previous studies; for instance, Hodson and Ferguson (1999) sampling every two-three hours, whereas Hodgkins et al. (2003) sampled every seventh hour with an ISCO-pump and every 20-103 hours manually. Bogen and Bønsnes (2003) state that 2-4 samples a day would provide a sufficient dataset to compute a linear interpolation and thus achieve an hourly SSC and cover the daily variation. The sampling frequency for this project was set to four samples a day, and the ISCO pump was programmed to sample every 360 minutes. Samples were stored bottles in the ISCO-pump canister, replaced with empty bottles every five-six days, and taken back to the lab for analyses, see *Figure 18* for a summary of the workflow. Sampling frequency was lowered to twice a day (720 minutes) from August 6th due to resource limitations and upstream construction work from August 4th. The timing for water sampling was based on Bogen and Bønsnes (2003) and aimed to capture the diurnal fluctuations, as discharge and SSC were thought to be at a maximum in the late afternoon and minimum in the early morning.

3.2.2 Suspended sediment concentration

SSC was determined according to the gravimetrical method described in Bogen and Bønsnes (2003). All samples were filtered through pre-weighed Whatman GF/F 47mm filters with a retention size of 0.7µm using an electric underpressure pump. During the most intense sediment transport, two or three filters had to be used as the relative retention size rapidly decreasing as sediment clogged the filters. Accurate volumetric measurements were made of each sample after filtration using a measuring cylinder. Filters from a given sample were placed in a small pre-weighed aluminium container and labelled. Bogen and Bønsnes (2003) recommend that all samples should be dried at 500ºC for two hours to eliminate all moisture and organic material. SSC was calculated after re-weighing the containers one dried. Hourly SSC data from June 12th until August 31st were further computed based on linear interpolation. SSY was computed by extracting corresponding discharge and SSC values. The workflow is summarized in *Figure 18*.

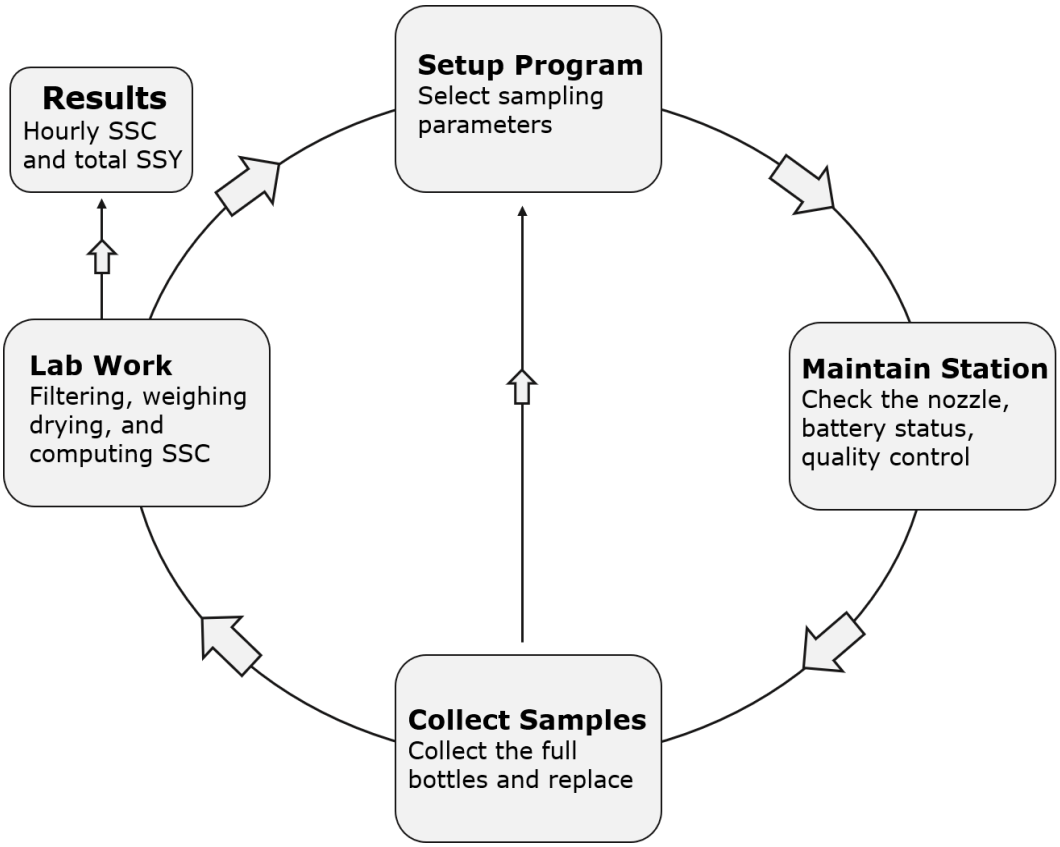

Figure 18: Workflow for collecting and calculation of suspended sediment concentration (SSC) and suspended sediment yield (SSY) in Longyearelva.

3.3 Bedload monitoring

The nature of glaciofluvial braided rivers in the Arctic makes bedload measurements challenging, and different research methods have been utilized. Sediment traps like the one used in Bellsund by Kociuba (2014) require daily maintenance - challenging in unstable Arctic conditions. A more manageable and less resource-demanding method is to use coloured passive tracers; a variety of passive tracers have been used on mainland Norway for bedload investigations (Møen et al., 2010; Engvik, 2011). The chosen method for qualitative measurements of bedload in Longyearelva is painted passive tracers due to its simplicity and low cost.

3.3.1 Coloured passive tracers

The coloured passive tracer method is described by, e.g. Laronne and Carson (1976). It relies on painted sediment (typically pebble, cobble, and boulder size) positioned at the riverbed for bedload monitoring. The researcher tries to detect the coloured tracers after a flooding event or a given period, thereby estimate bedload and transport capacity when combined with discharge data. Laronne and Carson (1976) further discuss the relationship between the tracer size and retrieve rate as large tracers are more easily retrieved. The chosen grain size for this project aimed to represent the natural grain size distribution in the Longyearelva system. Class 1 is numerous as the smaller tracers are harder to retrieve, and tracers <50mm were excluded as they were considered unretrievable. Rocks with a rounded, spherical shape were chosen, as they were anticipated to represent the particles easiest to be transported and reflected the specific fluvial sediments. 135 rocks were collected and measured according to sampling methods described in Bunte and Abt (2001).

The chosen tracers represent pebbles, cobbles, and small boulders, divided into four classes as presented in *Table 1*.

Table 1: Classes and characteristics of rocks that were used as passive tracers for monitoring bedload in Longyearelva.

Class	Size, mm	Number of tracers	Average weight
1-smal	50	45	160g
2-medium	100	30	537g
3-large	150	30	2.2kg
4-extra large	200-250	30	6.1kg

All tracers were washed, weighted, painted red, and labelled with a unique number. A water-based paint was chosen to minimize the environmental impact, based on the criteria used by The Norwegian Trekking Association for marking hiking trails (DNT, 2019).

The tracers were grouped and placed into three sections along the river, fifteen from Class 1 and 10 from the remaining classes, in total forty-five tracers in each section. The different starting positions were named: Huset (Hu-pt), Hallen (Ha-pt), and Polarriggen (Pr-pt), see *Figure 19*.

Figure 19: Initial starting position for the colored passive tracers (pt) for bedload measurements in Longyearelva. Huset-pt (Hu-pt), Hallen-pt (Ha-pt), and Polarriggen-pt (Pr-pt).

Hu-pt is located upstream of the sedimentation dam, thus outside the part of the river with permanent flooding mitigation. This section would be closer to the natural, braided river system, although bulldozers have reworked it regularly (Bjordal and Hoseth, 2017). The Ha-pt starting position was chosen because of an increased inclination of the channel between the sedimentation dam and Veg 501. This section holds the most recent constructions of flooding mitigation, see *Figure 9*. The third starting position (Pr-pt) is located closer to the outlet into Adventfjorden and situated where the construction of the flooding mitigation started in 2016 (*Figure 9*).

The schematic illustration in *Figure 20* shows how the passive tracers were placed in the river channel. Ten tracers from Class 4 put in a line across the channel, ten tracers from Class 3 in a new line, two-three meters upstream, and so on. The same principle was applied at all three starting positions.

The tracers were placed in the river channel on June 17^{th,} 2020, and monitored during the whole fieldwork period until September 15th. The thalweg migrating laterally within the channel occasionally exposed tracers, and regular inspections along the river channel made it possible to document transport during the monitoring period, not only at the end. Drone

orthophotos on three different occasions contributed to the transport data throughout the monitoring period. The red paint provided a good contrast to the grey gravel-bed, although conditions with high suspended sediment concentrations made it challenging to locate tracers once submerged.

A thorough examination of the riverbed was initiated towards the end of the monitoring period at minimal discharge (September 15th). In addition, a drone flight on the 11th of September provided high-resolution orthophotos for both mapping and locating tracers.

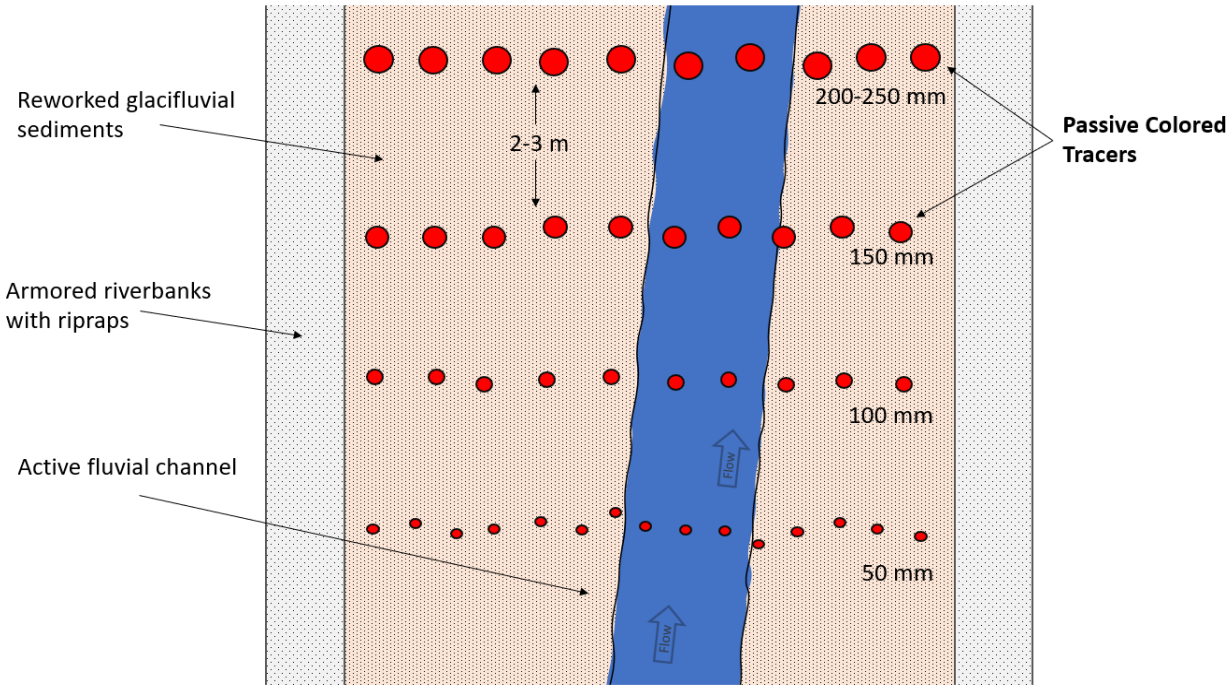

Figure 20: Schematic illustrations of placement of colored passive tracers in the fluvial channel.

3.4 Field observations and geomorphological changes

Part of the fieldwork was to map geomorphological changes with a relatively high temporal resolution, thus discuss fluvial erosion and the adequacy of the flooding mitigation. A combination of visual observations and remote sensing was used to cover the glaciofluvial system and hydrological engineering. Some locations of high interest, such as the sedimentation dam, sills, and the moraines, were photographed from fixed points at least twice a week. Hydrological- and weather conditions were noted in addition to the photographs.

3.4.1 Remote-sensing

Remote-sensing provides the opportunity to access areas or outcrops otherwise inaccessible and acquire data without being physically present (Rød, 2015). The combination of geographic information systems (GIS) and terrain models makes remote sensing and terrain analysis highly effective (Longley et al., 2015; Rød, 2015). Drones have revolutionized the remote-sensing methodology as they are becoming more available and user-friendly (Carrivick et al., 2013).

3.4.2 Drone survey and photogrammetry

Photogrammetry is the technic to obtain three-dimensional information based on feature recognition from two or several pictures (Rød, 2015). Structure-from-motion (SfM) is a method relying on photogrammetry to create three-dimensional models of a landscape. Algorithms detect and recognize features from overlapping images retrieved from a drone (or a hand-held camera) and generate a point cloud where each point has a position in a three-dimensional coordinate system (Carrivick et al., 2013). Georeferencing the model can be done through ground-control points (GCP) or with the internal GPS in the drone as in this project. Both Westoby et al. (2012) and Cook (2017) underlines how the usage of drones and photogrammetry with SfM is an effective branch of remote sensing. Westoby et al. (2012) further describe the accuracy to be within ±0.5m of a traditionally terrestrial laser scanner – which is more expensive and resource-demanding. Cook (2017) also describes the usage of drones and photogrammetry as an appropriate method for mapping changes in a fluvial system within the scale of Longyeardalen valley.

A DJI Mavic 2 Pro drone with a Smart Controller was utilized to get a bird-view perspective. The drone acquired high-resolution images covering an area of interest for further SfM and analysis. The drone was additionally used to obtain overview images from different views of the whole field area.

Three flights were conducted during the campaign, early July, early August, and middle of September. The former was implemented by a third-party company on behalf of the NVE, accompanied by the writer. The two latter were carried out by the thesis writer following the method described in *Figure 21*. A camera, attached to a drone or not, relies on the reflected light from an object (Rød, 2015). The weather, surface roughness, relief, and lighting conditions during the flight will thus be important for the final result (Westoby et al., 2012). Drone flights were thus conducted during calm and overcast weather conditions. The proximity to the airport and infrastructure required a close dialogue with the airport control tower and the Logistics Department on UNIS to ensure safe flights.

The Pix4d Capture software allows preprogrammed flight plans to be uploaded to the drone before takeoff (see *Figure 21*). The software automatically operates the drone and photographs the designated mapping area based on the pre-set parameters. Flight height was set to 70m, a compromise between ground pixel resolution and flight time. The fluvial channel from Veg106 to the outlet in Adventfjorden could be covered within two hours, divided into five missions with approximately one battery per mission and one thousand photos. Safety regulation required a pilot (the writer) on stand-by, always observing the drone - ready to take manual control over the drone if needed.

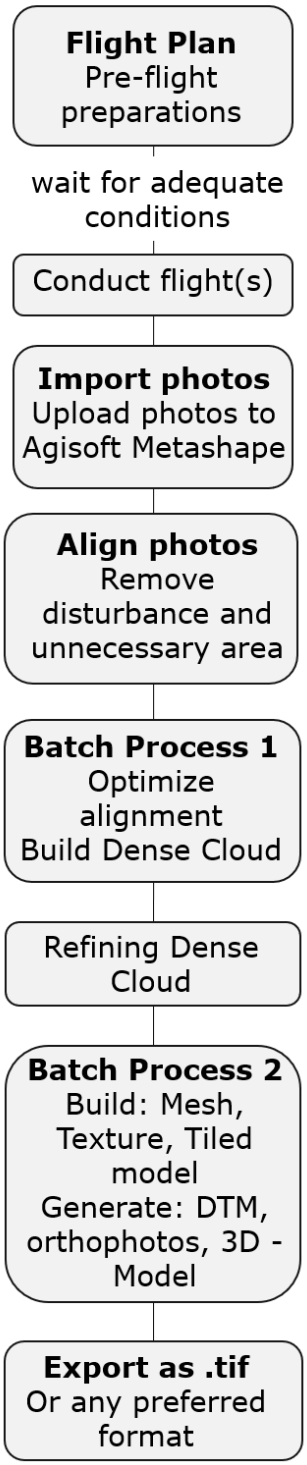

Figure 21: Simplified workflow for drone flights and postprocessing. Digital Terrain Model (DTM)

The AgiSoft Metashape Professional software was used in the post-processing for producing digital terrain models (DTM) and orthophotos. Spending some time removing unnecessary features from the point cloud decreased the processing time in the following steps, illustrated in *Figure 21.* After some initial editing, a series of operations were initiated using the batch module with pre-determined parameters. Running the whole model in medium quality took about 20 hours, including importing pictures and editing the first point cloud.

The Mavic 2 Pro uses the internal GPS to store the position for each picture, thus allowing directly georeferencing. Once imported to AgiSoft Metashape Professional, the models can be automatically georeferenced and exported as a .tif-file. The above allows the models to be imported into a GIS, ArcGIS Pro in this case and further analyzed.

3.4.3 Geomorphological mapping

A combination of field observations and remote sensing was utilized to map morphological changes in the Longyearelva fluvial system, similar to the methodology used by Kociuba et al. (2019). The geomorphological mapping was based on a combination of the DTM and orthophotos from the SfM, and DEM from the Norwegian Polar Institute (NPI). The DTM could be processed into a hillshade, aspect analysis, or hydrological gradient to characterise the system better. The Longyearelva catchment was calculated and illustrated using appropriate toolboxes in ArcGIS Pro and a 5x5m digital elevation model (DEM) over Nordenskjöld Land.

3.5 Challenges and adaptations

Continuous field observations and a good maintenance plan proved essential, although no major problems arose. Minor challenges were detected and solved right away, which ensured a representative dataset. Improvements and recommendations for further research are presented in *5.7 Suggested improvement.*

Discharge measurements with the SDM became challenging during high flows, such as on July 27th. Fast-flowing waters and unstable riverbanks made it challenging to place the EC-probe directly in the main current without risking being swept away. Attaching the sensor at the end of a rod allowed the operator to acquire good EC-reading even during demanding conditions. Using a phone to record the EC-meter while wading in the river made the process easier and more accurate than taking notes manually.

SSC samples from June 17th are missing due to a power shortage to the ISCO-pump. However, field notes indicate low discharge and SSC at the time, and the daily maintenance plan intercepted the problem so the battery could be replaced. Sven samples from July 21st to 23rd are missing due to human error. Once the stored samples were collected on the 21st, the program was not restarted, as it was mistakenly believed that the ISCO-pump would continue the program from sampling bottle 24 to 1. Field notes show low SSC at the time, and the mistake was immediate corrected once detected early on July 23rd.

During high water levels and discharge, the nozzle on the water-sampling tube was bouncing on the water surface. Different placements and weights attached to the nozzle were tested on June 24th. The solution was to adjust the placement and weight according to the fluctuating discharge for the rest of the monitoring period, keeping the nozzle submerged without reaching the bottom and possibly collecting bedload sediments. Controlling the nozzle, removing potentially jammed sediments, and adjusting the weight secured sufficient data.

The pressure sensor for water-stage measurements was buried in sediments during high flows and massive bedload on July 29th. The sensor was quickly retrieved and tested for potential damage before it was placed back in the river, a few centimetres higher. The new position required another discharge measurement for recalibrating the water-stage discharge correlation.

Laronne and Carson (1976) indicate potential drawbacks regarding the use of passive tracers, such as tracers can be hard to locate after an event or season, and precise quantitative data can thus be hard to achieve. Continuous observations of tracers during this fieldwork provided some data on bedload transport during the season, even though the tracers in question may be buried or washed away at the end.

The sampling frequency for SSC had to be adjusted over the monitoring period due to construction work in the river and resource considerations. From June 12th to June 17th, the ISCO-pump was programmed to sample at a four-hour interval, starting at midnight. Six samples a day proved too ambitious, considering the resources spent on post-processing. From June 18th to July 23rd, the sampling frequency was six hours, starting at 4:00 am. From July 24th, the frequency was changed to 8 hours, starting at midnight. Due to construction work next to Nybyen from August 5th, the frequency was changed to twice a day (6:00 am and 6:00 pm). Sampling intervals were still within the recommendations in Bogen and Bønsnes (2003), and the results are, therefore, believed to be representative.

4 Results

The following data was acquired over the monitoring period June 5th to September 15th. Key findings regarding the quantification of discharge and sediment transport are presented in *Table 2* and are further described in the following subsections. The fieldwork also resulted in field notes, thousands of images (both drone and hand-held camera), DTMs, water temperature, and electrical conductivity (EC) were acquired over the monitoring period, in addition to the quantitative results. The findings assessing the scour- and flooding mitigation are presented in Chapter 4.5, and ideas for a successful long-term program are presented in Chapter 4.6.

Table 2: Summary of key findings for quantification of discharge and sediment transport.

	Occurrence	***Quantity***
Mean discharge	11.06-15.09	1.5m^3/s
Highest discharge	28.07, time 04:00 pm	8.6m^3/s
Suspended Sediment Concentration (SSC)	25.07, 04:00 pm	24.1g/l max 1.9g/l average
Highest Suspended Sediment Yield (SSY)	25.07	252t/day/km^2 5594t
Total SSY	12.06-31.08	41 050t, 1866t/km^2/yr
Bedload	17.06-15.09	3.8% of the Passive Tracers were retrieved, documenting transport of all four classes
Longest transport distance as bedload	17.06-15.09	Class 3, 175m from Polarriggen starting position

2020 can be described as a relatively cold and dry year based on summarized weather data from Svalbard Airport meteorological station (MET, 2021), even though record-breaking air temperatures (max 21.7ºC) were recorded in late July. Precipitation in 2020 was 31% lower than the thirty-year average and 38% lower than the last five-year average. 2020 was 13% warmer than the thirty-year average, however 35% colder than the five-year average considering air temperature. Numbers are displayed in *Table 3* below.

Table 3: Weather- and climate data from Svalbard Airport meteorological station (MET, 2021) for comparing the conditions in 2020 with the 5-year and 30-year average.

	1991-2020	***2016-2020***	***2020***
Precipitation [mm]	202	223	139
Temperature [ºC]	-3.9	-2.2	-3.4

4.1 Hydrology

The hydrograph in *Figure 22* illustrates the daily mean discharge ($Q_{dailymean}$) in Longyearelva during the monitoring period and meteorological conditions (MET, 2021) from June 11th to September 15th. The average hourly discharge in Longyearelva during the 2020 monitoring period was 1.5m^3/s, and discharge exceeded the average for 998 hours or 43% of the monitoring period based on a duration curve. The hourly hydrograph displayed in *Figure 23* illustrates diurnal fluctuations in discharge that seem to correspond with air temperature changes throughout the monitoring period. Discharge remains stable at 0.5m^3/s during 14th-18th of June, with air temperatures around 1-2ºC and 7.6mm of precipitation. The air temperature increased from June 19th to June 24th, which correlates with the first increase in discharge. The discharge decreased and remained relatively stable at 0.7m^3/s on June 25th – 29th, before a new rise occurred early in July. The discharge remained stable with diurnal fluctuation between 1-3m^3/s until late July.

A heatwave caused record-high air temperatures at the end of July (24th- 30th), which correlates with a considerable peak in the hydrograph, hereafter named the Late July Flooding. A new temperature record (21.7ºC) on the afternoon of July 25th corresponds with a discharge of 6.2m^3/s. However, peak hourly discharge, 8.6m^3/s, was recorded at 4:00 pm on July 28th, see *Figure 23* and *Figure 24B-C.* The discharge dropped to 0.8 m^3/s at 2:00 am on July 31st, as the temperature gradually decreases to less than 10ºC. Diurnal fluctuations were especially noticeable over several days in August, as the discharge shifted between 3.5m^3/s and 0.5m^3/s for the day- and nighttime, respectively. Discharge and temperature continued to gradually decrease throughout August.

The discharge remained stable around 0.2m^3/s from August 25th and reached a minimum (0.05m^3/s) on September 2nd. Daytime temperature in the same period was 3-4ºC and close to 0ºC at nighttime. Precipitation (9.8mm) as snow on August 30th did not yield any increase in discharge, see *Figure 24D*. However, a precipitation event started on September 3rd and peaked on September 5th with 8.7mm combined with increased air temperature (10.5ºC). This event correlates with increasing discharge (*Figure 23)* and a distinct drop in EC*.* Discharge peaked at 2.7m^3/s on September 4th, before gradually decreasing to <0.5m^3/s. Another rise in temperature on September 10th did not produce a significant discharge increase.

The hypsographic curve presented in *Figure 25* illustrates the elevation distribution in the Longyearelva catchment. Approximately 40% of the area are under 450m.a.s.l (the height of the flat plateaus mountains) and 45% of the area is between 450-650m.a.s.l.. The remaining 15% are the most elevated areas, 650-1050m.a.s.l.

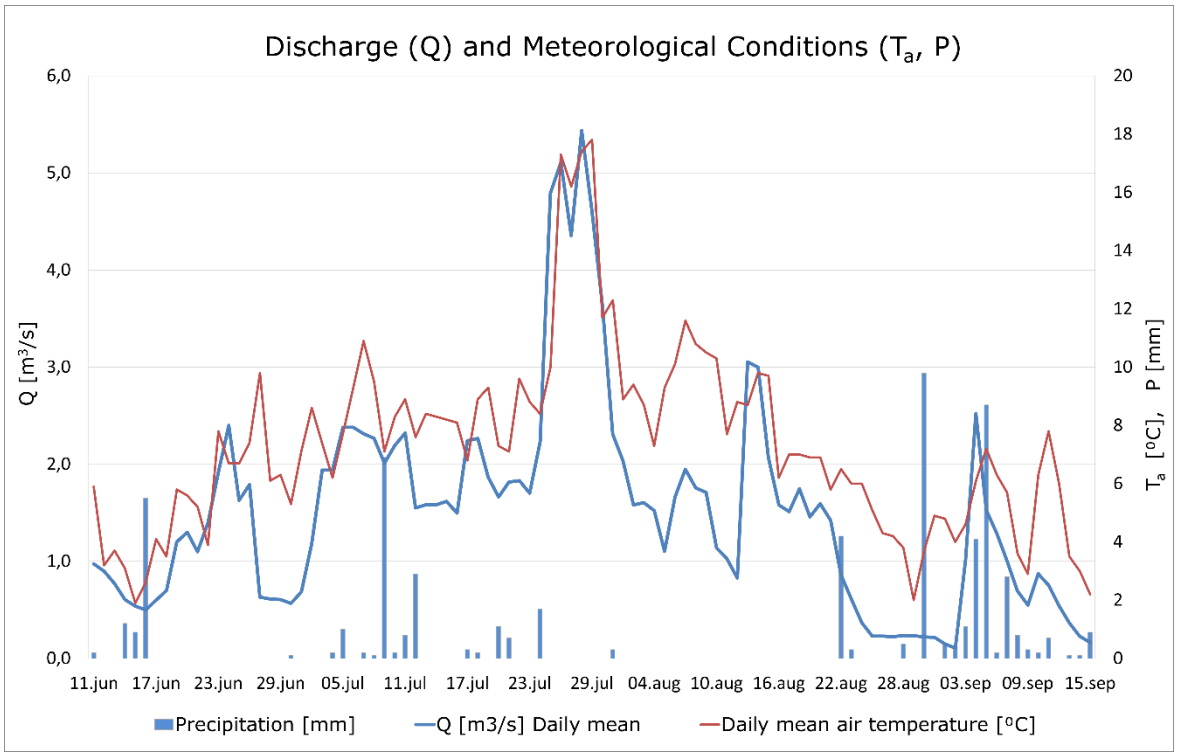

Figure 22: Daily average hydrograph from June 11th to September 15th. Daily mean air temperature and precipitation from Svalbard Airport meteorological station (MET, 2021).

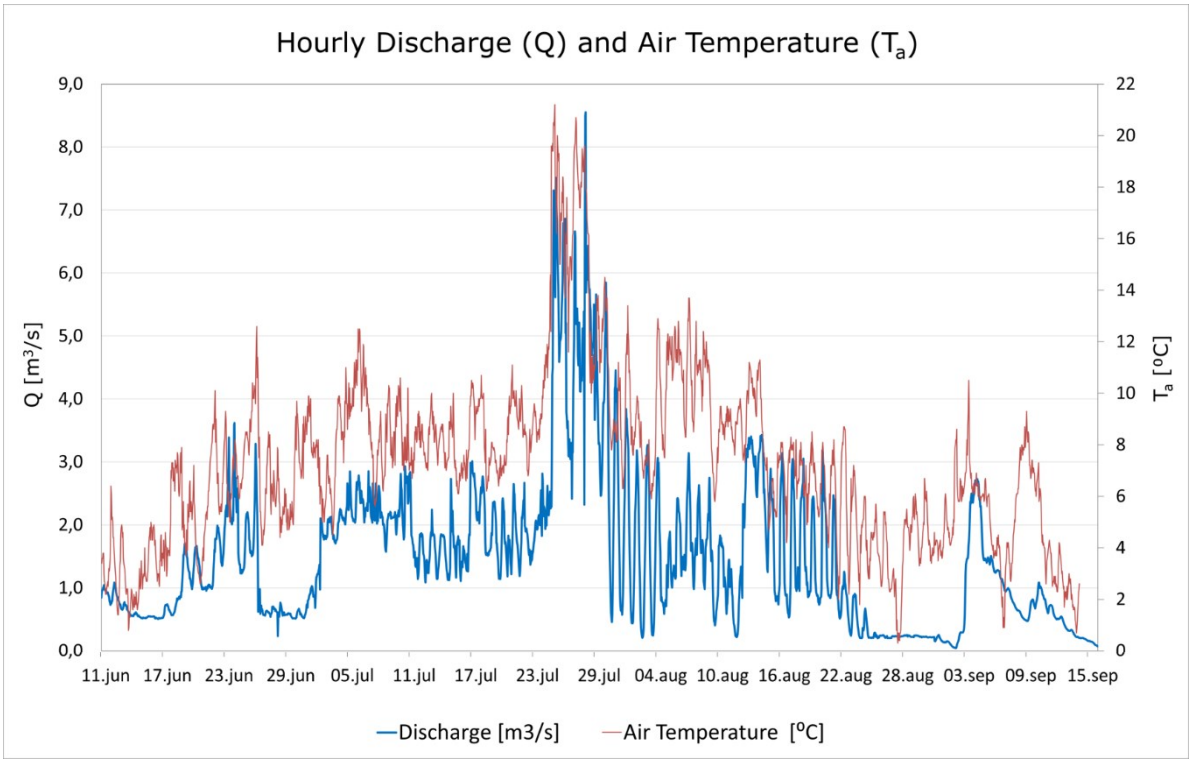

Figure 23: Hydrograph from the monitoring period, June 11th to September 15th. Hourly resolution displays the diurnal fluctuations throughout the summer, particularly in mid-July and August. Hourly air temperature data from Svalbard Airport meteorological station (MET, 2021).

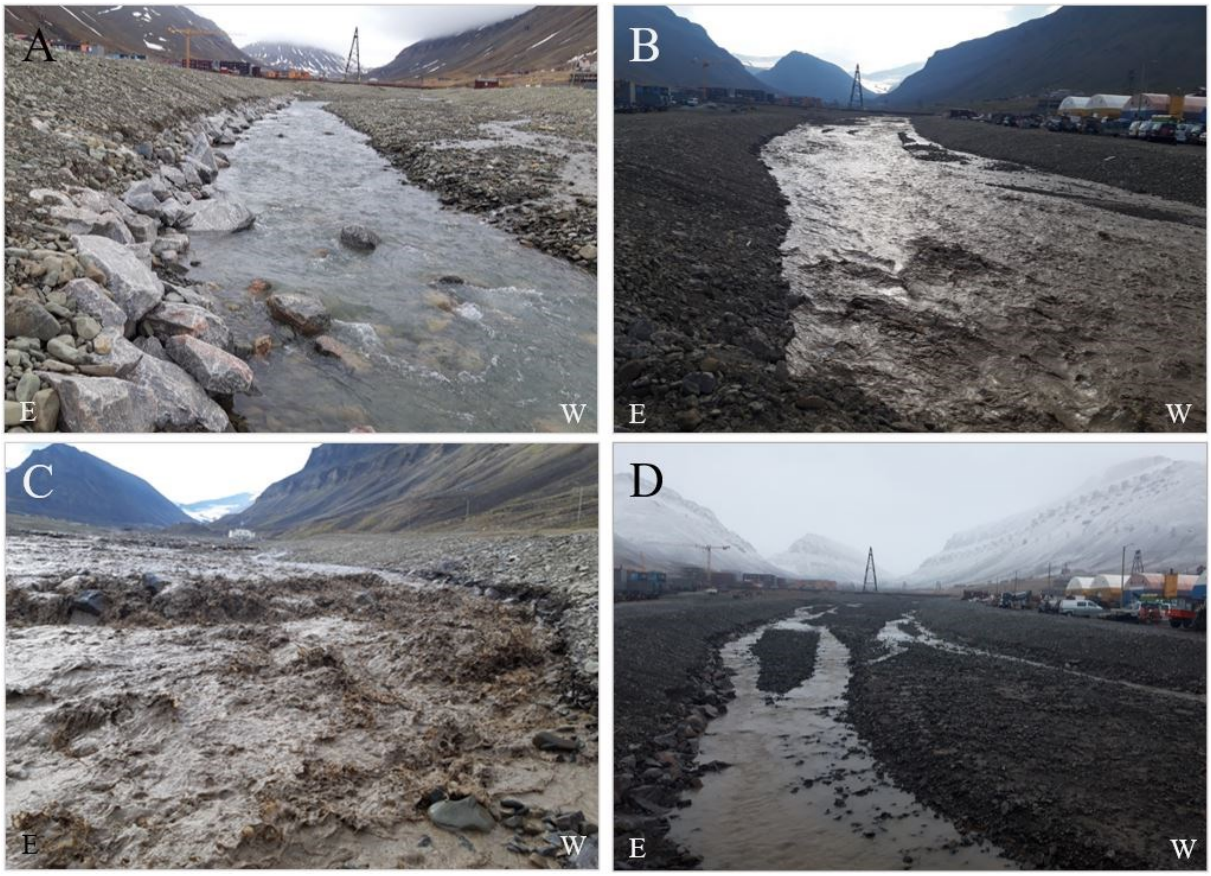

Figure 24: Photo A, B and D are from directly upstream Veg 600. **A**) Low discharge and Suspended Sediment Concentration June 5th. **B)** July 28th, the highest discharge recorded at 8.6m^3/s during record high temperatures. **C)** July 28th, the highest discharge recorded 8.6m^3/s flowing over the western side of Sill 6**. D)** First snowfall on August 28th, snowline roughly at Skjeringa 50m.a.s.l, low discharge at <0.5m^3/s.

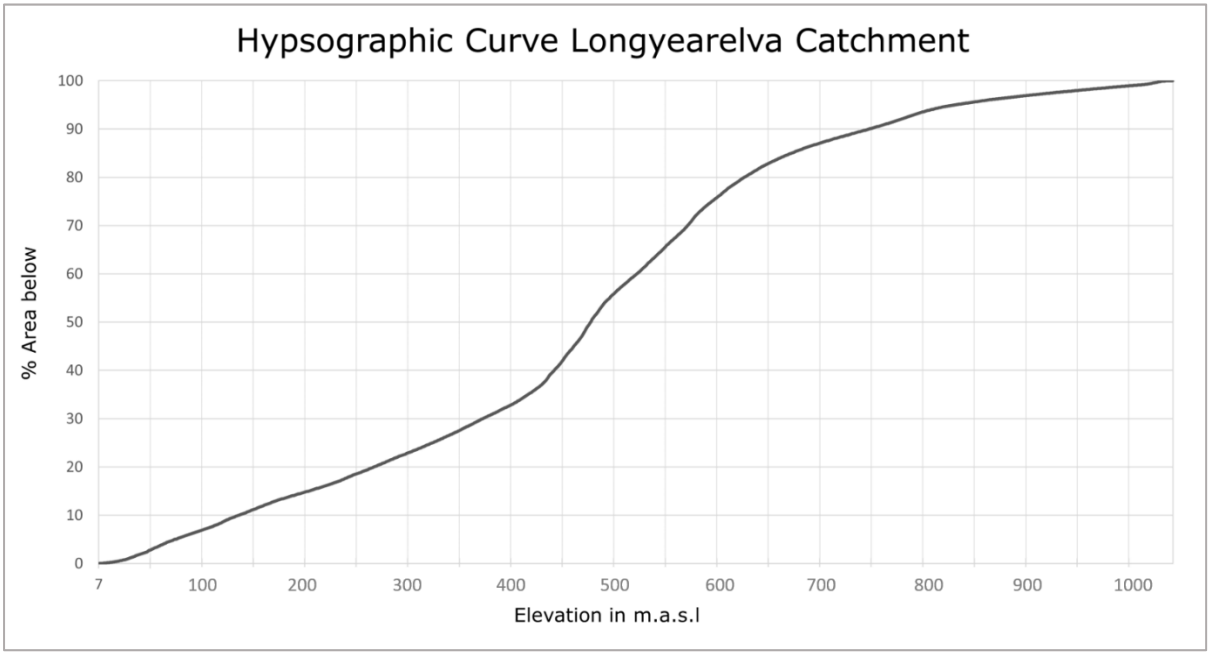

Figure 25: Hypsographic curve of the Longyearelva catchment, illustrating the area distribution with respect to the elevation throughout the catchment. Highest point 1051 m.a.s.l at Nordenskjöldfjellet mountain. The curve is generated based on a 5x5m digital terrain model.

4.2 Suspended sediment yield

SSC variated from low sediment transport and clear waters, in strong contrast to periods of high SSC when the water was dark brown and untransparent, as in *Figure 26*. 254 SSC samples were acquired from June 12th to August 31st and used for SSY computations. The average SSC for the 2020 monitoring period was 1.9g/l and a total SSY of 41 050t, which implies a specific SSY of 1866t/day/km^2 for the Longyearelva catchment. Plotting the SSC samples against the corresponding computed discharge reveals a correlation with $R^2 = 0.58$.

The highest SSC correlates with the rising limb of the hydrograph in the Late July Flooding. Highest SSC was 24.1g/l recorded at 5:00 pm on July 25th, and the corresponding discharge was 5.6m^3/s, see *Figure 26* and *Figure 27*. July 25th also produced the highest specific SSY, at 252t/day/km^2 for the catchment. A total of 5594t of suspended sediment was exhausted that day, illustrated in *Figure 28.* July 28th was a close runner-up, with 248t/day/km^2, and an SSY of 5411t, despite a lower SSC (14.2g/l at 5:00 pm, and 5.7m^3/s), see *Figure 28.* The Late July Flooding event generated 57% of the total SSY for the monitoring period in 2020.

Figure 26: Mid-day on July 25th, discharge 5.6m^3/s. The highest suspended sediment concentration was measured later that day: 24.1g/l and 7.3m^3/s at 4:00 pm.

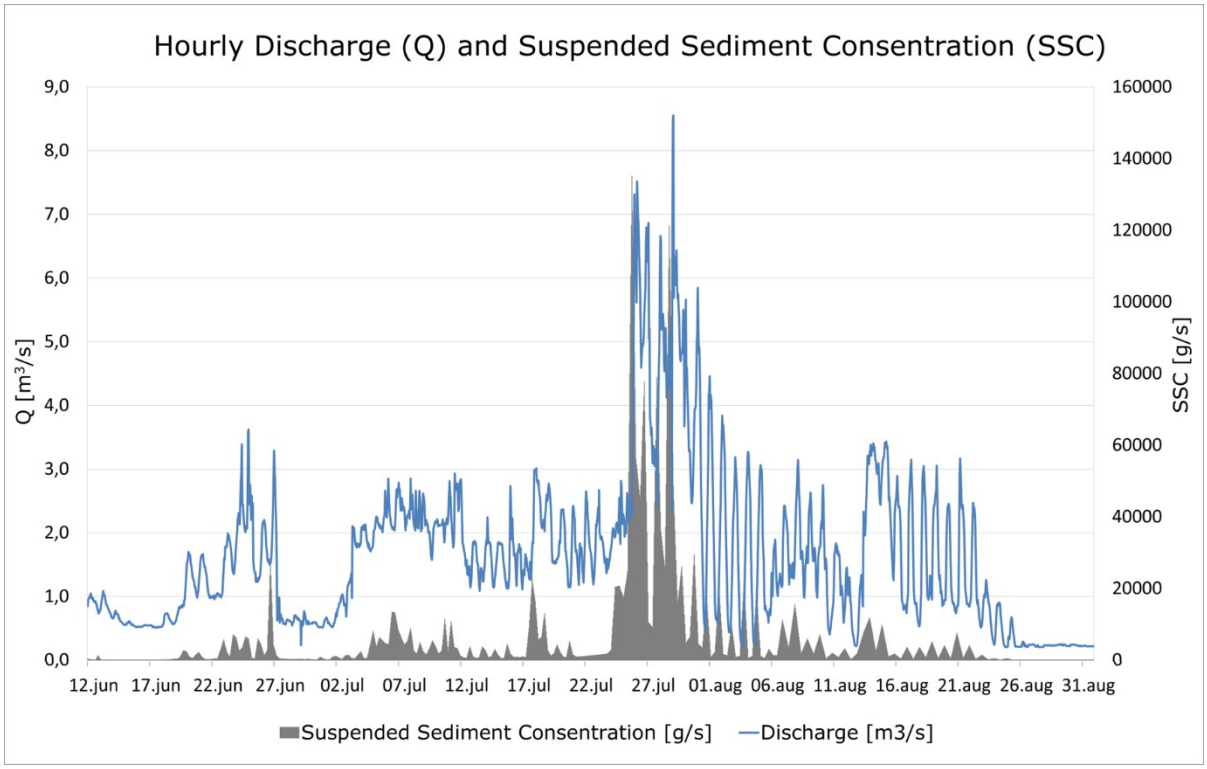

Figure 27: Hourly discharge and suspended sediment concentration (SSC). Highest SSC on July 25th, 24.1g/l. Average SSC during the monitoring period was 1.9g/l.

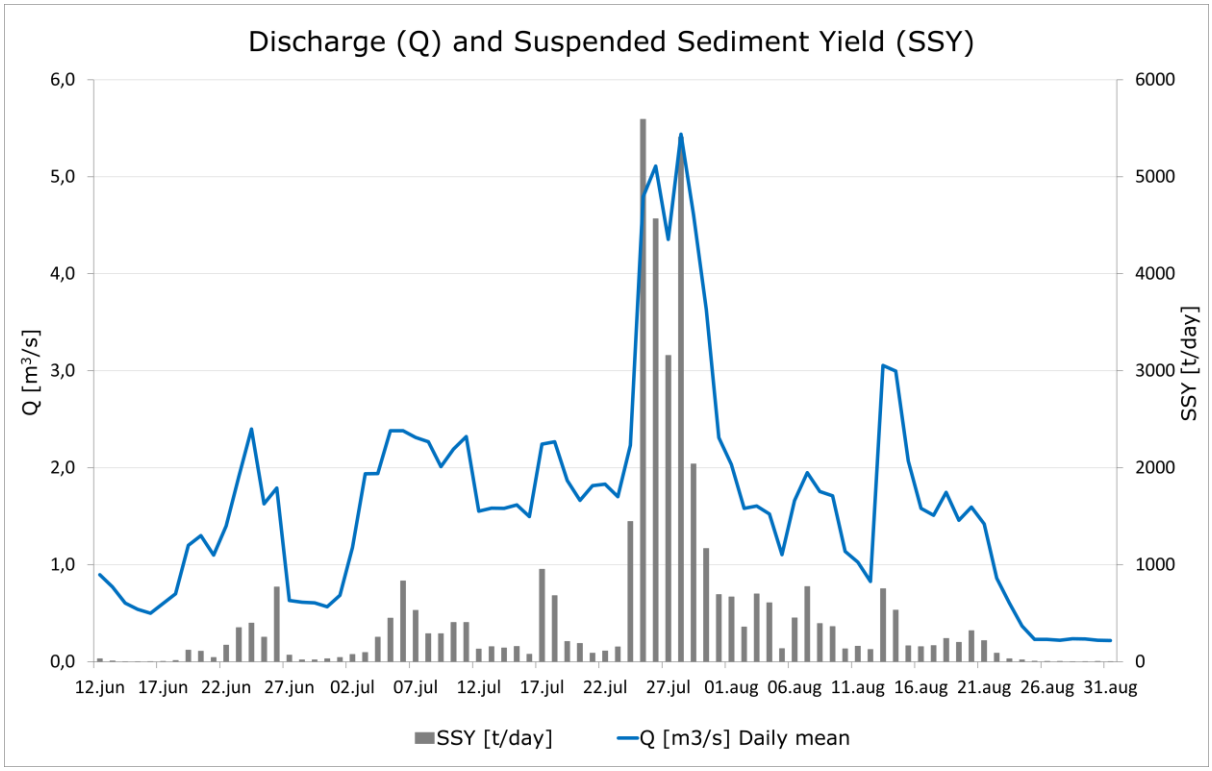

Figure 28: Dily discharge and suspended sediment yield (SSY). 57% of the total SSY traces back to the flooding event in late July. The highest SSY was recorded during the first days of the event.

4.3 Bedload transport

Coloured passive tracers were placed in the fluvial channel (see *Figure 19*) to monitor bedload and evaluate the discharge threshold for bedload transport and erosion in the Longyearelva river, see *Figure 29*.

All forty-five tracers from Hu-pt were transported as bedload and not relocated at the end of the monitoring period. However, movements were documented on June 24th, after a slight rise in the hydrograph and discharge up to 3.6m^3/s. Three tracers from Class 1 and two tracers from Class 2 were transported 8m and 5m, respectively. Tracers from Class 4 could be observed at their starting position until the Late July Flooding.

Tracer number 21 (Class 1) and number 92 (Class 2) from Ha-pt, were not reached by the water during the monitoring period and remained stationary throughout. However, they can be used as an argument for thalweg migration or rather the lack of migration. Tracer 125 (Class 3) was transported 150m downstream from the Ha-pt starting position and retrieved at Sill 4, which includes movement over Sill 3 (see *Figure 29C).*

Four tracers were retrieved from the Pr-pt starting position: three from Class 4 and one from Class 3. The bedload transport from Pr-pt includes transportation over Sill 18, although the sill was covered with sediments in June. The three tracers from Class 4 were found only a few meters apart, 80-90m downstream from their starting position, see *Figure 29 D.* All three were stationary after August, as the thalweg migrated westwards and left them on the dry riverbed. The one tracer from Class 3 moved 175m in total, which includes 2-3m during an increase in discharge on August 13-14th, 3.1m^3/s and 3.0m^3/s, respectively.

Of the 135 passive tracers placed in the river on June 17th, seven tracers were retrieved, a 5.2% retrieve rate. In total were 133 (98.5%) of the tracers placed in the channel on June 17th, reached by the water, and transported as bedload, summarized in *Table 4*. Of these 133, were 5 (3.8%) retrieved in September and abled further quantified movement. The 128 missing tracers include the largest tracers from Class 4, 200-250mm in size and an average weight of 6.1kg. The largest passive tracer not retrieved measured 250mm and 13kg, marginally classified as a small boulder. Boulders and cobbles could be observed rolling over the concrete culvert under Veg106 on several occasions, especially during the Late July Flooding, even at high SSC. Massive bedload could also be noticed, and even heard on the glaciofluvial fan emerging from the Larsbreen moraine.

Table 4: Summary of the bedload transport monitoring in Longyearelva over the 2020 ablation season

Class	***Tracers retrieved***	***Movement***
Class 1, small	0 = 0%	Yes, threshold < 3m^3/s
Class 2, medium	0 = 0%	Yes, threshold < 3m^3/s
Class 3, large	2 = 6.7%	Yes, 150-175m, threshold ~ 3m^3/s
Class 4, extra large	3 = 10%	Yes, 80-90m, Threshold > 3m^3/s
Total	3.8 %	Competence: Cobbles, small boulders

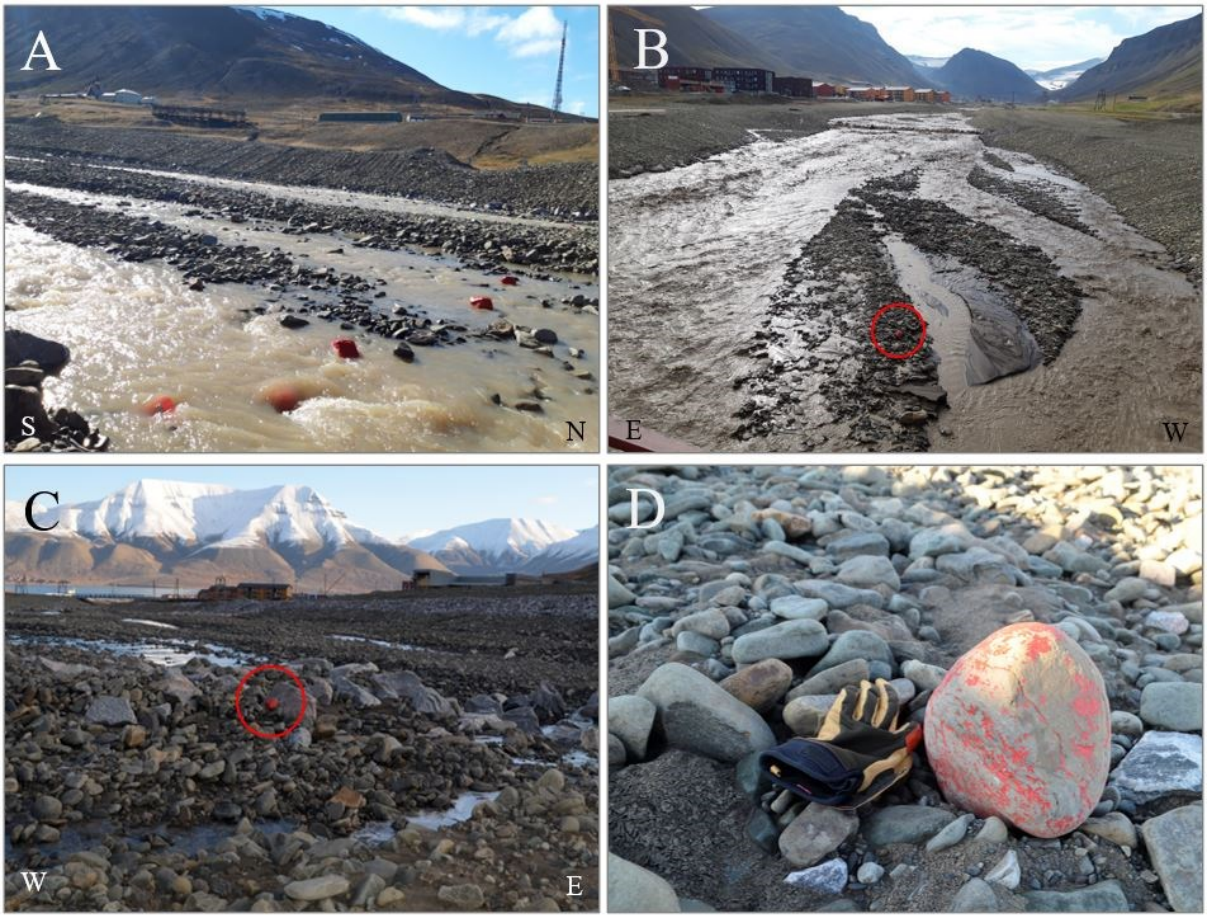

Figure 29: Coloured tracer in Longyeraelva. **A)** Initial placement of Class 4 passive tracers at Polarriggen (Pr-pt) starting position, June 17th. **B)** One Class 3 tracer at Pr-pt during high discharge in late July. **C)** Passive tracer 125, Class 3, from Hallen starting possition (Ha-pt) was transported 150m, ending up at the second sill downstream, Sill 4. **D)** Class 4 tracer retrieved downstream Pr-pt, transported 80m. Loss of paint indicate rough conditions on the riverbed and made the tracers less pronounced and thus channenging to locate.

4.4 Geomorphological features in the moraines

4.4.1 Larsbreen moraine

The Larsbreen moraine is split in half by a deep ravine running from the glacier snout through the ice-core moraine with a fluvial fan at the end, as shown in *Figure 30*. The meltwater stream from Larsbreen is confined in the ravine until it emerges on the fluvial fan, where it erodes, transports, and deposits sediments as it migrates. The ice-core is exposed in some sections due to active layer detachments on the inclined surface, documented in *Figure 30B*. The steep sides of the ravine show signs of fluvial toe-erosion, repeatedly slumping, and active layer detachments, as illustrated in the geomorphological mapping in *Figure 31*. Material from the gravity mass movements is accumulating in the fluvial channel. Active layer detachments and thermokarsts are recognised all over the moraine.

On the western side of the fluvial fan, a 1.5 m high, 20m long, and 5m wide bar could be seen in July, *Figure 30C – D.* This bar was eroded or covered with sediment during the second half of the monitoring period, as is cannot be seen in *Figure 30A* from September 2nd. Scars after fluvial erosion and braided channels have been observed over the monitoring period and are included in *Figure 31.* The eastern side of the fan is dominated by a large pile of mine waste, introducing a different material of mechanically stronger sandstone of Firkanten Formation, in contrast to the softer shales from Frysjaodden Formation that dominate the Larsbreen till.

The rock glaciers on the eastern side of the channel and fan have not been investigated. However, back scarps of small detachments at the foot are mapped. Meltwater was flowing out from these scarps, a contribution to the glacier runoff from Larsbreen.

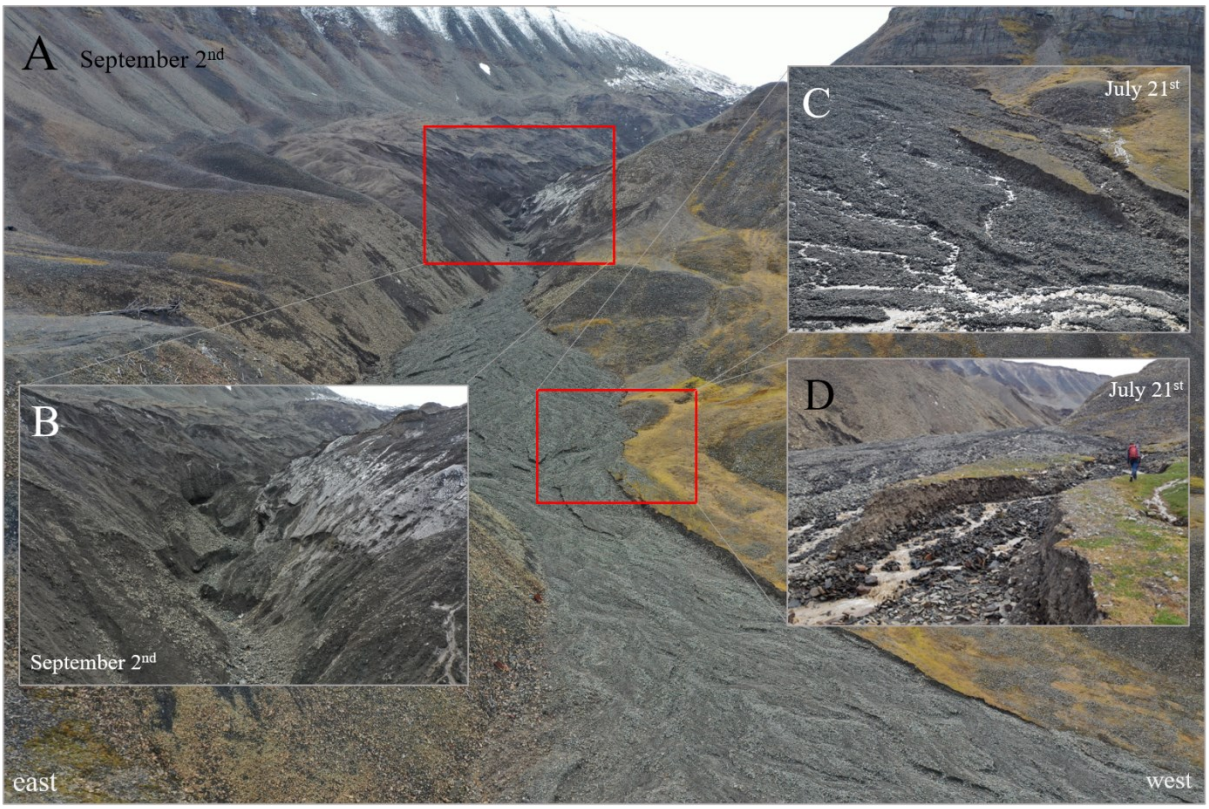

Figure 30: Larsbreen moraine and glaciofluvial fan. **A**) Drone-picture from September 2nd of the glaciofluvial fan and moraine at Larsbreen. **B)** Detailed drone-picture of the V-shaped channel through the moraine. On the right side can the ice-core be seen after active layer detachments. **C)** A 1.5 m high bar could be seen on the western side of the fan on July 21st. **D)** The same bar as in C, from a different angle and with e person for scale. This bar disappeared by the end of the season, illustrated in A.

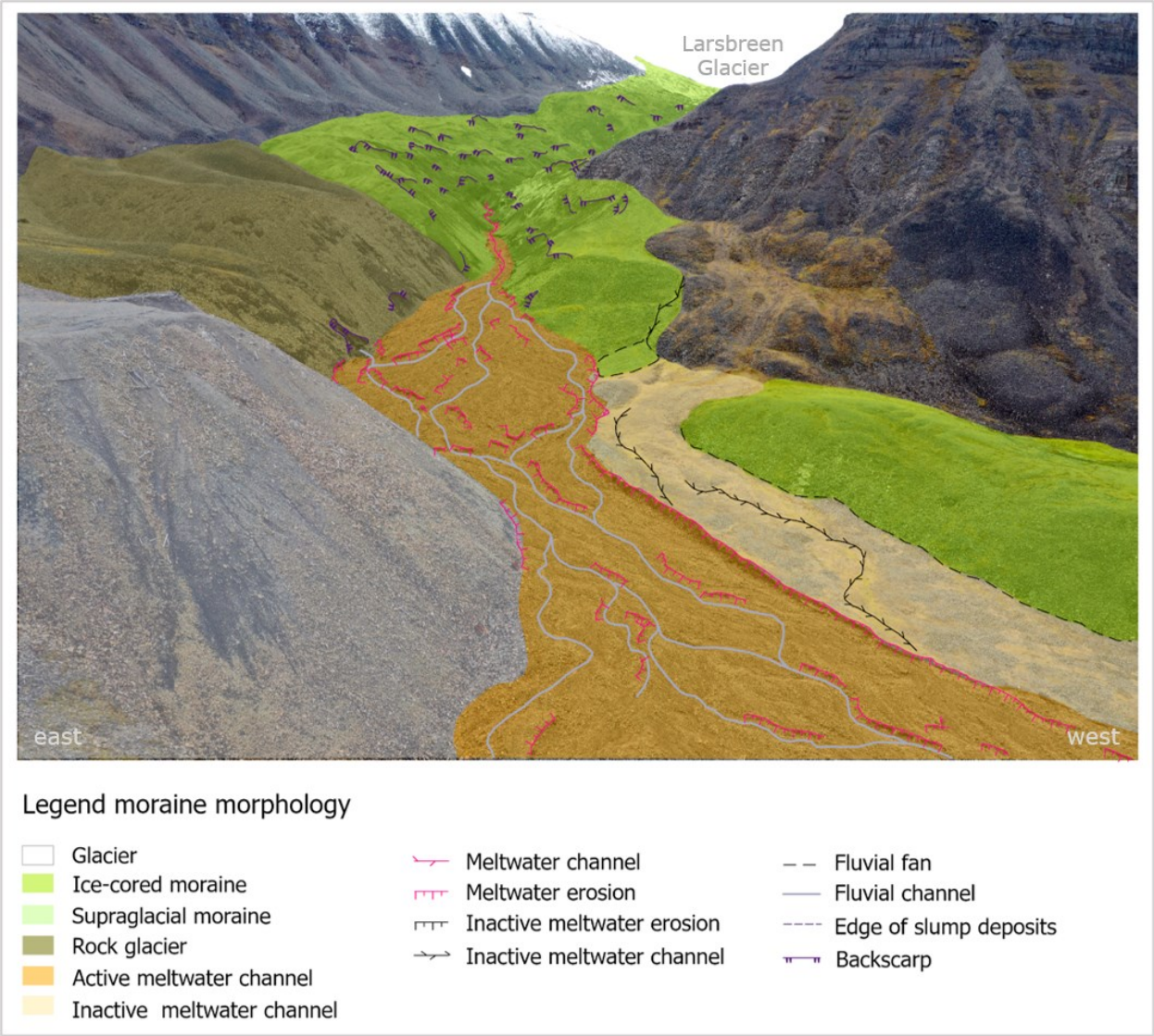

Figure 31: Geomorphological mapping, illustrated on an oblique image of Larsbreen moraine and fluvial fan.

4.4.2 Longyearbreen moraine

The Longyearbreen moraine has been dominated by lateral meltwater channels on the western and eastern flanks, illustrated in the geomorphological mapping in *Figure 33*. Some meltwater was directed through the former during the Late July Flooding (see the hydrograph in *Figure 22*). The latter remained dry and abandoned for most of the 2020 ablation period, and minimal runoff was only observed over the first days of monitoring (June 5th to June 12th). The main meltwater flow in 2020 was through the middle of the moraine, shown in *Figure 32* and *Figure 33*. Two prominent back scarps can be seen in the middle of the moraine in *Figure 32A-B,* in adjunction to the eroding meltwater channel. The snout of the glacier is at a slightly lower elevation than the highest point of the moraine, and a small sandur with braided streams can be seen directly in front of the glacier. The western side of the glacier is partly covered with two ridges of supraglacial debris.

The geomorphological features of Longyearbreen moraine illustrated in *Figure 33* documents the complex system of active fluvial channels, erosion, thermokarst, and active layer detachments. *Figure 33* also highlights the outlines of previous meltwater channels and landslide activity in the moraine.

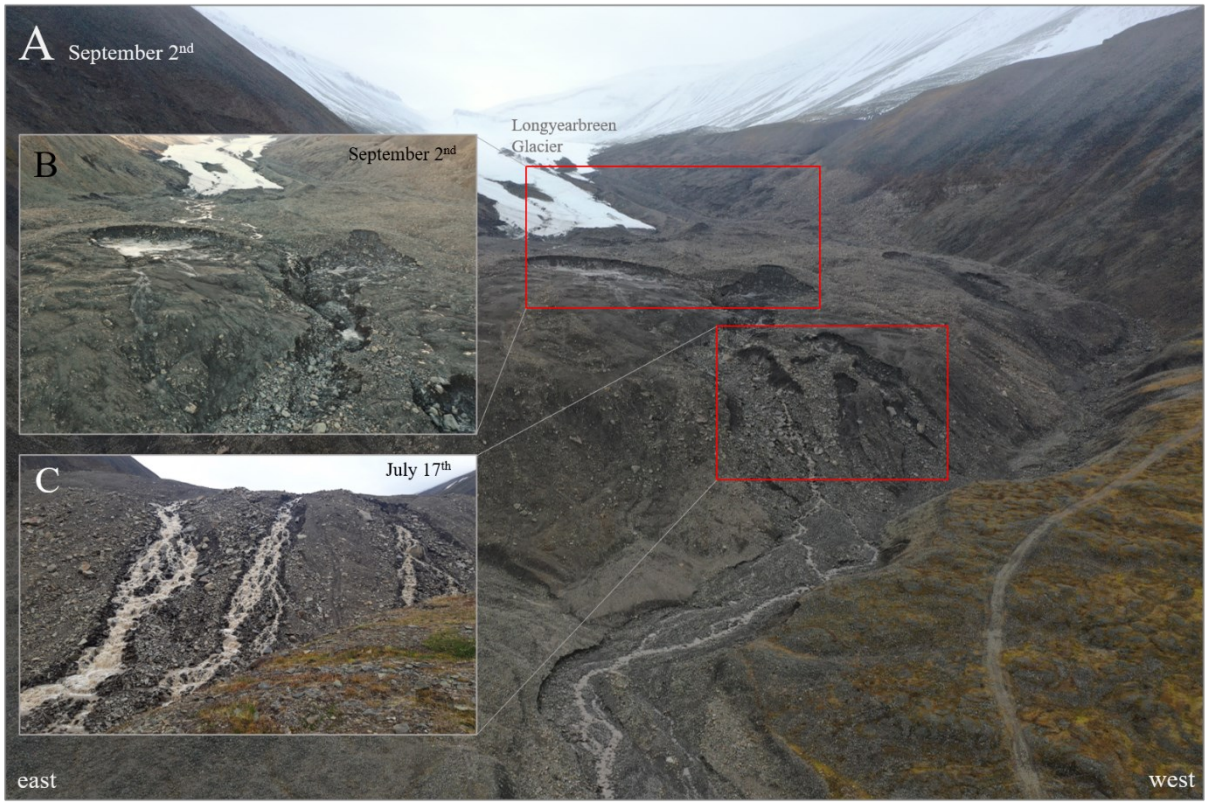

Figure 32: Longyearbreen moraine. **A**) Longyearbreen moraine and sandur on September 2nd. **B**) Detailed image of slumping, thermokarst and deep channels due to fluvial erosion over the summer. **C)** Meltwater runs down and erode the front of the moraine on July 17th.

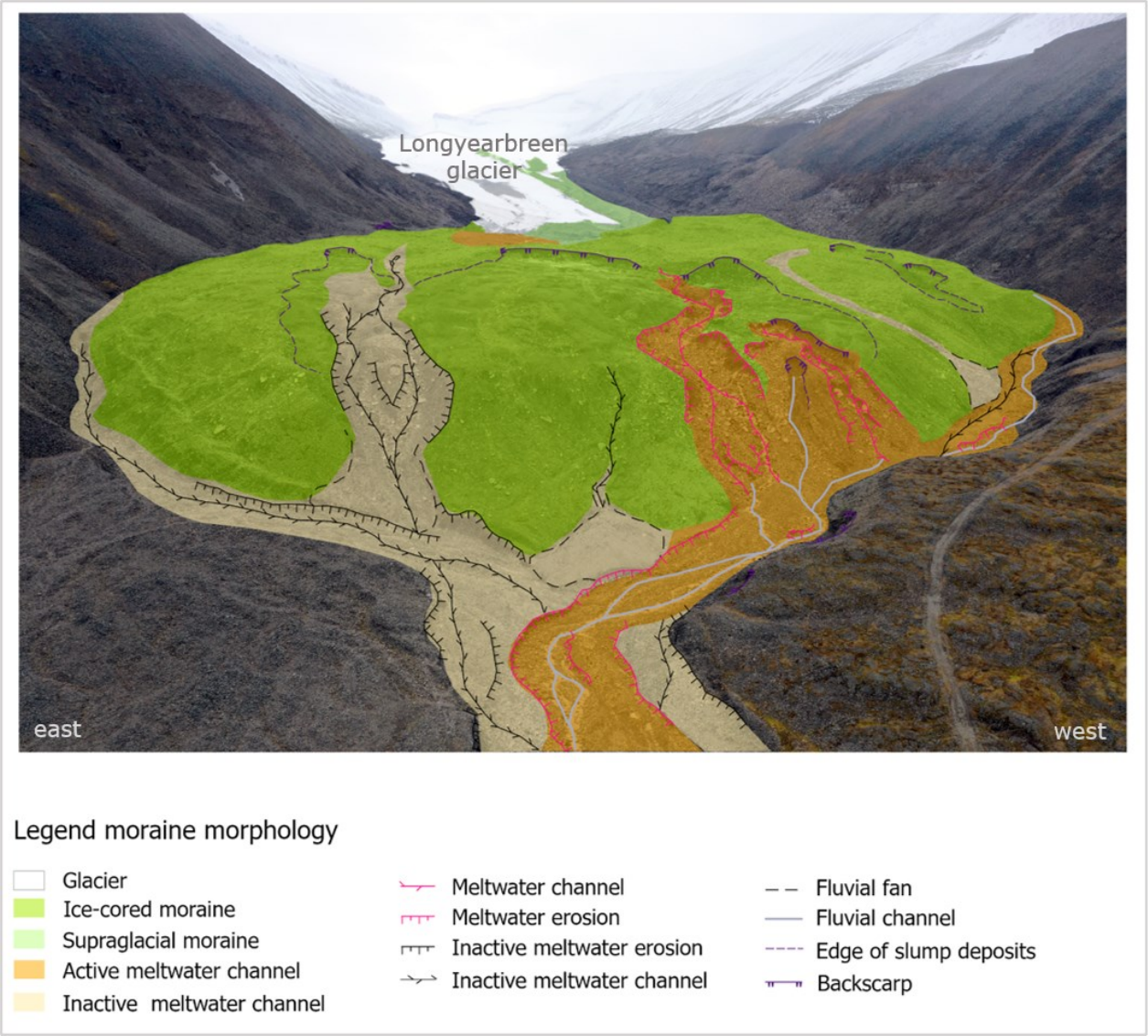

Figure 33: Geomorphological mapping illustrated on an oblique image of the Longyearbreen moraine.

4.4.3 Fluvial morphology

The sediments in the glaciofluvial system vary in size, from silt, sand, gravel, to boulders, illustrated in *Figure 34* and *Figure 35 C-D.* The deposits are rounded to subrounded sand- and siltstone, cubic, and disc shape reflecting the local geology of the CTB. Besides the local lithology, angular cobbles and small boulders (<500mm) of granitic gneiss used for riprap and sills are entrained and mixed in the glaciofluvial sediments, see *Figure 34B.* Sorted sediments in the constructed fluvial channel were observed and documented in *Figure 34A-B.* Imbrication of disk-shaped cobbles and boulders was documented in the Longyearbreen meltwater stream, ~200m downstream from the moraine (*Figure 34C*). The sediments in *Figure 34D* are unsorted and exposed in a 1.5m high and several meters long fluvial erosion scarp on the eastern levee between the sedimentation dam and Veg106. The channel between the sedimentation dam and Veg 106 is wider than the channel from the dam and downstream. More lateral migration and braided streams were documented in the broader section, see *Figure 35A* and *B*.

The sills and riprap in the constructed channel force the system into a channelized and concentrated stream the last 2.5km towards the outlet in Adventfjorden. Longitudinal bars and small terraces developed between some sills, documented in *Figure 35.* Sediments accumulated upstream the sills, while erosion dominated directly downstream (see chapter *4.5.1 Sills and riprap*).

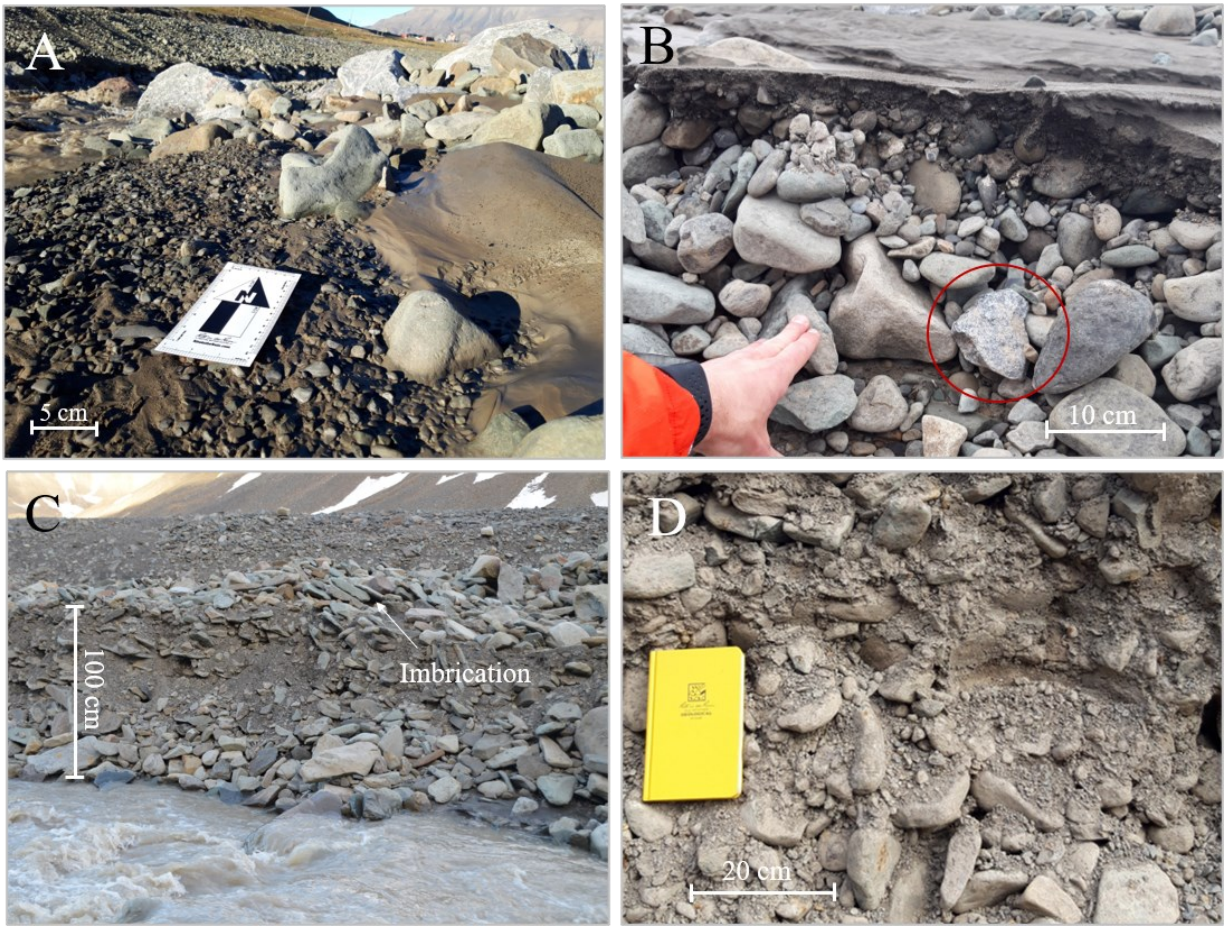

Figure 34: Fluvial sediments and qualitative grain size distribution in Longyearelva. **A**) Sand, gravel, cobble, and small boulders. Large boulders of granitic gneiss. **B**) Fines (silt and sand) on top, coarsening downwards to gravel and cobbles, note the small cobble of granitic gneiss highlighted in the red circle. **C)** Imbrication of cobbles and boulders in proximity to the Longyearbreen moraine. **D**) A wide range of mixed sediments from sand to boulders, unsorted, exposed in a 1.5m high, several meters long erosive scarp on the eastern side of the channel between Veg106 and the sedimentation dam.

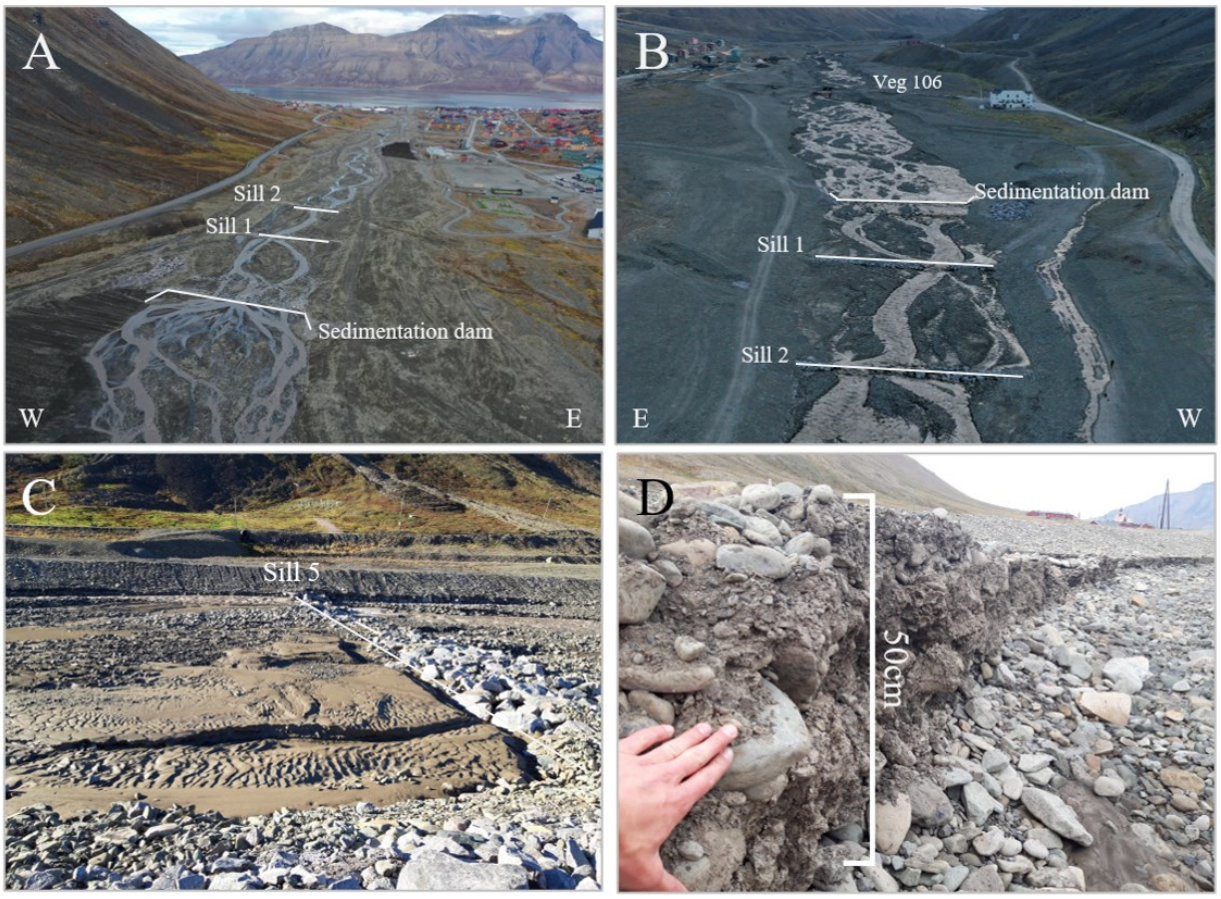

Figure 35: Fluvial morphology in Longyearelva. **A**) Drone image from September 11th, illustrating the braided channels upstream the sedimentation dam, and the more channelized system from Sill 1 and 2. **B**) Drone image from August 6th, illustrating the braided channels upstream the sedimentation dam to Veg 106, and the more channelized system from Sill 1 and 2. Note additional meltwater runoff on the western side of the channel. **C)** Sill 5 photographed on August 10th, note the fine sediments accumulated along the nearest bank. **D)** Fluvial terrasses from erosion and channel degradation, mix of sediment size from sand to cobble.

The fluvial sediments between Nybyen and Veg106 were excavated and reworked from August 4th and for the rest of the monitoring period, see *Figure 36. This part of the river* was therefore excluded from the fluvial morphological mapping.

Figure 36: Excavation of fluvial sediments next to Nybyen, deepening the channel to keep the river from migrating. The material is intended to be used in the construction of landslide mitigation in Lia. Picture from August 10th.

4.5 Hydrological engineering

An assessment of the newly constructed scour- and flooding mitigation is based on the methodology previously described. The observations related to the sills and riprap as well as the sedimentation dam are presented in the following subsections.

After an inspection accompanied by NVE on June 25th, it was decided that some sills (Sill 2, 3, 5, 6, and 8) needed repairs. The higher flows on June 23-26th (Q_{peak} 3.6m^3/s June 24th, 2:00 pm) caused limited damage, such as scouring and loss of interlocking between some of the boulders. The structure was reestablished with an excavator from June 29th to July 1st, see *Figure 37A.*

During the Late July Flooding (see *Figure 22*), a bulldozer was used to keep the river from eroding the levees both upstream Veg106 and downstream Veg600. The bulldozer dug out a new thalweg in the middle of the channel and strengthened the levees with more sediment, demonstrated in *Figure 37B.* One must underline that this work was performed outside the constructed channel, but was still essential to avoid water reaching and potentially damage infrastructure.

Figure 37: Immediate maintenance had to be done during floods. **A**) After the first minor flooding on June 24th, an excavator was used to reassemble damaged sills. **B)** July 27th, discharge 6.2m^3/s. Bulldozer performing critical maintenance downstream Veg 600 to keep the river from eroding the levees and threatening to flood the red pump-house.

4.5.1 Sills and riprap

Observations and quantitative characteristics of each sill are presented in *Table 5*. An overview of all sills and riprap is shown in *Figure 38*. All sills are displayed in *Figure 39*, *Figure 40*, and *Figure 41* at the end of the monitoring period, September 16th. In addition, sills of special interest were studied, and geomorphological features were illustrated on annotated figures, see *Figure 42*, *Figure 43*, and *Figure 44*. The SfM-method proved valuable for determine gradient, width, spacing, and general mapping. The river can, in general, be divided into four sections, where the different sections can be described as followed:

- Section 1, Sill 1-8, has a 2.2⁰ gradient with an average width of 35m, 77m average spacing, and the sills have in general partly collapsed, subsided and been eroded downstream *Figure 39*. Sill 8 has collapsed on the eastern side with severe undercutting, and erosion on the downstream riprap was documented, see *Figure 43*.
- Section 2, Sill 9-13, has an average width of 29m, 1.8⁰ gradient, and 95m average spacing, see *Figure 40*. Sill 9 is narrow (13m), and sediments accumulated as the channel widens downstream. The sills in this section are partly covered with sediments and little to no erosion on sills or riprap.
- Section 3, Sill 14-17, has an average width of 23m, an average spacing of 79m, and a 1.5⁰ gradient, see *Figure 40* and *Figure 41*. Some downstream erosion, but little to no subsidence or collapse. Sill 15 is the exception as it was buried entirely in early June and yet visible in September.
- Section 4, Sill 18 and 19, is the narrowest section at 21m on average, the highest spacing (146m), and the lowest gradient at 1.4⁰, see *Figure 41*. Sill 18 was not visible early in the season; however, the western side was exposed in September. Sill 19 was almost completely buried initially, and the situation was unaltered over the monitoring period.

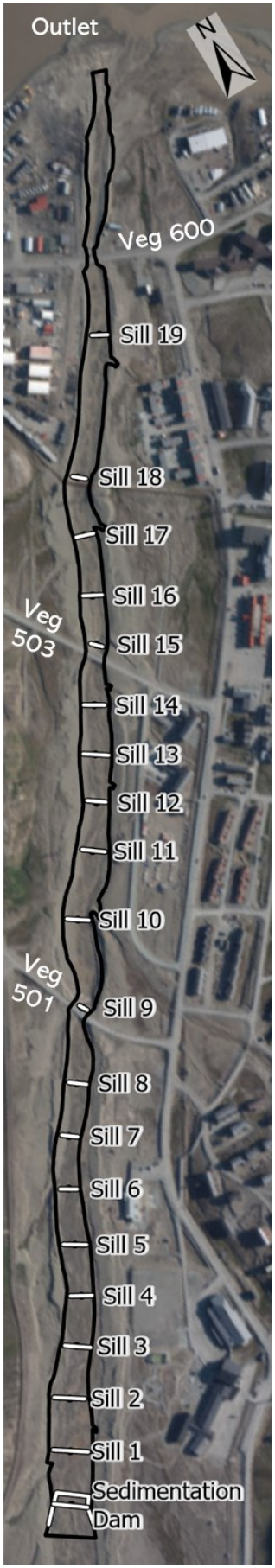

Figure 38: Overview of Longyearelva from the sedimentation dam to the outlet, 2.2km further down. Annotated with the placement of each sill and important roads.

Table 5: A summary of characteristics and observations of the different sills at the end of the monitoring period. The gradients are calculated based on the elevation difference from the sill upstream. Regarding Sill 1 is the crest of the sedimentation dam used for gradient calculation.

Sill number	Gradient [Deg.]	Width [m]	Spacing [m]	Observations
1	3.1	51.1	80.2	Collapse and subsidence in the middle, downstream erosion, especially on the eastern side. Some downstream erosion, no scour hole
2	2.3	45.3	75.6	Subsidence on the eastern side, some downstream erosion, otherwise in-flush and intact. Minimal scour hole
3	2.0	36.2	76	Minor downstream erosion, minor subsidence in the middle, otherwise in-flush and intact with a minimal drop, Passive tracers for bedload measurements were transported over this sill.
4	2.1	30.4	73	Downstream erosion, subsidence in the middle, displacement on some blocks. Small scour hole, see *Figure 42A.*
5	2.2	34.4	74.1	In flush on the eastern side, gradually more downstream erosion, and scour hole development towards the western side. Subsidence and partial collapse on the western side
6	2.0	25.4	81.8	In flush on the eastern side, gradually more downstream erosion. Subsidence and collapse with scour hole development towards the western side. Riprap eroded on the western side, see *Figure 42B.*
7	1.8	27.1	76.2	In flush on the western side, subsidence and partial collapse on the eastern side
8	1.7	27.7	76.6	In flush in the middle, severe collapse and subsidence on the eastern side with eroded riprap downstream. Downstream erosion and minor scour hole development on the western side, see *Figure 43*.
9	2.2	13	108.6	Buried in early June, erosion and gradually channel degradation has left it more exposed. Minor subsidence on the western side otherwise in flush, no scour hole development.
10	1.7	32.2	127	In flush towards the sides, sediments accumulated on the crest towards the centre.
11	1.6	35.1	102.2	Some downstream erosion and scour hole development on the eastern side. Otherwise, in flush and partly buried towards the centre. See *Figure 44A.*

12	1.5	28.6	71.2	Minor downstream erosion and scour hole development on both sides. The center is in flush.
13	1.9	37.2	67.8	Minor downstream erosion and scour hole development, more in flush towards the sides.
14	1.5	30.3	71.7	Severe downstream erosion and scour hole in full depth on the sill, undercutting has started to develop towards the centre.
15	1.7	9.8	88	Buried in early June, overburden eroded on the western side down to the sill crest. No scour hole development and remained entirely covered on the eastern side.
16	1.5	27.4	69.7	Some downstream erosion, minor scour hole development on the western side, otherwise in flush and no subsidence.
17	1.4	26.1	88.1	Downstream erosion and scour hole development on the sides, more pronounced towards the east. Centre more in flush, see *Figure 44B.*
18	1.6	20	83.5	Buried in early June, eroded overburden on the western side down to the sill crest. No scour hole developed, and sediments accumulated on the eastern side. Passive tracers were transported over this sill.
19	1.2	22.9	207.7	In flush on the sides, sediments accumulated towards the centre.

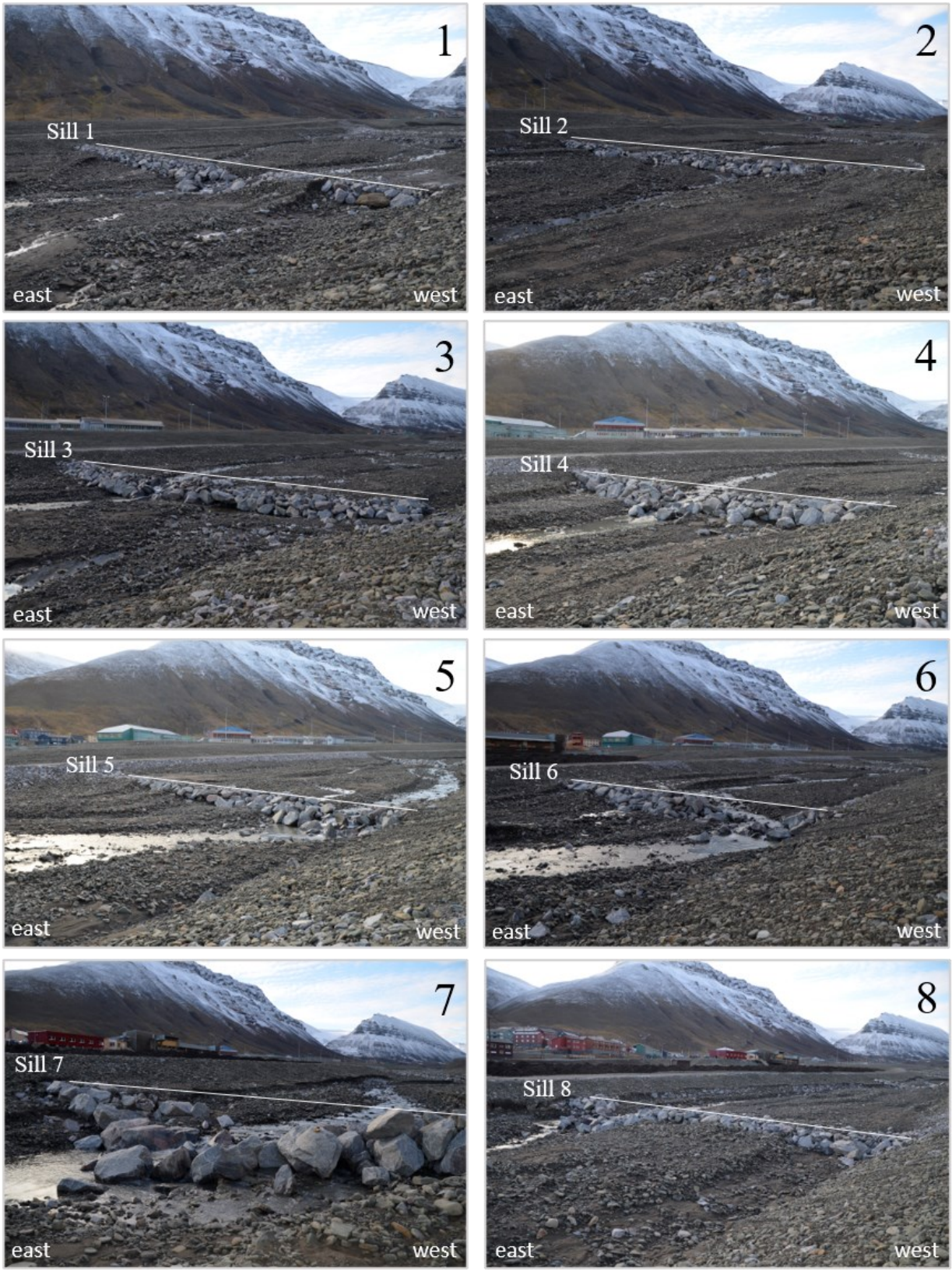

Figure 39: Sill 1-8 at the end of the monitoring period. Pictures from September 16th, at 9:00 am,dDischarge less than 0.1m^3/s. First day with icings on the riverbed. All sills have collapsed to some extent, where Sill 7 and 8 suffered the most pronounced subsidence and deformation. Sill 2 remained relative intact, with little deformation and erosion. Important to mention that the Sill 2, 3, 5, 6 and 8 needed minor repairs with an excavator the first days in July. The largest granitic boulders are approximately 1-1.5m.

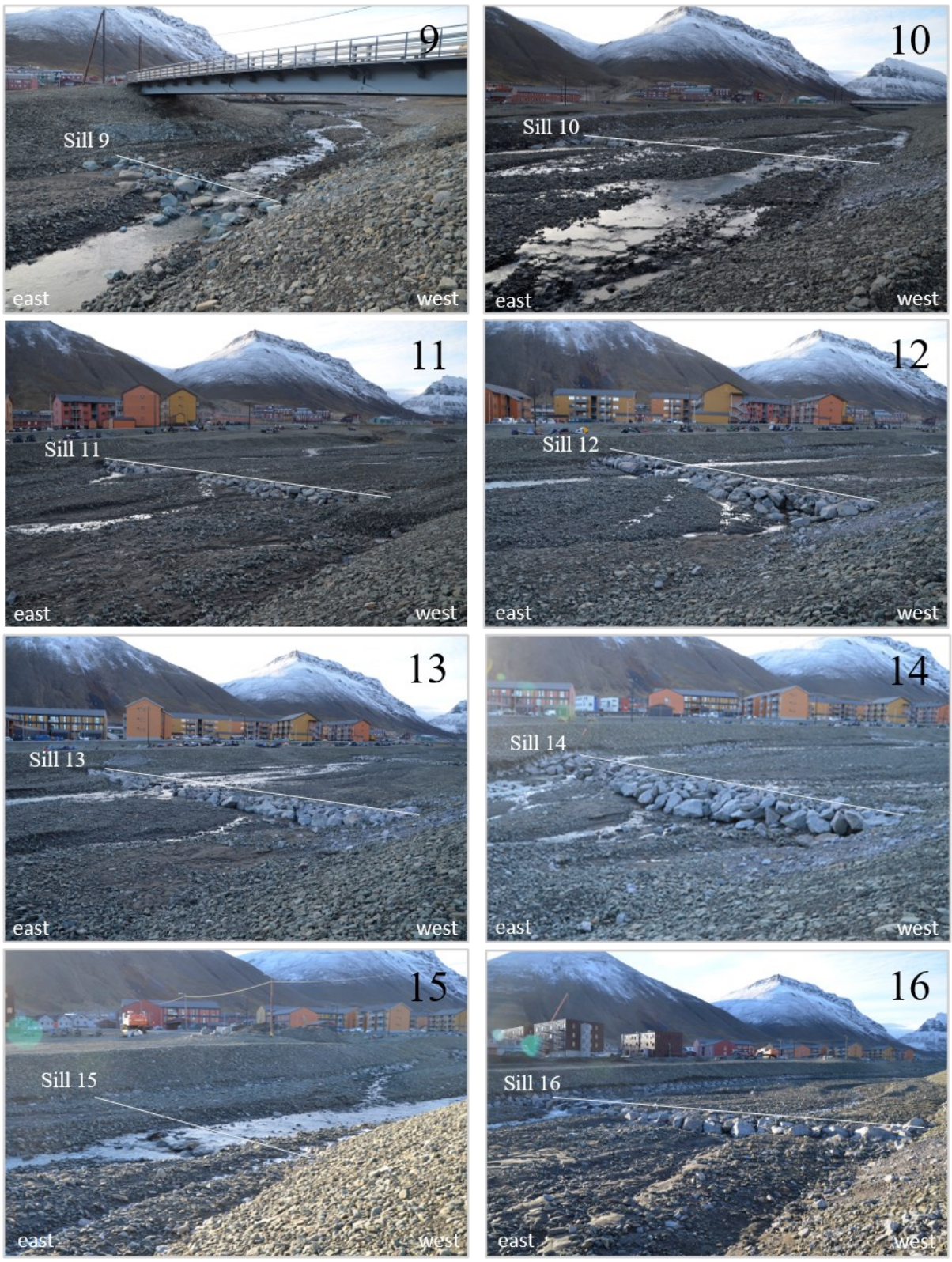

Figure 40: Sill 9-16 at the end of the monitoring period. Pictures from September 16th, at 9:00 am, discharge less than $0.1 m^3/s$. First day with icings on the riverbed. Sill 9 and 15 was covered with sediments in early June, but erosion has partly exposed them. Sills 10, 11 and 16 are relative in flush with the riverbed, and partly buried due to accumulated sediments. Sill 12, 13, 14 are intact but with some downstream erosion. The largest granitic boulders are approximately 1-1.5m.

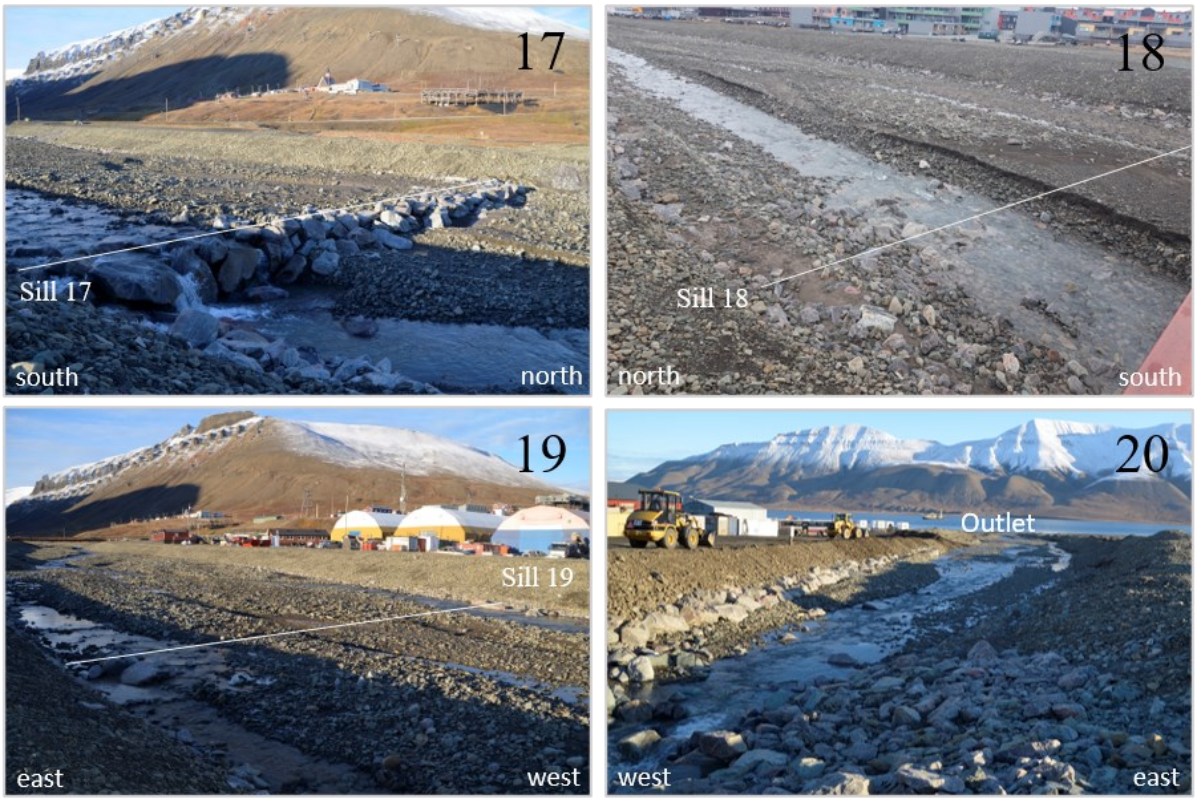

Figure 41: Sill 17-19 at the end of the monitoring period. Pictures from September 16th, at 9:00 am, discharge less than 0.1m^3/s. First day with icings on the riverbed. Sill 17 is intact, but with severe downstream erosion. Sill 18 was covered with sediments in early June, but channel degradation has partly exposed it. Sill 19 is partly covered with sediments, and accumulated sediments over the monitoring period. **20)** Riprap and scour protection downstream the bridge at Veg600. Riprap on the western side remained intact, but a bulldozer had to be used to keep the river from eroding the eastern levees during high flows (up to 8.6m^3/s) in late July.

4.5.2 Morphological mapping of sills and riprap

Based on the observation listed in the previous subsection (see *Table 5*), a selection of sills was mapped to enhance distinctive morphological features. The chosen sills reflect the general trends observed and highlight the problems with subsidence, collapse, scour hole development, and downstream erosion around the transition from sill to riprap. Sills from all four sections are represented, but as Sill 8 is most damaged, it is displayed from two perspectives (*Figure 43*) to stress the morphological features.

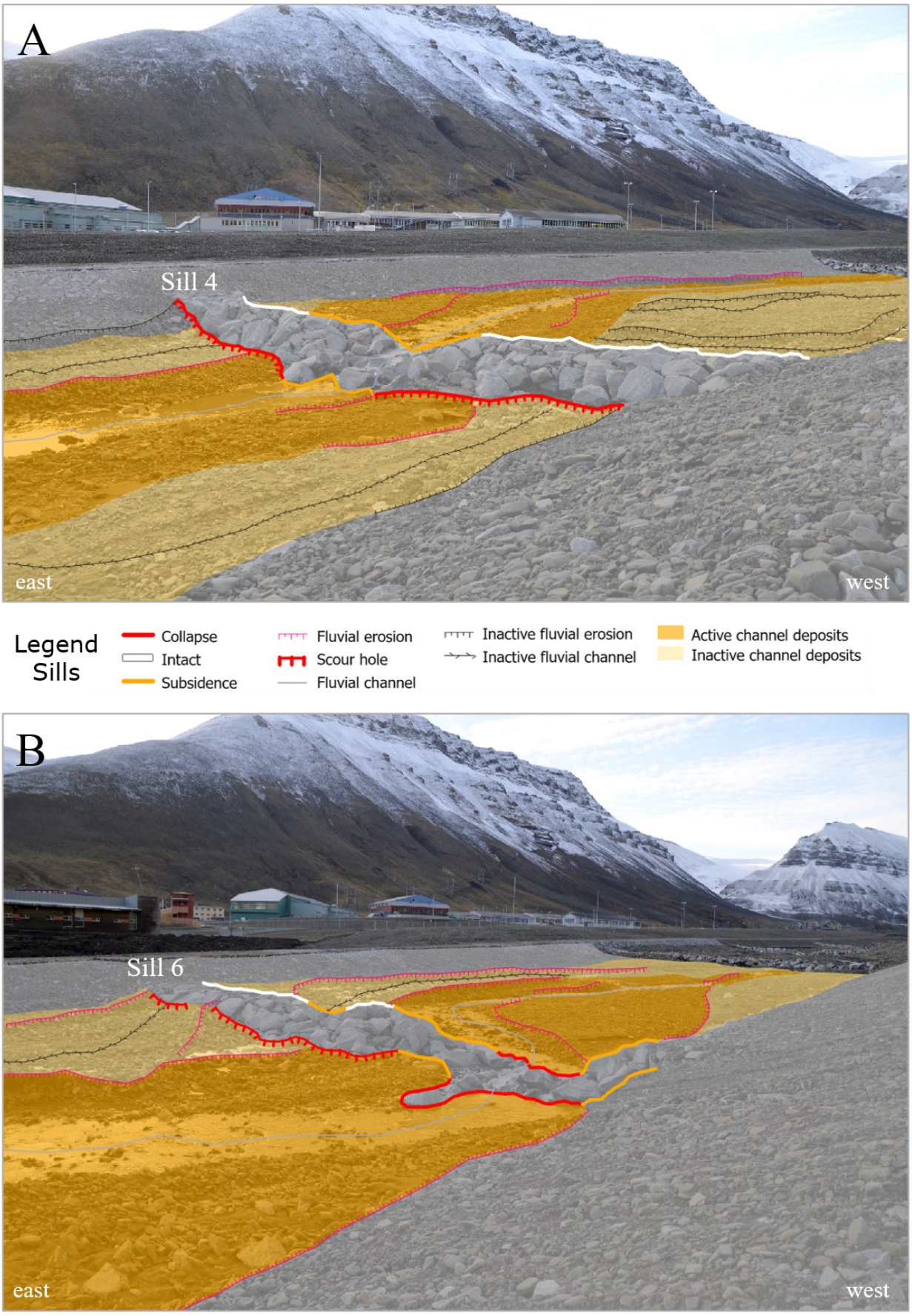

Figure 42: September 16th, discharge <0.01m^3/s, end of the monitoring period. **A**) Sill 4 annotated to illustrate morphology. Not the erosion induced drop on the downstream side of the sill and subsidence in the middle of the sill. **B)** Sill 6 annotated to highlight erosion and collapse and subsidence on the western side of the sill.

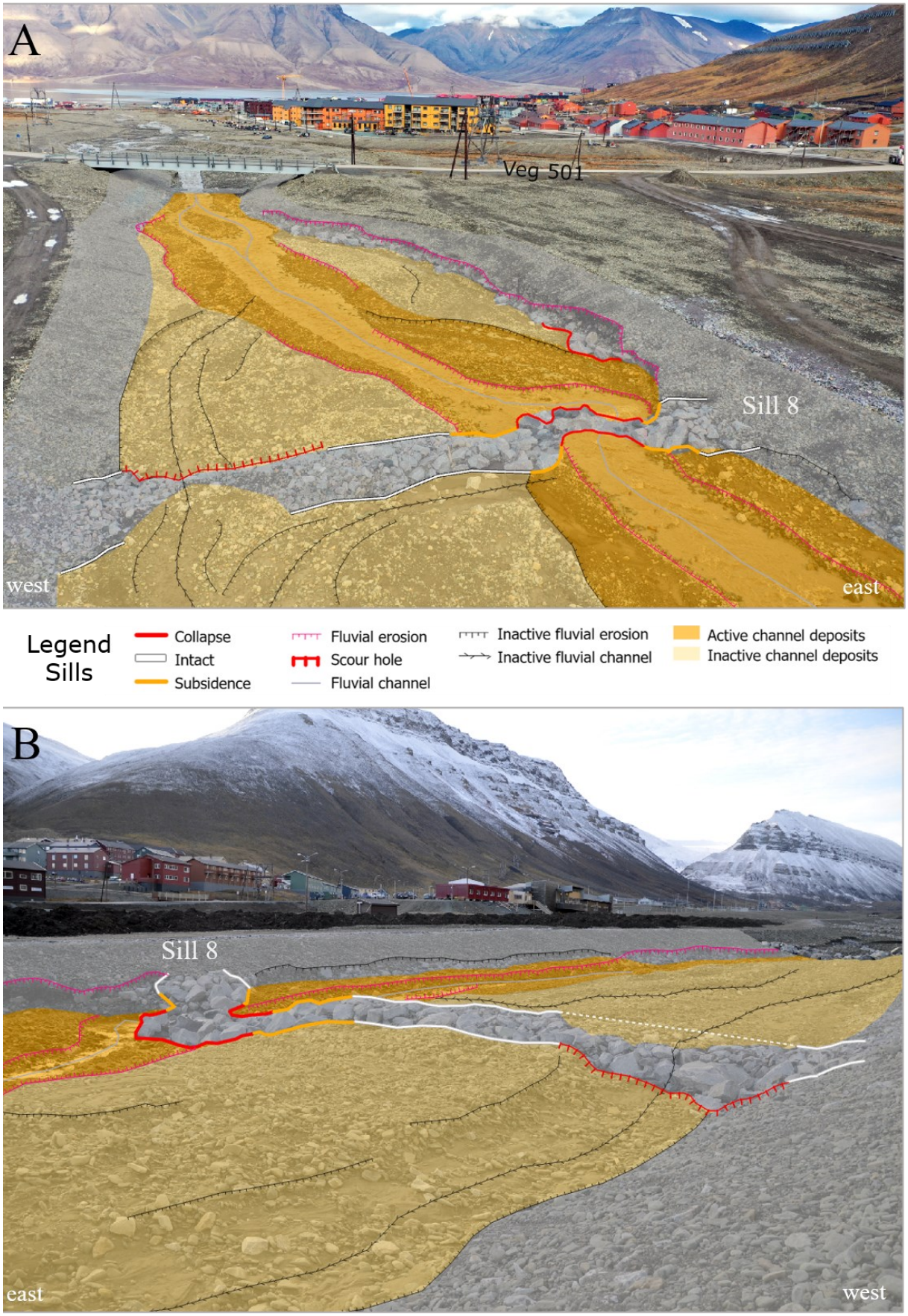

Figure 43: Picture from September 16th, discharge <0.01m^3/s, end of monitoring period. **A**) Annotated drone picture of Sill 8 to illustrate the morphology. This perspective show both the collapse on the eastern side and damage to the riprap directly downstream. **B**) Annotated picture to document downstream erosion and how Sill 8 has collapsed on the eastern side and how the riprap directly downstream has been eroded and collapsed.

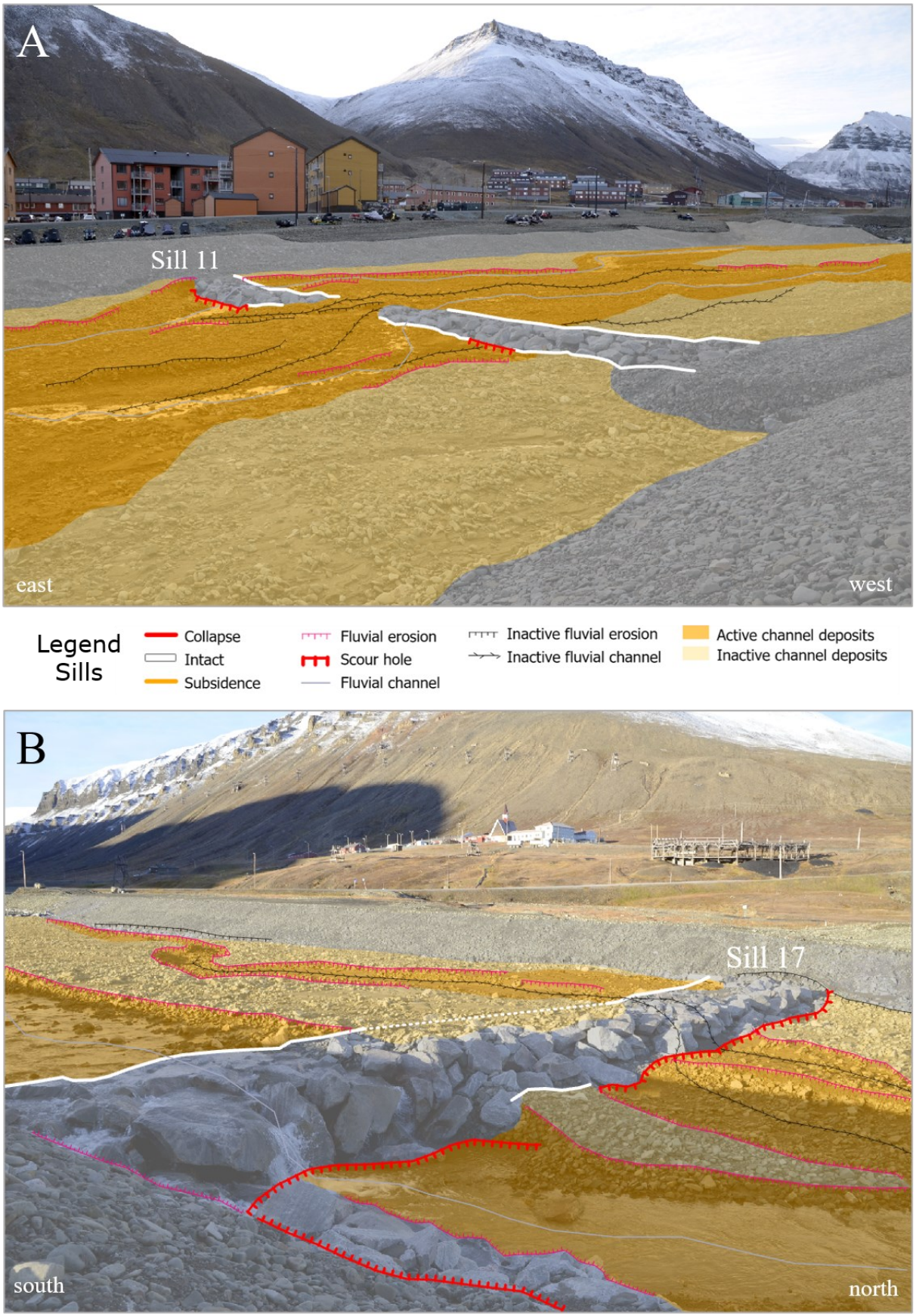

Figure 44: September 16th, discharge <0.01m^3/s, end of the monitoring period. **A**) Sill 11, mostly in flush both up- and downstream, only minor downstream erosion on the eastern side. **B)** Sill 17 remained intact and in-flush upstream, however, severe scour hole development caused a 1m drop over the sill. In strong contrast to the in flush crest and riverbed at the start of the monitoring period.

4.5.2 Sedimentation dam

The sedimentation dam next to Huset aims to limit bedload transport by controlling the sediment supply. The dam accumulated at least 30 000m^3 sediments from June 5th to September 15th. A considerable volume of sediments accumulated during a minor flooding event (June 24th-26th) with discharge up to 3.6m^3/s, lifting the bed by 40-50cm (see *Figure 22* and *Figure 23* for daily and hourly hydrographs). As *Figure 45* illustrates, the sedimentation dam gradually accumulated sediments until it was full and overflooded during the Late July Flooding.

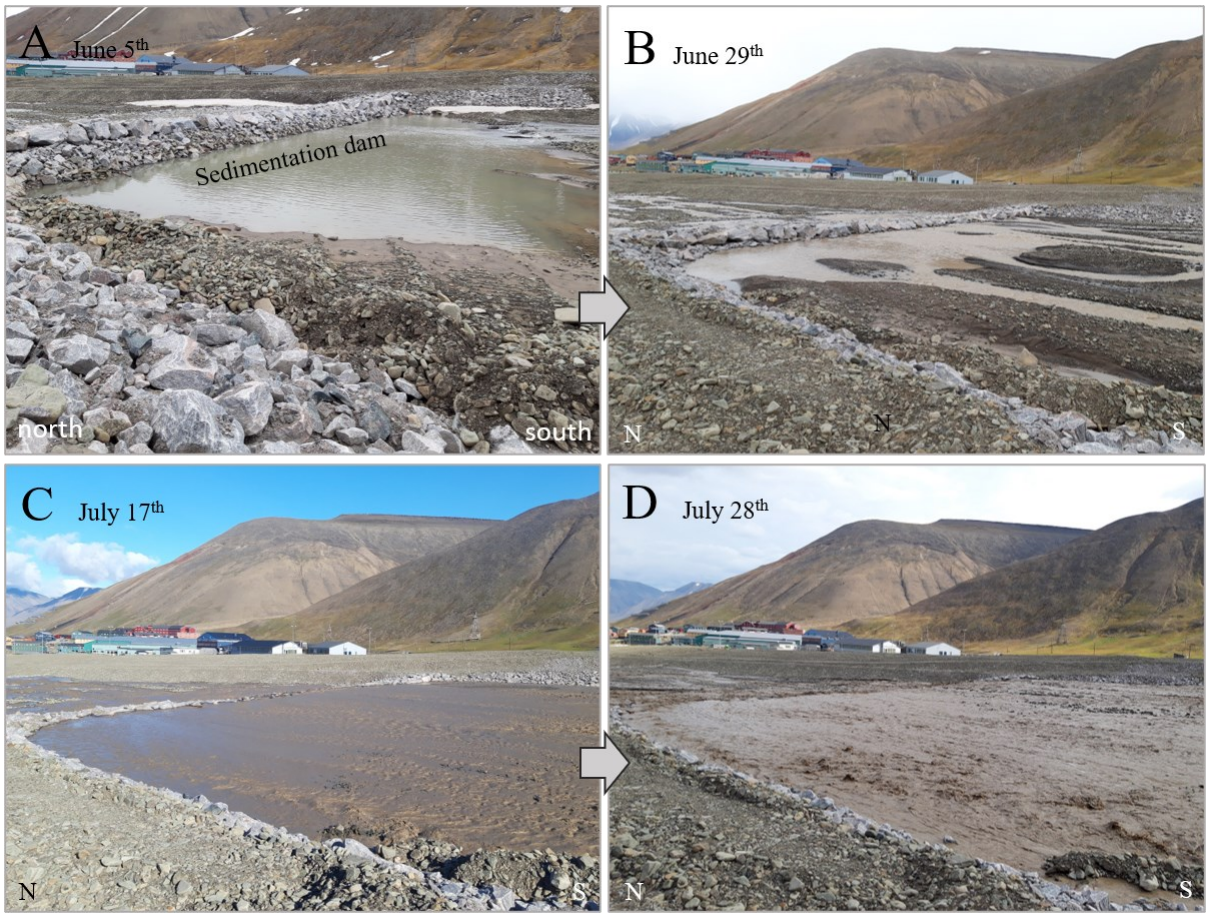

Figure 45: Gradually filling of the sedimentation dam during the summer. **A**) June 5th, first day of monitoring. Notice larger boulders on top of the weir, the crest is 100cm above the water surface at the time. **B**) June 29th discharge 0.6m^3/s. Water level now 60cm below the weir crest, and bars has developed upstream. **C**) July 17th, discharge 3.0m^3/s. Considerable volumes of sediments accumulated, water in full width of the dam, overflowing in the middle. **D)** July 28th, discharge 6.7m^3/s. Weir overflowing in full width, accumulated sediments filling the whole dam, 30 000m^3, and bedload has started to accumulate on the apron. Longitudinal bars of sediments can be observed in the middle of the dam.

After the dam had reached its maximum capacity, sediments started to accumulate on the apron, illustrated in *Figure 46*. The non-functional dam had to be excavated on August 11th. *Figure 46B* show a full sedimentation dam on September 11th, with low discharge and a braided stream through a top layer of fine sediments, in contrast to the turbulent waters in *Figure 45D* transporting pebbles, cobbles, and small boulders.

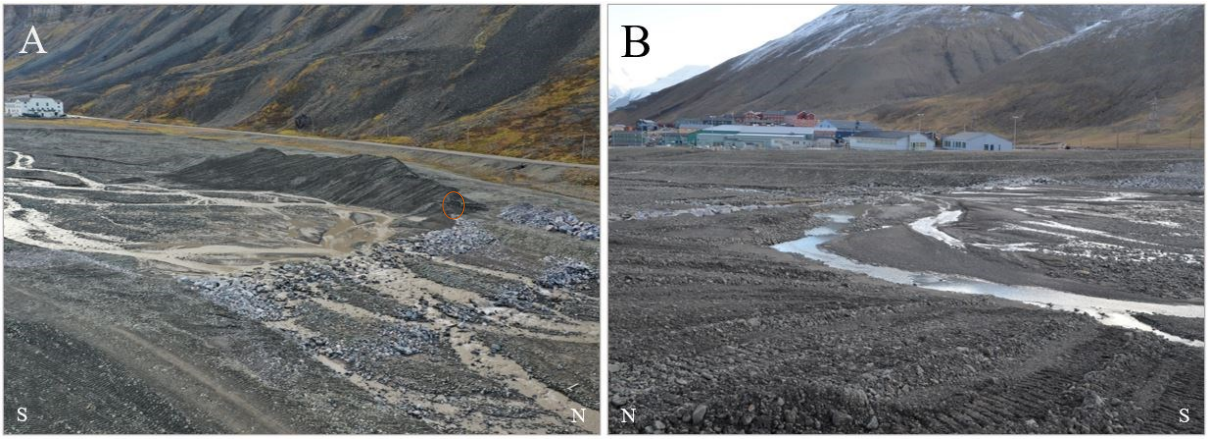

Figure 46: Sedimentation dam at the end of the monitoring period**. A**) September 11th, discharge 0.7m^3/s. Overview of the sedimentation dam. Braided stream and bars upstream, in flush with the weir crest, bedload accumulated on the apron and further downstream. Person for scale in the red circle. **B)** September 16th, discharge 0.1m^3/s, braided stream trough the top layer of fine sediments in the full sedimentation dam. Icing could be observed, especially on granitic gneiss used for construction.

4.6 Contribution to the long-term monitoring

All results presented in Chapter 4 above can serve as a baseline dataset for further research and contributes to the long-term monitoring, which is part of the overall intention of this project. An important aspect is how to ensure that data is made available as the project develops. Investigations that need to be continued (as planned) or started are listed below.

- Discharge and water stage measurements to produce an hourly hydrograph (planned).
- Monitor suspended sediment transport and bedload transport (planned).
- Document development at all sills and riprap. A combination of remote sensing and in situ measuring are favourable.
- Investigate the ground thermal regime with several thermometers in boreholes in and around the fluvial channel.
- Set up a server at UNIS, preferably cloud-based, where updated data is saved and made available after each field season.

The discharge, erosion and sediment transport monitoring are continued by Nowak and Rubensdotter (2021) with a ten-year perspective for now (Research in Svalbard (RIS) ID 11641). Master students affiliated with the projects start their fieldwork in June 2021.

5 Discussion

The findings presented in Chapter 4 are examined, reviewed, and put in context with other relevant publications in the following subsections. The results regarding discharge, sediment transport and sources are tackled first. Arguments for assessing the scour and flooding mitigation follows, and lastly, future recommended research questions.

5.1 Hydrograph and discharge measurements

Yde et al. (2008) differentiate the ablation season into three periods based on meltwater characteristics; the hydrograph from 2020 is hence divided into early ablation season, peak flow period, and late ablation season. 2020 was a relatively dry and cold year, and the snow cover was thin and limited to the elevated ravines and glaciers at the beginning of the monitoring period.

5.1.1 Early ablation season

The first rise in the hydrograph over three days on June 21st – 24th corresponds to increased air temperature and no precipitation. These observations indicate snowmelt as the main reason for the increasing discharge. The low EC in this early ablation period correlates with the findings from Yde et al. (2008) and could be explained by the water is flowing on top of the frozen sediments without collecting any solutes. Snowmelt induced floods early in the ablation season are common and observed in several hydrological studies on Svalbard (Grønsten, 1998; Etzelmüller et al., 2000; Bogen and Bønsnes, 2003; Riger-Kusk, 2006), this is arguably also the case in Longyearelva. The magnitude of the flood is considerably less than in the peak flow period.

5.1.2 Peak flow period

The record-high air temperatures in late July correlates with a massive peak in discharge during the Late July Flooding (see *Figure 22* and *Figure 23*). It is hence likely that the flood was caused by glacier melt. The water balance equation presented in *2.3 Hydrology* can be used to determine the source of the Late July Flooding. Arguments point in the direction that the flood was induced by glacial ablation, considering most of the snow had already melted during the early ablation season, and no precipitation was recorded. Glacier ablation and thawing of ground ice decrease the storage parameter (ΔM) and thus increase discharge. A correlation between daily average discharge and daily air temperatures was also documented in a different catchment by Nowak and Hodson (2013). Ground-water contribution cannot be excluded, but there are no direct measurements from this project to determine the exact contribution. Thawing of ground ice and increasing active layer thickness can allow water to percolate through the relative coarse fluvial sediments in Longyearelva and contribute to total discharge. However, the volumes from groundwater flow are likely insignificant compared to the input from glacier meltwater.

5.1.3 Late ablation season

The air temperature began to decline through August, which arguably caused the observed decrease in discharge and diurnal fluctuation. The daytime air temperature causes increased melt and runoff, while the discharge rapidly decreases as the temperature drops at nighttime. Diurnal fluctuations are recognized as a typical pattern in hydrological studies at the archipelago (e.g Etzelmüller et al., 2000; Hodgkins et al., 2003). The diurnal fluctuations are observed until August 23rd, where the discharge remains stable for nine days, despite close to 10mm of precipitation on August 29th. The fact that the temperature was close to zero at the measuring station on August 29th suggests precipitation as snow,

especially when considering the hypsographic curve from the catchment and the temperature-elevation relationship discussed in Nowak and Hodson (2013). Field observations confirm snow accumulating on the ground down to Skjeringa (50m.a.s.l) and minimal discharge in late August.

On September 3rd, both precipitation and air temperature increased, causing a minor peak discharge. It can be argued that an increase in storage caused stable discharge in late August since precipitation was solid, not liquid, the runoff was delayed. The peak in discharge on September 4th is, therefore, a result of saturated snow starting to melt, decreasing storage and precipitation as rain contributes to saturation of the snow and discharge. A distinctive drop in EC underlines the increased meltwater input, and the contribution from water from the active layer less noticeable. Despite high temperatures on September 9th, only a minor rise in the hydrograph could be observed. Most of the snow had melted at this point, precipitation was minimal, and the air temperature was likely not high enough to cause further change in storage, e.g., though glacial melt. A warm-swell in early September with increasing precipitation and discharge was also documented by Yde et al. (2008), and Nowak and Hodson (2013) found a correlation between precipitation and runoff in September-October. The low discharge continued after the monitoring period ended, and the time of final freeze-up is part of the data.

EC increases as the discharge decreases in August, potentially a combination of less meltwater that obscures the groundwater contribution and a deeper active layer capable of releasing more material to be diluted. Increased EC in the late ablation season is also recognized in previous work in Longyearelva by Yde et al. (2008). However, the EC measurements from 2020 are inconclusive for the actual groundwater contribution. Nevertheless, groundwater flow can constitute an increasing contribution to the water balance given the climate scenarios in NCCS (2019) with potential degradation of permafrost due to climate changes, and may no longer be neglected as discussed by Bense et al. (2009). The fact that geotechnical drilling by LNSS (2016) detected water at 5-6m depth at Sjøområdet could indicate groundwater, although the proximity to the fjord could mean that it is water from the fjord. Springs revealed as ridges of ice on Elvesletta (Pedersen, 2018) and pingos in the nearby Adventdalen (Hodson et al., 2020) are also signs of groundwater flow in the area.

5.1.1 Previous discharge measurement

Nowak et al. (2021) describe a westward bias regarding hydrological work on the archipelago, as a matter of fact, this can be an advantage for discussing the finding in this thesis, as the climatic conditions are similar. Work by NVE presented in Bogen and Bønsnes (2003) show discharge and sediment transport data over several years from Endalselva (1994-98). Previous work in Longyearelva by Grønsten (1998); Etzelmüller et al. (2000); Riger-Kusk (2006) has been limited to one, two, or three ablation seasons, in line with the general trend of individual projects running for only a relatively short period (see *Table 6*). However, they are still comparable to the results from 2020.

Table 6: Previous discharge monitoring projects in Longyearelva relative to the results from the monitoring conducted in 2020.

Reference	Year	Max [m^3/s]	Q mean [m^3/s]	Occurrence Q_{Max}
Etzelmüller	1993-95	6.7*		
Grønsten	1995	10	2.2	July 13th
Grønsten	1996	21	1.2	August 4th
Grønsten	1997	22	2.8	August 31st
Riger-Kusk	2004	16.5	0.9	July 3rd
	2020	**8.6**	**1.5**	**July 28th**

Comparing the data from previously discharge monitoring projects with the observations from 2020 reveals a decrease in peak discharge from the Longyearelva catchment and a Q_{mean} slightly under average. A result that is supported by the finding by Nowak et al. (2021) - smaller valley and cirque glaciers have already passed the peak runoff stage, even though the NCCS (2019) climate report predicts increased runoff as a result of climate change. The numbers from Etzelmüller et al. (2000) are uncertain, as no complete hydrograph was presented, only a description of discharge in the range of 2-4m^3/s from Longyearbreen and further stating that 60% of the total discharge in Longyearelva originate from Longyearbreen meltwater stream. The peak discharge in previous studies is typically recorded in the mid-to-late ablation season (July – August), and especially the timing of peak discharge from 1995 and 1996 corresponds with the results from 2020. The fact that most of the major floods are recorded in July-August, coincides with Hoseth and Daae (1996) preliminary catchment description, where late summer floods constitute the greatest hazard for the nearby infrastructure such as roads and pipelines that cross the valley floor.

The peak discharges from Grønsten (1998) and Riger-Kusk (2006) are considerably higher than the highest estimated discharge from 2020. However, there could be more to it than just the decreasing glacier coverage and available meltwater. Extreme events, such as precipitation outburst or record high temperatures, can cause considerably increased discharge – which was the case during the Late July Flooding. Preliminary flooding calculations by Sværd (1996) present an annual discharge estimate with Q_{peak} at 20m^3/s and a Q_{daily} at 10m^3/s, with a ±25% uncertainty. However, new calculations from Stenius (2016) presented in *Table 7* cast doubt on the previous flooding calculations and are based on updated data combined with new models.

Table 7: Preliminary and updated flooding calculations from Longyearelva, Q# indicate the expected return interval for the calculated floods.

Longyearelva	*Q2 daily (Q_{middle})*	*Q2 peak*	*Q100 daily*	*Q100 Peak*
NVE - Stenius (2016)	6.6m^3/s	9.9m^3/s	16.4m^3/s	24.6m^3/s
NVE - Sværd (1996)	10m^3/s	20m^3/s	24m^3/s	40m^3/s
2020 measured discharge	Q_{daily} = 5.4m^3/s	Q_{peak} hour 8.6m^3/s		

The updated flood values are used in designing the flooding mitigation in Bjordal and Hoseth (2017). Stenius (2016) poses more moderate discharge values both concerning Q_{peak} and daily average. The report further argues that the values from Sværd (1996) are too high due to limited data series and that the specific method used for the calculations tends to produce an overestimate. The numbers from Grønsten (1998) and Riger-Kusk (2006) are validated based on Sværd (1996) and could therefore be an overestimate as well. However, there is a possibility that the discharge from the catchment peaked during the turn of the millennium and has decreased ever since, an explanation supported by Nowak et al. (2021). Another possible explanation is that the high discharges are a product of annual fluctuations, which is something this long-term monitoring program aims to reveal.

The observed discharge from 2020 is relatively close to the Q_{2daily} values from Stenius (2016) presented in *Table 7*, meaning that the discharge observed during the 2020 ablation season should occur every other year (on average). However, record high temperatures were followed by considerable glacier melt. Therefore, the measured discharge from 2020 could be an underestimate, given that the temperature conditions were extreme.

The highest discharge measured was 7.4m^3/s at 9:08 pm July 28th, 1.2m^3/s lower than the highest extrapolated discharge, 8.6m3/s at 4:00 pm the same day. A lower discharge is expected in the evening compared with the afternoon as the temperature typically decreases. A 1.2m^3/s decrease in discharge over five hours is thus plausible. However, the air temperature remained relatively high, within the range of 10-12ºC, which could argue against such a drop in discharge. During the Late July Flooding, the high discharge caused severe erosion and sediment transport and further accumulation of sediments on the bridge weir. The pressure sensor became buried in sediments for a short period on July 29th and had to be manually retrieved and quickly recalibrated. Although the problem was fixed immediately, a discussion of the accuracy of the extrapolated discharges is required. The discharge from the 28th (evening) to the 29th (morning) could be underestimated and the actual discharge in the period was potentially higher. The record high temperatures could generate extreme glacier melt, which could have produced discharge higher than the estimated Q_{2peak} from Stenius (2016). However, the flooding calculation accounts for precipitation and ‘’worst-case events’’. There was no precipitation during the Late July Flooding, all the snow in the catchment had previously melted and general precipitation was under average in 2020. It is also a possibility that the computations from Stenius (2016) over-estimate, as Nowak et al. (2021) conclude that the runoff from small, glaciated catchments is decreasing, and the calculations are based on models, not specific data. Stenius (2016) also highlights the importance of better discharge data to validate the estimates the report presents - which this project aims to provide over the next ablation seasons.

The problems encountered during the monitoring period underlines the challenges with hydrological work in an Arctic environment. Despite minor challenges, the hydrological station was operative without any serious setbacks for the whole monitoring period, June 11th to September 15th. Ideas for improvements regarding the hydrological station are presented in *5.7 Suggested improvement.* Nevertheless, the hydrograph presented in this thesis illustrates the trend throughout the measuring period, even though the extrapolated values estimate the actual conditions during high floods in 2020. Problems were limited to the peak floods, >5m^3/s (2.5% exceedance), and fixed as quickly as possible.

5.2 Erosion and sediment transport

Longyearelva, with a constructed channel and anthropogenic disturbance, is far from the natural state of a High Arctic fluvial system, and this project will hopefully reveal how this will affect erosion and sediment transport. The SSC and SSY are based on the discharge, and potentially inaccuracies regarding discharge may be inflicted on the sediment transport calculations. The discharge data used for sediment transport calculations are therefore considered absolute henceforth. However, the results for sediment transport must be considered as an estimate and consequently used with caution.

5.2.1 Fluvial morphology and sediments

The fluvial sediments in Longyearelva have previously been described by Lied and Hestnes (1986) as coarse-grained, with limited content of fines, and the findings presented in this thesis support the general description. The qualitative observations are inconclusive for determining if Longyearelva can be defined as a gravel-bed or cobble-bed river according to the criteria in Bunte and Abt (2001). However, it is plausible that the term gravel-bed is suitable, given the mechanically week lithology and the observed quantities of granules and pebbles. The low content of fines means that the cohesive forces described in Self et al. (1989) are most likely not relevant in Longyearelva. Although the high SSY indicates large quantities of fine sediment exposed for erosion and suspended sediment transport – the lack of fines in the fluvial deposits can be due to the relatively short and turbulent flow regime. Imbrication between disk-shaped cobbles and small boulders, in proximity to the Longyearbreen moraine, coincides with the geomorphological mapping by Lied and Hestnes (1986) and the description of other Arctic sandar in Boothroyd and Ashley (1975). The disk-shape could originate from the horizontally bedded sandstones being crushed in rockfalls and frost weathered, as Lied and Hestnes (1986) state that frost weathering is the dominant process. Frost weathering in sedimentary rocks like the ones in the Longyearelva catchment has also been documented by Rudberg (1988).

The sorting of deposited sediments varies from absent to fining upwards. The sediments deposited between sills during 2020 show some grading as fines are deposited when the water flow declines. However, as the riverbed has been reworked with bulldozers for decades, the original sorting in the channel is uncertain. The deep erosive scarp in *Figure 34D* illustrates an absence of sorted sediments, arguable because bulldozers have reworked the deposits.

The Longyearelva is closer to its natural braided channel system upstream of the sedimentation dam. At the same time, it can be described as anastomosing, with relatively stable bars and less migrating thalweg from the dam and downstream where the riprap and sills affect the braiding.

5.2.2 SSC and SSY

In June-July, the daily SSY fluctuates with the discharge with higher peaks, compared to the more stable daily SSY in August. The observation described above is arguably due to the exhaustion of in-channel stored sediment during the snowmelt-induced floods, while the sediment supply is more consistent in August. Flushing of inter-channel stored sediments early in the ablation season is also recognized by Bogen (1980). The SSC follows the diurnal discharge fluctuations over the monitoring period, with a slight delay between the peak discharge and peak in SSC. The coupling between discharge and SSC is observed in several projects (e.g., Hodson et al., 1998; Hodson and Ferguson, 1999); Bogen and Bønsnes (2003); (Hodgkins et al., 2003). However, the correlation between discharge and SSC is not constant; for instance, Hodson et al. (1998) show increased SSC over the ablation period. A shift from high SSC in the rising limb of the hydrograph to a lag between peak discharge and peak SSC was observed in Hodgkins (1996). Hodson et al. (1998)

argue that as the active layer thickness increases over the ablation season. More sediments are made available for fluvial transport, and the coupling between SSC and discharge may shift. Increased SSC was observed with increasing discharge in Longyearelva without a clear correlation. However, an R^2 of 0.58 is a moderate correlation, considered the numbers of variables in nature. A slightly higher SSC with the same discharge later in the ablation season is most likely a combination of a higher sediment supply due to increasing active layer thickness and the construction work in the channel next to Nybyen. Etzelmüller et al. (2000) also highlight variations within the same catchment, as a good correlation between SSC and discharge was observed from Longyearbreen and the contrary from Larsbreen.

Bogen (1980) motivates an explanation that sediments are temporarily stored within the channel, and the highest SSC will hence occur during the rising limb of a flood as the accumulated sediments are flushed out. Hodson et al. (1998) documented a higher SSC during the rising limb of the hydrograph in a small, glaciated catchment – which supports the findings in Bogen (1980). The same was observed in Canada, as Hammer and Smith (1983) recorded the highest SSC during the rising limb of the hydrograph during floods, as well as an increased SSC as the active layer thickens. The findings from Longyearelva in 2020 correspond with the results from the projects mentioned above, as the highest SSC was documented at the beginning of the Late July Flooding, and observations after the flood confirm storage of sediment within the channel, potentially avaliable to be flushed by the next flood. Sediment sources are further discussed in *5.2.4 Sediment sources*.

Etzelmüller et al. (2000) measured sediment transport from the glaciers in Longyeardalen in 1993-94 and found SSC at average 0.5g/l and peaks above 6g/l ($Q=3m^3/s$) from Longyearbreen meltwater stream in 1994. The sediment transport was further characterized as high from both glaciers, although the correlation between SSC and discharge was different.

Riger-Kusk (2006) measured SSC up to 13.7g/l in the meltwater stream from Longyearbreen and a mean SSC at 1.3g/l for the 2004 ablation season. Bogen and Bønsnes (2003) present data from Endalselva, and the SCC annual peak were measured to 2.5-10g/l at discharges from $7m^3/s$ to $13m^3/s$. The results from the research projects are presented in *Table 8*, and are all lower than the highest SSC measured in 2020. The mean SSC at 1.9g/l in 2020 is a 46% increase from Riger-Kusk (2006) and a 280% increase from Etzelmüller et al. (2000).

There can be several reasons for the increased SSC in Longyearelva compared to the earlier work. As mentioned, Longyearelva is relative unique due to the anthropogenic influence, and the changes in the moraine system in front of Longyearbreen are discussed in detail later. An abundance of sediment is available for transport due to erosion and slumping in the moraines. More sediments might be available at the channel be as 2020 was the first year after construction work was finished. The straightening and narrowing of the river from the dam to the outlet might have increased the erosive forces in this section (discussed in more detail in *5.4 Effect of sills and riprap*). There is a possibility that the fluvial system needs time to exhaust sediment left by the heavy machinery during construction before it stabilizes, and a trend in SSY can be noticed.

Directly comparison of the SSC results from this project, and the SSC monitoring from Etzelmüller et al. (2000) might be problematic. Etzelmüller et al. (2000) did not cover the same timespan as in this project, nether the whole Longyearelva catchment - only the SSC from each meltwater streams. The highest peaks in SSC could be missing from Etzelmüller et al. (2000) if a significant sediment source was located downstream of the measuring

point. The same problem could be the case for Riger-Kusk (2006), which only investigates the Longyearbreen meltwater stream, although covering the same period of the ablation season as this project. The specific suspended sediment yield is consequently more comparable as it accounts for the catchment area.

As discussed, the discharge did not exceed the estimated mean annual flood, but the SSC is higher than in the comparable data series. The SSY from Longyearelva in 2020 is higher than the presented data from catchments with approximately the same size and glacier coverage. Numbers regarding SSC and specific SSY from catchments on Svalbard and this project are presented in *Table 8*.

Table 8: Comparable sediment transport and discharge, from Bogen and Bønsnes (2003) and Riger-Kusk (2006)

Catchment	**Size [km^2], glacier coverage [%]**	**SSC max/mean [g/l]**	**SSY [t] Max/mean**	**Specific sediment yield [t/km^2/yr]**
Bayelva (1990-01)	30.9, 55%	11.5/0.3	22 797 / 11 104	359
Endalselva (1994-98)	28.8, 20%	9.0/0.6	16 359 / 8102	281
Longyearbreen (2004)	10.7, 43%	13.7/1.3	8910	830
Longyearelva (2020)	**22.2, <26%**	**24.1**	**41050**	**1849**

Based on the data presented above, Longyearelva is, in fact, more comparable to a catchment with a warm-based or polythermal glacier (see *Table 9*), e.g., the sediment yield from the warm-based Finsterwalderbreen glacier meltwater stream (Hodson and Ferguson, 1999) (Hodgkins et al., 2003). However, the data is 20 years old, and a conclusion cannot be made based on a singular season. The site-specific weather condition in the particular projects is not accounted for, and the anticipated increased erosion due to climate changes could already be prevalent.

Table 9: Sediment transport from glaciers with different thermal regimes (Hodson and Ferguson, 1999; Hodgkins et al. 2003)

Glacier /catchment	**Thermal regime**	**Mean discharge [m^3/s]**	**Mean SSC [g/l]**	**SSY [t/km^2/yr]**
Finsterwalderbreen	Warm-based	4.0	2.0	1800-2700
Austre Brøggerbreen	Cold-based	2.1	0.1	-
Erdmannbreen	Polythermal	2.2	1.5	-
Longyearelva (2020)	**Cold-based**	**1.5**	**1.9**	**1849**

Thus, the high sediment transport can be due to something else than the thermal regime in the glaciers alone. Etzelmüller et al. (2000) estimated SSY from Longyearelva to be 1500t/km^2/yr, which adds weight to the results from 2020. The NCCS (2019) report predicts increased erosion rates and sediment transport as the runoff increases with a

changing climate. However, the increased erosion might be discussable, as the increasing discharge is contested by Nowak et al. (2021). The 2020 ablation season sediment yield could be an anomaly due to the record high temperatures and construction work. The findings from Bogen and Bønsnes (2003) and Hodgkins et al. (2003) all show relatively large annual fluctuations for sediment transport, which support a hypothesis that 2020 is an irregularity. An alternative explanation may well be that the observed erosion and sediment transport are a part of the projected increased erosion rates. With that said, the Longyearelva catchment may not be representative of the projection in the NCCS (2019) due to the anthropogenic disturbance. The characteristics of erosion and the sediment yield in the catchment can truely be investigated as the monitoring in Longyearelva is continued.

5.2.3 Bedload transport

Sediment transport as bedload has been observed and measured over the monitoring period from June 5th to September 15th. 5.2% of the passive tracers were retrieved, although the actual retrieving rate was 3.8%, as two (1.5%) of the tracers placed in the river were not in contact with the water over the monitoring period. The 3.8% is less than the 5% retrieving rate in Laronne and Carson (1976), but still acceptable for the method. The larger tracers were easier to monitor during high floods and relocate at the end, illustrated by a 10% retrieving rate for Class 4 tracers, 6.7% of Class 3, and 0% retrieving rate of Class 1 and 2. The decreasing retrieving rate with decreasing grain size, coincides with the findings in Laronne and Carson (1976) and projects on the Norway mainland (Engvik, 2011). The two tracers from Class 3 were transported over a longer distance than the three tracers from Class 4, as expected, based on the Shield parameter and the Hjulstöm Curve.

None of the passive tracers from Hu-pt was found at the end. They have most likely accumulated and buried in the sedimentation dam. There is a possibility that the Hu-pt tracers were buried at their starting position, although the documented transport further downstream indicates transport of all classes. The channelizing of the water can have increased the erosive forces, and the transport capacity downstream of the sedimentation dam might be higher than upstream. The sediment that accumulated on the bridge pier and buried the pressure sensor on July 29th was in the range from sand to pebble, meaning that Class 1 sediment was transported as bedload. Class 1 and 2 from Pr-pt could have been transported into the fjord, but that would mean 650m travel distance. The missing tracers are believed buried or impossible to locate if the colour has disappeared.

The largest classes are of interest to determine the competence of the river. The largest tracer missing measured 250mm and weighed 13kg, and transport of three other Class 4 tracers was documented. Thus, the competence of the channelized section of Longyearelva during the 2020 ablation season is at least large cobbles or small boulders at ~250mm. The actual competence is hard to establish, as none of the tracers remained stationary at their starting position after being submerged. The shear stress working on the riverbed changes with the channel morphology and dimensions, based on the parameters explained in Chapter *2.4 Erosion*. Hence, the competence could be changing over the length of the river. The effect of a potential armouring layer of larger sediments as described in Pitlick et al. (2008) has not developed in Longyearelva, although some sorting was documented in the constructed channel. As the frequent use of bulldozers and massive bedload transport decreases with the ned constructions, it is plausible that sediments under the transport capacity will be removed, and the remaining boulders will protect underlying sediments between the sills. The scour mitigation can be considered highly successful if

the system develops into a naturally armoured channel that remains stable until an extreme flooding event triggers extensive erosion.

The mass of the transported tracers is 274kg. However, the total mass or volumes of sediments transported as bedload in Longyearelva during the 2020 measuring period is challenging to estimate with the available data. The sedimentation dam was constructed to hold 30 000m^3 of sediments; it was filled and emptied over the monitoring period, which indicates that at least 30 000m^3 of sediment were transported in the upper part of the river. The total volume and mass of bedload transport further downstream to the outlet are harder to estimate. However, preliminary investigations by Øvereng (1989) suggest 2500-6000m^3 of bedload for the system, which is only 8-20% of the volumes accumulated in the sedimentation dam and are therefore considered to be a modest estimate. Øvereng (1989) discusses how bedload can be approximately 30% of the SSY and potentially even higher given the characteristics of Longyearelva. The 30% SSY estimate would mean a bedload yield of around 12 000t, twice the preliminary estimate by Øvereng (1989). The sediment transport review by Orwin et al. (2010) illustrates bedload transport ranging from 600 to >40 000 t/yr, and the estimate from Longyearelva is within this wide range. In the end, accurate quantification of the bedload is highly uncertain, both regarding mass and volume.

An approximation of bedload transport distance in Longyearelva could be based on the results from the passive tracers. If the discharge in 2020 is the typical flow regime, the cobbles and boulders from Class 3 and 4 would need 13-26 years to move the 2200m from the sedimentation dam to the outlet. Regarding pebbles and small cobbles, the transport distances are more uncertain as no tracers from Class 1 and 2 were retrieved. Despite the lack of transport distance data, an estimate could be made of the following hypothetic figment.

Transport (8m) of Class 1 and 2 was documented at discharge up to 3.7m^3/s on June 24th. Based on setting 3.0m^3/s as a threshold for transport of Class 1 and 2 and an analysis of the hourly hydrograph, and approximate transport speed on June 24th is 2.7m/h. The 3.0m^3/s threshold value is based on observed transport of Class 3 at discharge down to 3.1m^3/s. Hypothetical transport distances for Class 1 and 2 could further be estimated based on the duration curve of 2020 and 3.0m^3/s as the threshold. The duration curve indicates an 8.3% exceedance (or 189 hours) of the defined threshold discharge during the 2020 monitoring period. Combing the 2.7m/h transport on June 24th with the 189 hours with discharge over the threshold, hypothetical transport distance for Class 1 and 2 could be in the range of 300-500m. The numbers are highly uncertain, as the conditions and parameters involved in both the Shield parameter and Du Boys equation will change over the length of the channel, and Class 1 would have a lower threshold for transport than the larger Class 2. The same discharge can cause a range of shear stress on the channel bed depending on the water depth, gradient, and roughness. The transport could also be considerably faster during the peak floods. Additionally, a migrating thalweg could have left tracers outside the water, as was the case for three Class 4 tracers at Pr-pt. The 189 hours is, therefore, a maximum. None the less, one could argue that the construction work in August did not affect the observed bedload in the constructed channel and had a limited effect on accumulation rates in the sedimentation dam.

Bedload measurements in Scott River by Kociuba et al. (2012), determined threshold discharge at 1-1.3m^3/s for initial movement and bedload transport. Grain size is not particularly mentioned (introduced as a gravel-bed river), and a comparison with the

hypothetical threshold values from Longyearelva is therefore inappropriate. Sediment sources and how the sills and riprap influenced the erosion and bedload transport will be discussed further in *5.4 Effect of sills and riprap.*

The riverbed may have been extra unstable during the 2020 ablation season, as an armouring layer had not reestablished after being disturbed by the heavy machinery in 2019. Laronne and Carson (1976) further described how the painted tracers in their study were plausible more easily transported as the tracers were placed on top of the riverbed. The placement causes a reduction of the friction point illustrated in *Figure 12*. The passive tracers in Longyearelva are considered representative, as they were placed in a riverbed without a defined armoured top layer.

5.2.4 Sediment sources

The Late July Flooding accounts for the highest SSC and 57% of the total SSY, and it was undoubtedly high sediment transport at the time. However, the sediment sources may differ from other sites on Svalbard. The riverbed had been reworked by heavy machinery for decades, and the sills and riprap have arguably changed the flow regime as the wetting perimeter is more constant than in a natural braided stream.

A clear difference between the am- and pm-samples for SSC could be observed in the results after August 5th, when the construction work next to Nybyen started. While the discharge continued with the same diurnal fluctuations during weekends, the SSC was lower on Sundays and Monday mornings before the construction work resumed. The influence of construction work next to Nybyen has arguably increased the SSC in August.

Frost action is recognized as a prominent weathering process due to the mechanically week bedrock in the CTB (Hoseth and Daae, 1996). The combination of steep mountainsides and frost action leads to repeatedly rockfall and thus sediment input. Etzelmüller et al. (2000) discuss how the glaciers play a role as a conveyor belt for sediment accumulated from the steep slopes in the southern end of the valley and link the fluvial system and hillslope processes together. The cold-based glaciers in the catchment do not contribute to the sediment input with basal abrasion, a statement supported by the observations of in situ vegetation at the base in Humlum et al. (2005). However, the supra-glacial channels can transport material from the supraglacial moraines and into the fluvial system.

Permafrost with high ice content supports the grain structures and thus increases the mechanical strength of the soil until it thaws. As several articles conclude, more sediment is available for transport as the active layer thickness increases over the ablation season (e.g., Hammer and Smith, 1983; Hodson et al., 1998; Hodgkins et al., 2003; Kociuba, 2014). Thus, the available sediment source will change over the season. Etzelmüller et al. (2000) explore the different sediment sources in the catchment and propose the moraines as the primary sediment sources and the fluvial channel as a secondary contributor. Proglacial moraines and sandur are recognized as the main sediment source in several publications (e.g., Hodson et al., 1998; Orwin et al., 2010; Kociuba, 2014). Thermokarst and slumping in the moraines in Longyeardalen were observed in the 2020 season (see *5.5 Geomorphological changes*). The sediment input in the eroding meltwater streams is therefore unlimited with a one-season perspective. The anticipated increased erosion and sediment yield in NCCS (2019) is based on an increase in runoff and a deeper active layer. As discussed, the increase in discharge is debated, but a deeper active layer would make more sediment available for transport, and the active layer in Longyearbyen is increasing towards the river (Bjordal and Hoseth, 2017).

The sedimentation dam worked as intended until the Late July Flooding event, and most of the downstream bedload must therefore originate from sediment sources within the channel. The sedimentation dam was overflooded for approximately 1-2 weeks and acted as a sediment source for downstream bedload transport until it was emptied on August 11th. Suspended sediment transport continued throughout the season, but the suspended sediment does not constitute a problem for the flooding mitigation, as fines are mostly just flushed through (Øvereng, 1989; Bjordal and Hoseth, 2017). Nevertheless, flushing out all the fines in between the larger particles decreases the matrix support and increases the infiltration. Thus, potentially changing the properties for the active layer as the proportion of solids, water, and air are rearranged. High SSC increases the density of the water, and theoretically, this could cause increased shear stress on the channel bed. To what extent the SSC in Longyearelva sufficiently increases the shear stress is uncertain but considered limited.

5.3 Sedimentation dam

The sedimentation dam was built to control the sediment supply, and the goal was achieved apart from a short period in July-August. The dam should have the capacity for accumulating sediments in 2021 after being excavated in mid-august. However, if 2020 represents a typical year considering sediment yield, the dam will need to be emptied every year. It could therefore be beneficial to schedule excavation of the dam early in June. As the anticipated highest discharge occurs during the peak flow period, the capacity would then be at a maximum before the highest bedload. Increasing the depth in the dam would increase the available volume if it proves to be a limitation. However, excavation towards the sides and crest must be done with caution, and the thalweg should be kept in the middle of the channel to avoid undercutting and potential dam-break.

According to Hoseth and Daae (1996), shutting off the sediment supply would escalate the downstream erosion and channel degradation. A complete stop in sediment supply might, therefore, not be ideal. It could be a possibility to accept limited sediment supply and intentionally allow the sediment budget downstream to stabilize gradually.

Construction work next to Nybyen from early August could have increased the bedload and led to a higher accumulation rate. Although, it must be considered whether the work, in reality, contributed to an increased bedload. Cobbles (150-250mm) would need 4-9 years to be transported the ~800m from the construction site in Nybyen to the sedimentation dam (based on the recorded transport distance for the passive tracers of Class 3 and 4). Sand, gravel, and cobble (<150mm) could accumulate in the dam earlier, maybe even in 2020, as threshold discharges for movement are decreasing with decreasing grain size.

A bulldozer had to dig out a new thalweg and reinforce the levees with gravel directly upstream the weir under Veg106 during the Late July Flooding. The combination of digging and high discharge at the time could have escalated bedload, but only for a limited period. Therefore, it is believed that most of the accumulated sediments in 2020 originates from the fluvial plane downstream of Veg106.

5.4 Effect of sills and riprap

The completion of the scour and flooding mitigation in 2019 marks a new period in the expansion of Longyearbyen. Longyearelva is now limited to a 30-40m wide channel, unrecognizable from the 3-400m wide sandur with a braided meltwater channel.

5.4.1 Construction and design

Construction started in 2016, with testing and reinforcement around bridge weirs. The construction plan by Bjordal and Hoseth (2017) describes a problem with the sills after the first flood, as the initial quarry rock was too small compared to the competence of the river. The statement is supported by the findings from 2020, as gravel and cobbles of granitic gneiss mixed with the fluvial sediments. The sills southwards from Veg501, including the sedimentation dam, were completed in 2019. The fact that the construction took four years to complete can be part of the explanation of why the sills have responded differently. The oldest sills, Sill 9, 15, 18, and 19, have accumulated sediments and are partly or entirely buried on September 15th. These oldest sills were built according to the construction plan by Bjordal and Hoseth (2017) and the recommendations in Fergus et al. (2010). Whereas the youngest sills, from Veg501 to the sedimentation dam was constructed with a downstream drop, meaning that the sills were not in flush with the channel bed (personal communication with Anders Bjordal (*NVE*) and Øyvind Hellum (*former LL*)). The downstream drop causes increased speed and erosive forces directly downstream the sills, creating scour holes. These downstream drops and scour holes are particularly prominent in the annotated figures in *4.5.1 Sills and riprap*. Erosion causes loss of downstream support for the sills, and the chance of collapse and or subsidence could increase. Hence, the scouring and flushing of downstream sediments contributed to the collapse of Sill 8. The fact that Sill 17 also developed a 50-100cm downstream drop without collapsing implies a more intricate explanation than the lack of downstream support alone.

The larger boulders, >800mm, are more frequent in the youngest sills from Veg 501 and southwards to the sedimentation dam (section 1). However, even boulders (1000mm) of granite gneiss have moved out of their initial position during the monitoring period, e.g., on Sill 7. The movement is more likely due to fundament scouring and subsidence rather than forces induced by the water. The boulder size granitic gneiss is in general sufficient for construction, despite some displacement. The sills that are in flush, with intact downstream support (as initially planned), have remained stable during the monitoring period. A possible improvement of the construction could be to put the collapsed sills back together and further replace the eroded sediment downstream. Thereby minimize the drop, prevent a standing wave, and thus decrease the erosive forces. Simultaneous reestablish the downstream support of the sills could limit the displacement.

The sills are constructed perpendicular to the flow direction, straight across the channel. The erosive forces are previously described and could be decreased if the water is spread over the whole width of the channel. If the sills were built with a low angle V-shape pointing upstream, the interlocking between boulders may be more stable (Fergus et al., 2010). If the thalweg remained stable in the centre of the channel, each sill could act like a plough, splitting the water over a larger area and decreasing the erosive forces. However, in a dynamic system like Longyearelva, a static thalweg would be doubtful, and the construction would be exposed if the thalweg shifts towards the sides. Firstly, it would require even more blasted rock to be shipped from the mainland, thereby making the project more resource-demanding. Secondly, the thalweg has shifted repeatedly over the 2020 monitoring period; controlling the thalweg would require more construction work and background data. Nevertheless, since the sedimentation dam is shutting off the bedload sediment supply, it would imply a more stable thalweg. Reid and Church (2015) discuss how the full effect of scour protection is uncertain, as a fluvial system requires time to adjust. The actual results of the construction work in Longyearelva are a few years into the future. However, the number one objective for the scour and flooding mitigation is to

protect the Elvesletta area, not to investigate the geomorphological effect of riprap. Reinforcements should therefore be done before any potential problems and not postponed to see what happens.

5.4.2 Gradient and channel width

Part of the explanation of how the sills responded could be linked to the channel geometry. Channel width and gradient are not constant in Longyearelva, and as both parameters are importing regarding erosive forces, are they discussed in the following section.

The channel gradient decreases from Sill 1 to Sill 19, reflecting the general observation of more erosion upstream of Veg501, compared to the lower parts downstream Sill 15. The steepest gradient is between the dam-crest and Sill 1, with a fall of 4.3m over 80m (3.1º). The dam is built with a sufficient apron to reduce energy, and Sill 1 does not show signs of more damage than the other sills, despite the steepest gradient. For the rest of Section 1 (sill 1- 8), the gradient decreases, although there is a slight increase between Sill 4 and 5. The damage on Sill 2-7 is consistent, as the sills have the same characteristics and consequently similar shear stress and erosion. The damages indicate forces above the threshold shear stress for bedload transport, and the spacing in this section could with advantage been shorter to reduce the gradient. The exception is Sill 8, which has the most extensive damage, despite the lowest gradient in Section 1. The gradient can, therefore, not be the only factor. The low gradient (1.7º) from Sill 7-8 is increased by 29% between Sill 8-9 (2.2º). The combination of increased water speed, a westward curve, and narrowing of the channel (by >50%), can explain the severe erosion on the eastern side of the channel and Sill 8. Reid and Church (2015) state that riprap placed in the outer bend can increase the water speed and thus the erosive forces. Larger boulders would help improve the channel roughness and further reduce the water speed. Reid and Church (2015) describe potential problems with erosion in the transition between riprap and natural levees. The sills in Longyearelva are hence continuous on both sides to avoid the problem. These transitions (between sills, riprap and natural riverbed) are also emphasized as exposed locations in the building plan by Bjordal and Hoseth (2017). Observations in 2020 confirm erosion in these locations, despite the concern in the building plan. Scour hole development and undercutting of riprap can, over time, expose the underlying gravel and escalate the damages to the construction. The eastern bank upstream Veg 501 and Sill 8 are therefore in need of repair and reinforcements, as the observations from 2020 point at this section as an exposed area.

Sill 9 is narrow, directly under the bridge at Veg501, and built at the same time as the bridge weir was upgraded (Larsen, 2016). Sill 9 has limited damage despite the increasing gradient from Sill 8. The channel widens and flattens directly downstream, and sediments accumulated over Sill 10 and 11. Considering the severe erosion downstream Sill 8, and the documented transport distances in the river, the accumulated sediments could originate from the area around Sill 8.

Accumulation of sediments as the gradient decreases and the channel widens is also observed at Sill 15-19, as they are in flush with the bed or partly buried. The exception is Sill 17, which has a pronounced scour hole over the whole width of the sill. Despite average width, spacing, and relative low gradient, an 80-100cm drop has developed at Sill 17, and riprap is exposed for undercutting. The explanation could be an increasing gradient from Sill 17 to 18, only from 1.4º to 1.6º, a 14% increase, but in combination with a marginal westward curve, the product could be higher shear stress and erosion. The channel characteristics around Sill 8 and 17 have some similarities, and these sills show severe

downstream erosion. The combination of increased gradient and a curve downstream is arguable critical.

Glover et al. (2012) reviews erosive measurements in Norwegian rivers and point out an upper limit of 2m/km gradient for check dams or steps - Section 1 in Longyearelva has a 38m/km gradient. Downstream erosion has reworked the sills into steps, and as there are no aprons or energy-reducing construction downstream the sills, the damages will impair if the sills are not repaired. The report further highlights the importance of spacing related to the slope of the channel, and the spacing in section 1 is too long, as previously addressed. Both spacing and gradient are too costly or impossible to rearrange at this point in Longyearelva. A potential solution could be to establish an energy-reducing structure by extending the sills downstream and create a small step in the middle. Digging a new ditch downstream the damaged sills, e.g., 2m wide and 1.5m deeper than the existing crest, making a 5m broad sill, with a 0.5 step for energy reduction, illustrated. This solution would not change the gradient, nether the channel width, although it would reduce the energy of the water over each sill. Constructing a ‘’step-sill’’ should be considered for sills in Section 1 and sills with downstream erosion in the other sections, such as Sill 17.

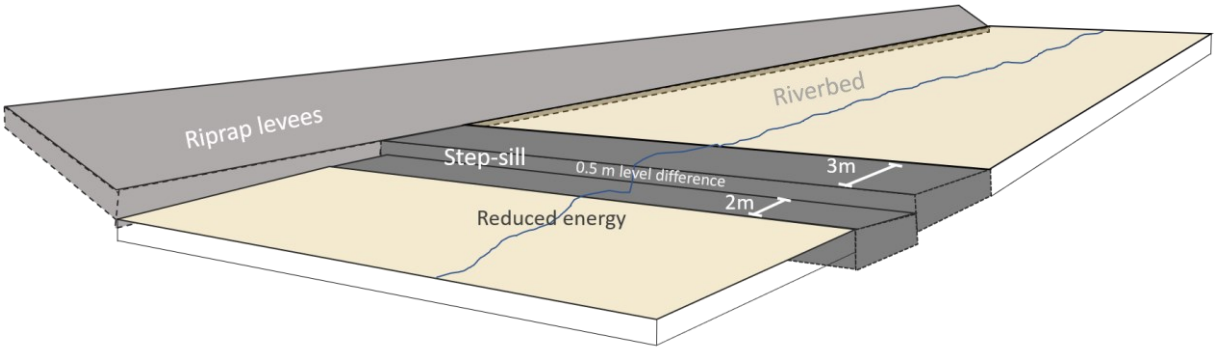

Figure 47: Based on the discussion in the text, the figure illustates the suggested expansion of damaged sills, creating a level-difference for reducing the energy of the water.

Several sources (e.g., Fergus et al., 2010; Bjordal and Hoseth, 2017) claim that sections, where the channel narrows down should be added more protection, such as under bridges and in curves. The sills connected to bridges and narrow stretches of the Longyearelva river were constructed in 2016-2017. Sills 9, 15, and 18 are entirely or partly buried in sediments, despite expectations of enhanced erosion as the channel narrows down. Sediments could have accumulated during the years of construction, as the sills and riprap in Sections 2-4 were operative before the sediment supply was controlled.

5.4.3. Thermal regime

As described in chapter *2.2 Heat flow and thermodynamics*, the mechanical strength of sediments increases as the grain skeleton is reinforced with ice. The explanation for the collapse and subsidence of the sills can be linked to changes in the thermal regime. Several factors arguably affect the ground thermal regime:

- Reworking the fluvial sediments in 2019 (September-October) could have postponed the natural freeze-up.
- Foreign lithologies (granitic gneiss) with different thermal properties were used as a building material
- Increase the ground moisture by channelizing the water.

The factors above, combined with record high temperatures in 2020, have most likely affected the ground thermal regime. Increased temperature of the ice-rich permafrost could have decreased the foundation's mechanical strength. Increased moisture could have produced a high-temperature gradient through the ground, but temperature readings are necessary to test the hypothesis. The lack of ground temperature readings in the channel causes this discussion to be based on previous work and assumptions of the local thermal properties, especially if the ground properties have changed. The channel characteristics around Sill 8 and 17 are described as quite similar; however, Sill 8 collapsed while Sill 17 remained intact despite downstream erosion. Could the explanation be related to reestablishing the permafrost after construction work?

The permafrost on Svalbard tends to be deeper in bedrock than in sediments due to different thermal properties (Larsen, 2016). The boulders of granitic gneiss could act as heat bridges since they have a higher thermal conductivity than the local sedimentary lithologies. The 1m deep ditch where the boulders were placed allows the energy to be transported into the active layer, both through the boulders and as water instantaneously percolates down. A deeper active layer can consequently develop underneath the sills. The increased load from the sills on a mechanically weakened grain structure can explain the observed subsidence. The subsided parts and the thalweg seem to overlap, but whether the water caused subsidence or the subsidence causes a favourable water path is unclear. Arguably, the thawed ground could be more exposed for erosion, and smaller grain sizes might be washed away as the thalweg remains stable over a collapse or subsided part. A potentially constant scouring could have weakened the foundation and escalated the problems.

Preliminary investigations by Bjordal and Hoseth (2017) revealed a deeper active layer in the river channel than the surroundings, probably due to the water-air conductivity ratio. The channels in an undisturbed sandur will migrate and continuously rearrange the thermal properties of the uppermost sediment layer as the water content shifts. Water in Longyearelva is confined, and the ground is presumably constantly saturated. Woo and Xia (1996) accentuate the importance of water content in the active layer as it strongly influences the ground thermal properties and the heat flux through the sediments.

Christiansen et al. (2021) described thaw depth down to 500m at Hornsund and introduced groundwater flow as part of the reason combined with the high conductivity of the specific lithology. Suggesting that groundwater flow causes increased thaw depths are of high interest for the active layer development around Longyearelva. The average water temperature in Longyearelva in 2020 was 2.9ºC, which implies an effective way of transferring energy through the active layer given the high thermal conductivity of water. Cooper et al. (2002) investigated groundwater flow through the active layer in the sandur

at Finsterwaldbreen, 80km south of Longyearbyen. The findings indicate groundwater recharge from the meltwater streams, and lakes and an inverse correlation of meltwater discharge and groundwater flow as the latter increases late in the ablation season. The observed increased EC in Longyearelva in August and September could point toward increased groundwater flow through the active layer over the ablation season. The increased active layer thickness gives a postive feedback, as more water is allowed to migrate through the sediments, thus acelarete the heat flux.

As snow and ice accumulate in the Longyearelva channel during winter, the insulation from cold temperatures is increased. Refreezing of the active layer could be slowed down, and the thawing over the next summer could penetrate even deeper. The above are only speculations, nevertheless of interest when considering the long-time effect of the channelization and the expected lifetime of the sills. The climate changes and temperature increase in the Arctic are of high importance regarding the thermal properties in the ground (NCCS, 2019). A deeper active layer leads to additional groundwater flow and thus a self-destructing system where a combination of several factors pulls in a negative direction concerning the mechanical strength of the ground and, therefore, the stability of the sills. It must be stressed that all the parameters discussed in the previous sub-sections affect each other and underscores the complexity of a High Arctic fluvial system like Longyearelva.

An explanation to why the sills responded differently could be linked to how the permafrost reestablished after the construction work and if the ground retained its initial strength. Construction work in September-October delays the refreezing of the ground and disturbs the natural temperature fluctuations. Problems with frozen ground as a building material are well known. After building the Svalbard Global Seed Vault, artificial cooling of the construction site was necessary to re-establish the permafrost and achieve the anticipated foundation and avoid further problems (Statsbygg, 2019). Settling damage caused by changes in the ground thermal regime has also been challenging for buildings in Longyearbyen (Instanes and Rongved, 2017; Larsen, 2016). The permafrost under Sill 17 has had two years to re-establish, while the sills in Section 1 had only one winter, and the construction work late in autumn postponed the natural refreezing. Therefore, the foundation is not as strong as in the rest of the channel, this combined with parameters as width and gradient, could explain the different response over the 2020 ablation season. The subsidence and collapse of sills in Section 1 are thought to be linked to declining foundation strength, a statement supported by the mentioned related problems for other constructions in the area.

5.5 Geomorphological changes

The geomorphological changes will be more pronounced as this project continues in the coming years, as the data for detecting and evaluating changes will grow. However, previous research in the Longyearelva catchment allows some discussion of geomorphological features observed in 2020.

Bigger slumps or landslides are anticipated in the Arctic, given the current climate changes presented in NCCS (2019). Increased thermokarst activity as a consequence of extreme summer climate has already been documented by Lewkowicz and Way (2019) in Arctic Canada. Considered the record high temperatures in Longyearbyen in 2020, the observed landslide activity in the moraines could hence be expected. Akerman (2005) investigated the connection between active layer thickness and solifluction, as the mass movement increases with a deeper active layer. Akerman (2005) also found a correlation between air

temperature and movement and further emphasizes the importance of soil moisture related to ground thermal regime – which adds weight to the arguments of decreasing mechanical strength as the ground thaws at river channel. Lewkowicz and Way (2019) highlight how ice-rich permafrost in their study area is extra vulnerable to increased summer temperatures, a statement directly transmissible to the permafrost conditions in Longyeardalen as Wawrzyniak and Osuch (2020) documented how Svalbard is heating up faster than the rest of the Arctic.

It is unlikely that increased sediment input in the moraines contributed to filling the sedimentation dam in 2020, based on the bedload monitoring. However, a continuous increase in sediment input to the fluvial system could lead to more rapid filling of the sedimentation dam and thus increase the workload and maintenance cost. Therefore, the true value of this project is to investigate changes over time and discuss the finding versus climate models presented in NCCS (2019).

5.5.1 Larsbreen moraine and alluvial fan

The deep ravine is a distinct feature in the moraine and is vital for the morphological development and sediment supply in the fluvial system. Thermokarsts and active layer detachments described in Etzelmüller et al. (2000) were also documented during the 2020 monitoring period. The active layer detachments and fluvial toe-erosion are escalating the processes of increasing active layer thickness, in addition to the ground thermal regime. Each time material is removed from the slopes, new ice or previously frozen sediment are exposed to the heat exchange with the air. The impermeable permafrost provides a low friction gliding surface as the active layer becomes saturated and potentially detach. Permafrost serving as a gliding surface for landslides is also recognized by Larsen (2016). As the slope toe is eroded during floods, the gravity mass movements could increase as the sides of the ravine becomes steeper.

Climate-related increased thaw depth combined with intense precipitation could cause sizable mass movement events into the narrow ravine. A potential damming of the meltwater stream followed by a dam-break and meltwater outburst constitutes a hazard for Nybyen and infrastructure further down the valley. It is plausible that the active layer in the moraine became deeper than usual, and the sediment input to the fluvial channel increased during record high temperatures in 2020. Therefore, monitoring the erosion and landslide activity in the moraine are of interest for hazard evaluation and potentially initiation mitigation measures.

The disappearance of the bar on the western side of the fluvial fan is a sign of high sediment transport during the monitoring period. To conclude, whether the whole bar has been eroded or sediments accumulated on top is challenging with the available data. It is likely a combination of erosion of the green vegetated surface and accumulation of sediments around, thus reducing the relief and distinct colour difference between the bar and fan. The fact that sediments accumulated on the vegetated and elevated area on the western side of the fan indicate sediment aggregation in the channel between the bar and the person in *Figure 30D*.

5.5.2 Longyearbreen moraine

The active meltwater channel cuts through the centre of the moraine, flanked by erosive scarps, slumps, and thermokarsts. The same geomorphological features are described by Etzelmüller et al. (2000) except the meltwater channel. The most prominent channels are the lateral meltwater channels on the eastern and western sides – which were relatively inactive during the monitoring period. Only for a short period in the first days of June was

a small creak observed in the eastern channel, thought to originate from snowmelt in the hillside above and the recession. The western channel was active during the Late July Flooding. Both lateral channels drained meltwater when (Etzelmüller et al., 2000) conducted their fieldwork.

Riger-Kusk (2006) measured discharge and solutes from the eastern meltwater channel, as the water flow was prominent in the channel at the time. Measurements of discharge and suspended sediments by Etzelmüller et al. (2000) were conducted on the western channel. Both the later channels as been of interest for previous research, which illustrates that they have been the primary drainage system, in contrast to the situation in 2020. However, *Figure 33* demonstrates several inactive meltwater routes through the moraine, contradicting a theory of meltwater only being drained at the flanks. The active channel in 2020 holds features of deep fluvial incisions, erosive scarps, and mass movement deposits in a variety of sizes. Features associated with a former active channel can be seen east of the middle. The erosive scarps and mass movement deposits are less distinct than in the active channel, as the edges and deposits are weathered, but still a sign of shifts in the drainage system.

The reason for a shift in the meltwater path morphology can potentially be traced back to changes in the glacier surface. Glacier retreat can change the glacier surface inclination and thus alter the drainage channels. As the glacier surface has not been observed or mapped in detail, is it inconclusively at this point. Considering the climate changes described in NCCS (2019), thawing of the ice-core might lead to subsidence of the moraine, and further, change the drainage in the years to come. The development of a new meltwater channel through the moraine is thought to be significant regarding sediment input and transport. Increased sediment access would firstly influence the sandur directly downstream of the moraine, and bedload would eventually end up in the sedimentation dam. The effect of a new channel through the moraine has most likely not contributed to bedload and accumulation in the 2020 ablation season, given the transport distances. However, the high SSC can be liked to erosion and slumping in the moraine, which releases large quantities of fine sediments into the fluvial system. The erosion in the moraine could therefore contribute to the high SSY measured in 2020. Bogen and Bønsnes (2003) discuss how the sampling frequency is crucial to record peaks in SSC due to sudden sediment input in the system. 2-4 samples a day ought to reflect the general trend of sediment transport. However, pulses of high SSC caused by sudden input can be overlooked, depending on the length of the channel and transport velocity. The erosion and sediment input also applies to Larsbreen moraine.

With the current morphology in Longyearbreen moraine, the scenario with damming and outburst as described in Larsbreen is unlikely, as the meltwater is less channelized compared to Larsbreen moraine. Hence, a potential dam in the lateral channels would need time to fill, and countermeasures could be initiated in advance. However, a deeper active layer is associated with increasing mass movement events as the strength from the frozen ground decreases. If the meltwater continuous to erode, a ravine through the core of the moraine may well develop, resulting in a scenario similar as discussed for Larsbreen moraine.

5.6 Recommended research questions and topics

Contribution to the long-term monitoring of discharge, erosion and sediment transport has been one of the objectives for this thesis. Working with the fluvial and geological systems in Longyeardalen for three and a half months has demonstrated the complexity of the catchment. Additional objectives to the already established monitoring program (RIS ID 11641) have developed during the fieldwork and postprocessing. The discussion of the finding from this work and others reveals large annual fluctuations, and some questions cannot be answered based on a single season. Therefore, a continuous monitoring program like the one that is now ''up-and-running'' is needed to see the results in context. Listed below are the key areas for continuation and topics to investigate further:

- Continuous monitoring of discharge, erosion and sediment transport, as planned in RIS ID 11641.
- Initiate ground temperature monitoring in connection to scour and flooding mitigation and in the ice-core moraines.
- Geomorphological mapping of the glacier margins, moraines and fluvial channel

Discharge measurement to produce yearly hydrographs are the foundation for sediment transport computations. The fluvial system is the linkage between the geological processes and the most important mean of transportation in the system. Consequently, water stage and discharge correlation are needed every year. A more robust and permanent water stage measuring construction is recommended based on the challenges with sediment accumulation on the pressure sensor. Figuring out a way to guide bedload away from the pressure sensor without causing a false water stage is a foremost difficulty the installation must overcome. Maintaining a stable water stage reading from the bottom of the concrete weir would improve the data quality.

Continuing the SSC and SSY in the coming years will show if the 2020 ablation season was an anomaly, if the SSC decreases once the fines left by the heavy machinery are washed out, or if the erosion in the moraines is more important. Concerning the morphological changes in the moraines, the source-to-sink perspective of sediment transport is of interest. Bedload is more critical than suspended sediments when it comes to the sedimentation dam and a maintenance plan. Investigation of bedload could be divided; accumulation rate in the sedimentation dam for formulating a maintenance plan, the other focusing on the development around the hydrological engineering.

Based on the observations from 2020, it is believed the channelization of the river affects the ground thermal regime, and that decreasing strength of the thawing sediments damaged the constructions. Over several years, obtaining ground temperatures in and around the river channel is highly interesting to detect potential variations in the trumpet curve. Ground temperature readings have been conducted in different locations in the valley –background temperature readings are thus available for comparison.

For detecting morphological changes in the moraines and terminus of the glaciers, annual orthophotos must be acquired. Drones have proven to be quick and easy to use for remote sensing during the 2020 monitoring. Accurate DTM of the moraine may well be used to determine if the moraine is subsiding, perhaps a result of thawing of the ice core? Combined with ground temperature reading in the moraine, changes in the ice-core can be detected. Remote sensing and ablation stakes spread over the glacier surface can be used to find the explanation for the shift in drainage through the moraine. Low logistical challenges with the field area make the Longyeardalen valley a perfect site for Arctic

research. Increasing the knowledge of the High Arctic environment is vital to understand the effect of the ongoing climate changes.

5.7 Suggested improvements of the field techniques

The fieldwork conducted during the 2020 ablation season was successful, and data were acquired as planned, although some flexibility and adjustment were needed.

Forty-one discharge measurements were conducted, but due to adjustment to the pressure sensor, the stage measurements had to be divided into four sections with an individual rating curve. Discharge measurements were challenging during the Late July Flooding, at discharges over $5m^3/s$. Over 3.5kg of salt was diluted and injected into the river to record discharge ($7.4m^3/s$) on July 28th. However, when the bulldozer dug out a new thalweg downstream of Veg 600, an ideal stretch of a uniform channel of turbulent water was created and used for successful discharge measurement, including the $7.4m^3/s$ on July 28th. As mentioned, a more permanent stage-measuring installation should be built to maintain stable water level readings and avoid sediment accumulation.

During high flows with fast turbulent waters, the nozzle for the ISCO-pump was bouncing on the surface, which was solved with repeated adjustments and weights. A more permanent solution would be to fasten an eye-bolt in the concrete weir and make a rope-loop from the bridge to the bottom. Attaching the nozzle to the rope would make it possible to easily change the height to keep it in the middle of the water column while assuring easy maintenance. The suggested rope-loop would improve the data quality and make the job for the researcher easier.

Georeferencing the orthophotos was done with the internal GPS in the drone. It would be beneficial to establish precise and permanent ground control points that can be used every year and making it easier to compare drone data directly. The internal GPS in the drone proved too inaccurate to calculate areas of channel aggregation or degradation, as the DTMs from the different flights did not match on a cm-scale. Permanent ground control point could be bridges or other stable infrastructure alongside the channel, although more challenging to establish in the moraines.

Bedload monitoring should focus on more detailed data, perhaps using simple GPS-trackers on the tracers (e.g., Engvik, 2011). Sediment traps like those used in Scott Elva by Kociuba (2014) could be another option and would yield more info regarding threshold conditions.

6 Conclusion

This thesis is the products of an initiative between LL, NVE, and UNIS with the desire to enhance the knowledge of the local fluvial system and minimize the associated geohazards. The conclusions for each objective are presented below.

6.1 Discharge and sediment yield in Longyearelva

The aim to quantify discharge in the Longyearelva catchment has been achieved through continuous water stage measurements from June 11th to September 15th, producing an hourly hydrograph. Diurnal fluctuations are prominent, and discharge is thought to be closely linked to the air temperature. Snowmelt was the main water source in the early ablation season before glacier ablation took over in the peak flow period. Considerable glacier melt followed the record high air temperatures on July 24th-29th and triggered the Late July Flooding. The hourly discharge peaked at 8.6m^3/s in the afternoon on July 28th. Change in storage rather than precipitation generated most of the discharge in 2020 – except in the late ablation season, where increased discharge correlates with rainfall.

Suspended sediment measurement from June 12th to August 31st resulted in an average SSC of 1.9g/l, a total SSY of 41 050t, and a specific SSY of 1866t/km^2/yr for the Longyearelva catchment. A moderate correlation between SSC and discharge was observed, and 57% of the SSY can be traced back to the Late July Flooding. Evidentially, the moraines are the primary sediment sources, while inter-channel stored sediments constitute a secondary contributor. Despite the cold-based glaciers, the sediment yield in the Longyearelva catchment is high compared to nearby catchments with related characteristics and glacier inventory. However, the comparable data is sparse and might be outdated given the rapidly changing climate.

The competence of the channelized section of the Longyearelva river is >250mm, as large cobbles were transported as bedload. The available data is inconclusive for discharge threshold values for gravel <150mm but are within the range of 0-3m^3/s, and movement was documented at 3m^3/s for cobbles larger than 150mm. Bedload transport of at least 30 000m^3 is considered a modest estimate, and an accurate assessment of the mass is challenging with the available data. Bedload transport is generally high, given transport distances up to 170m for Class 3 passive tracers.

6.2 Scour and flooding mitigation in Longyearelva

The constructed channel effectively constrained the river, and the main goal of protecting the Elvesletta area and infrastructure has thus been achieved. The discharge recorded in 2020 has a short return period and how the construction will handle extreme events is unknown at this point. However, if the damages from this year are renovated, the height of the levees and capacity of bridge weirs are sufficient to hold larger floods based on water levels from 2020.

The sedimentation dam successfully accumulated bedload, thus limiting the sediment supply for the channel downstream. The initial capacity of 30 000m^3 was reached during the Late July Flooding, and the dam was consequently emptied on August 11th. Hence, a plan for annual excavation is advised, preferably during the early ablation season, thereby achieving maximum capacity before the expected high floods in July and August. However, it can be considered to increase the capacity by extending the pool upstream, reducing

annual maintenance costs. The construction remains robust and shows no sign of damage for the first year after completion.

The capability of the sills to reduce bedload transport is only partly accomplished, given the fact that passive tracers were transported over sills. Channel erosion is still occurring, a conclusion supported both by the movement of passive traces and scour hole development. Channel width, gradient, and the timespan in construction have caused more erosion in the youngest sills, while older sills have accumulated sediments. A probable explanation for the observed collapse and subsidence at some sills is that changes in the ground thermal regime have decreased the mechanical strength of the foundations. It is believed that over the coming years, the erosion will continue, and sediments will be transported downstream from the upper sections until the channel reaches equilibrium between available sediments and transport competence.

The youngest sills in Section 1 have the most severe damage, and it is recommended minor design improvements to reduce erosive forces and the economic footprint in the long run. The annual use of bulldozers will still be needed at this point if the sills are not reinforced. The suggested solution is to extend the damaged sills (Sill 1-8, 14, and 17) downstream and include a step for reducing the energy. Besides, all sills must be in-flush with the riverbed to eliminate the kick-point and further scour hole development. If the sills continue to lose integrity, undercutting can develop, and the cost of fixing the construction will escalate.

6.3 Further recommended research questions

As the extent of acquired data increases, trends and characteristic of the catchment can gradually be distinguished. The first complete monitoring season has been successful in establishing a baseline for discharge and sediment yield as well as identifying additional topics for further research. Two new Master students will continue the monitoring of discharge, erosion and sediment transport in 2021. An effective way of sharing data must be established, preferable a cloud-based server at UNIS. Additionally to the topics listed above, the following issues are advised to investigate in the years to come:

- Ground thermal regime affiliated to the constructed channel and ice-cored moraines. How does hydrological engineering affect permafrost characteristics?
- Geomorphological mapping of the catchment using both remote sensing and hands-on technics. Is there a connection between active layer detachments and potential degradation of the ice-cored moraine?

The ground thermal regime nearby the newly constructed channel and in the moraine complexes are of high interest. Investigating the active layer thickness and heat flux can potentially refute the hypothesis that the sills subsidence is linked to a decreasing mechanical strength of the ground as it thaws. Heat flux data from the moraine ice cores can detect increasing active layer thickness and be used to assess potential increased thermokarst and geomorphological changes as the climate changes continue. A broader dataset could be used to obtain a more accurate evaluation of the geohazards.

7 References

Akerman, H. J. (2005) Relations between slow slope processes and active-layer thickness 1972–2002, Kapp Linné, Svalbard, *Norsk Geografisk Tidsskrift-Norwegian Journal of Geography,* 59(2), pp.116-128. DOI: 10.1080/00291950510038386

Andersland, O. B., Ladanyi, B. & ASCE (2003) *Frozen Ground Engineering.* 2nd edn, New Jersey/Canada: John Wiley & Sons.

Arlov, T. B. (1994) *A short history of Svalbard.* 2nd edn, Oslo: Norsk Polarinstitutt (NP).

Arlov, T. B. (2020) *From Mining Camp to Family Society.* Svalbard Museum, Available at: https://svalbardmuseum.no/en/kultur-og-historie/moderne-tider/ (Accessed: 11.11. 2020).

Bense, V., Ferguson, G. & Kooi, H. (2009) Evolution of shallow groundwater flow systems in areas of degrading permafrost, *Geophysical Research Letters,* 36(22), pp.1-6. DOI: 10.1029/2009GL039225

Berggren, A.-L. & Finseth, J. (2019) *Grunnundersøkelsesrapport - Geofrost Coring og laboratorieanalyser fra Lia. Skredsikring Longyearbyen.*(Fagrapporter - Longyearbyen Lokalstyre, G-5599-07-GEODATA-001). Geofrost AS. Available at: https://www.lokalstyre.no/fagrapporter.488045.no.html (Accessed: 10.04.2021).

Bintanja, R. & Andry, O. (2017) Towards a rain-dominated Arctic, *Nature Climate Change,* 7(4), pp.263-267. DOI: 10.1038/nclimate3240

Bjordal, A. & Hoseth, K. (2017) *Tiltaksplan, Flom- og erosjonssikringstiltak i Longyearelva* (Vassdragnr. 400, 201601388). Longyearbyen: Norges vassdrag- og energidirektorat (NVE). Available at: https://www.lokalstyre.no/fagrapporter.488045.no.html (Accessed: 12.04.2021).

Björnsson, H., Gjessing, Y., Hamran, S.-E., Hagen, J. O., LiestøL, O., Pálsson, F. & Erlingsson, B. (1996) The thermal regime of sub-polar glaciers mapped by multi-frequency radio-echo sounding, *Journal of Glaciology,* 42(140), pp.23-32. DOI: 10.3189/S0022143000030495

Bogen, J. (1980) The hysteresis effect of sediment transport systems, *Norsk geografisk Tidsskrift,* 34(1), pp.45-54. DOI: 10.1080/00291958008545338

Bogen, J. & Bønsnes, T. E. (2003) Erosion and sediment transport in High Arctic rivers, Svalbard, *Polar Research,* 22(2), pp.175-189. DOI: 10.3402/polar.v22i2.6454

Boothroyd, J. C. & Ashley, G. M. (1975) Processes, bar morphology, and sedimentary structures on braided outwash fans, northeastern Gulf of Alaska, *Glaciofluvial and glaciolacustrine sedimentation, Society of Economic Paleontologists and Mineralogists,* Special Publication(23), pp.193-222. DOI: 10.2110/pec.75.23.0193

Brooks, K. N., Ffolliott, P. F. & Magner, J. A. (2012) *Hydrology and the Management of Watersheds.* 4th edn, USA/UK: John Wiley & Sons Inc.

Bunte, K. & Abt, S. R. (2001) *Sampling surface and subsurface particle-size distributions in wadable gravel-and cobble-bed streams for analyses in sediment transport, hydraulics, and streambed monitoring.*(RMRS-GTR, 74). Fort Collins, CO: US Department of Agriculture. Available at: https://www.fs.usda.gov/treesearch/pubs/4580 (Accessed: 10.04.2021).

Bårdseth, A. (2021) *Skred ved Nybyen idag.* SvalbardPosten Available at: https://svalbardposten.no/nyheter/skred-ved-nybyen-idag/19.13832 (Accessed: 12.04.2021).

Carrivick, J. L., Smith, M. W., Quincey, D. J. & Carver, S. J. (2013) Developments in budget remote sensing for the geosciences, *Geology Today,* 29(4), pp.138-143. DOI: 10.1111/gto.12015

Charlton, R. (2007) *Fundamentals of fluvial geomorphology*. London/New York: Routledge Taylor & Francis Group, e-Library, pp.1-275.

Christiansen, H. H., Gilbert, G., Neumann, U., Demidov, N., Guglielmin, M., Isaksen, K., Osuch, M. & Boike, J. (2021) *Ground ice content, drilling methods and equipment and permafrost dynamics in Svalbard 2016–2019 (PermaSval).*(SESS Report, 2020). The State of Environmental Science in Svalbard (SESS). Available at: https://epic.awi.de/id/eprint/53626/1/SESS2020_PermaSval-1(3).pdf (Accessed: 10.04.2021).

Cook, K. L. (2017) An evaluation of the effectiveness of low-cost UAVs and structure from motion for geomorphic change detection, *Geomorphology,* 278(2017), pp.195-208. DOI: 10.1016/j.geomorph.2016.11.009

Cooper, R., Wadham, J., Tranter, M., Hodgkins, R. & Peters, N. (2002) Groundwater hydrochemistry in the active layer of the proglacial zone, Finsterwalderbreen, Svalbard, *Journal of Hydrology,* 269(3-4), pp.208-223. DOI: 10.1016/S0022-1694(02)00279-2

Dallmann, W. K. (ed.) (2015). *Geoscience Atlas of Svalbard.* Tromsø: The Norwegian Polar Institute (NPI).

Day, T. J. (1976) On the precision of salt dilution gauging, *Journal of Hydrology,* 31(3-4), pp.293-306. DOI: 10.1016/0022-1694(76)90130-X

Dingman, S. L. (2015) *Physical hydrology* 3rd edn, Illinois: Waveland Press Inc.

DNT (2019) *Merkehåndboka - Tilrettelegging og synliggjøring av turruter.* 2nd edn, Oslo: Den Norske Turistforeningen (DNT), Innovasjon Norge, Friluftsrådenes Landsforbund.

DSB (2016) *Skredulykken i Longyearbyen 19. desember 2015 -Evaluering av håndteringen, beredskap og forebygging.*(DSB Rapport, September/2016). Tønsberg: Direktoratet for Samfunnssikkerhet og Beredskap (DSB) Available at: https://www.dsbinfo.no/DSBno/2016/Rapport/SkredulykkenSvalbard/?page=1 (Accessed: 10.04.2021).

Eckerstorfer, M. & Christiansen, H. (2011) The" High Arctic Maritime Snow Climate" in central Svalbard, *Arctic, antarctic, and alpine Research,* 43(1), pp.11-21. DOI: 10.1657/1938-4246-43.1.11

Eckerstorfer, M., Christiansen, H., Rubensdotter, L. & Vogel, S. (2013) The geomorphological effect of cornice fall avalanches in the Longyeardalen valley, Svalbard, *The Cryosphere,* 7(5), pp.1361-1374. DOI: 10.5194/tc-7-1361-2013

Elliassen, T. (2020) *Present Day Tourism.* Svalbard Museum, Available at: https://svalbardmuseum.no/en/kultur-og-historie/turisme/ (Accessed: 11.11 2020).

Engvik, T. (2011) *Bunntransport i Vekveselva: Et felteksperiment for å undersøke egnetheten til passive integrerte transpondere i fjellelver.* Master Thesis, Norges teknisk-naturvitenskapelige universitet (NTNU), Trondheim. Available at: https://ntnuopen.ntnu.no/ntnu-xmlui/handle/11250/265443 (Accessed: 12.04.2021).

Etzelmüller, B., Ødegård, R. S., Vatne, G., Mysterud, R. S., Tonning, T. & Sollid, J. L. (2000) Glacier characteristics and sediment transfer system of Longyearbreen and Larsbreen, western Spitsbergen, *Norsk Geografisk Tidsskrift,* 54(4), pp.157-168. DOI: 10.1080/002919500448530

Fergus, T., Hoseth, K. & Sæterbø, E. (2010) *Vassdragshåndboka: Håndbok i vassdragsteknikk.* 2nd edn, Trondheim: Tapir akademisk forlag.

Førland, E. J. & Hanssen-Bauer, I. (2003) Past and future climate variations in the Norwegian Arctic: overview and novel analyses, *Polar research,* 22(2), pp.113-124. DOI: 10.3402/polar.v22i2.6450

Gilbert, G., Instanes, A., Sinitsyn, A. & Aalberg, A. (2019) Characterization of two sites for geotechnical testing in permafrost: Longyearbyen, Svalbard, *AIMS geosciences,* 5(4), pp.868-885. DOI: 10.3934/geosci.2019.4.868

Gilbert, G. L., O'Neill, H. B., Nemec, W., Thiel, C., Christiansen, H. H. & Buylaert, J. P. (2018) Late Quaternary sedimentation and permafrost development in a Svalbard fjord-valley, Norwegian high Arctic, *Sedimentology,* 65(7), pp.2531-2558. DOI: 10.1111/sed.12476

Glover, B., Brabrand, Å., Brittain, J., Gregersen, F., Holmen, J. & Saltveit, S. J. (2012) *Avbøtende tiltak i regulerte vassdrag - målsettninger og susesskriterier* (Miljøbasert vannføring, 10/2012). Norges vassdrags- og energidirektorat (NVE). Available at: https://publikasjoner.nve.no/rapport_miljoebasert_vannfoering/2012/miljoebasert2012_10.pdf (Accessed: 15.04.2021).

Gregersen, O. (1995) *Grunnundersøkelser Elvesletta, Longyearbyen.*(Geoteknikk, 950080-1). Norges Geotekniske Institutt (NGI). Available at: https://www.lokalstyre.no/fagrapporter.488045.no.html (Accessed: 15.04.2021).

Gregersen, O. & Tuft, P. (1994) *UNIS-bygget på Svalbard - Grunnundersøkelser.*(Geoteknikk, 930060-1). Norges Geotekniske Institutt (NGI). Available at: https://www.lokalstyre.no/fagrapporter.488045.no.html (Accessed: 23.04.2021).

Grønsten, H. A. (1998) *Hydrological Studies and Simulations of a High Arctic Catchment Longyearelva, Spitsbergen* Master Thesis, The University of Oslo, Oslo. Available at: Printed, Fellesbiblioteket Universitetet i Oslo, (Accessed: n.d).

Hagen, J. O., Liestøl, O., Roland, E. & Jørgensen, T. (1993) *Glacier atlas of Svalbard and Jan Mayen.*(Meddelelser 129). Oslo: Norsk Polarinstitutt (NP). Available at: https://brage.npolar.no/npolar-xmlui/handle/11250/173065 (Accessed: 16.04.2021).

Hammer, K. M. & Smith, N. D. (1983) Sediment production and transport in a proglacial stream: Hilda Glacier, Alberta, Canada, *Boreas,* 12(2), pp.91-106. DOI: 10.1111/j.1502-3885.1983.tb00441.x

Hancock, H., Prokop, A., Eckerstorfer, M. & Hendrikx, J. (2018) Combining high spatial resolution snow mapping and meteorological analyses to improve forecasting of destructive avalanches in Longyearbyen, Svalbard, *Cold Regions Science and Technology,* 154(-), pp.120-132. DOI: 10.1016/j.coldregions.2018.05.011

Hansen, B. B., Isaksen, K., Benestad, R. E., Kohler, J., Pedersen, Å. Ø., Loe, L. E., Coulson, S. J., Larsen, J. O. & Varpe, Ø. (2014) Warmer and wetter winters: characteristics and implications of an extreme weather event in the High Arctic, *Environmental Research Letters,* 9(11), pp.1-11. DOI: doi:10.1088/1748-9326/9/11/114021

Helland-Hansen, W. (1990) Sedimentation in Paleogene foreland basin, Spitsbergen, *AAPG bulletin,* 74(3), pp.260-272. DOI: 10.1306/0C9B22BD-1710-11D7-8645000102C1865D

Hestnes, E., Bakkehøi, S. & Jaedicke, C. (2016) Longyearbyen, Svalbard-Vulnerability and risk management of an arctic settlement under changing climate -a challenge to authorities and experts.*The International Snow Science Workshop.* Breckenridge, CO, USA. 02.10.2016. Montana State University Library, pp.363-370, available at: https://arc.lib.montana.edu/snow-science/item/2293 (Accessed: 17.04.2021).

Hjulström, F. (1935) Studies of the morphological activity of rivers as illustrated by the river Fyris, *Bulletin Geological Institute Upsala,* 25(1), pp.221-527. DOI: -

Hjulström, F. (1939) The principles of construction of instruments for procuring samples of water containing silt, *Geografiska Annaler,* 21(1), pp.67-71. DOI: 10.2307/520002

Hodgkins, R. (1996) Seasonal trend in suspended-sediment transport from an Arctic glacier, and implications for drainage-system structure, *Annals of Glaciology,* 22(1), pp.147-151. DOI: 10.3189/1996AoG22-1-147-151

Hodgkins, R., Cooper, R., Wadham, J. & Tranter, M. (2003) Suspended sediment fluxes in a high-Arctic glacierised catchment: implications for fluvial sediment storage, *Sedimentary Geology,* 162(1-2), pp.105-117. DOI: 10.1016/S0037-0738(03)00218-5

Hodson, A., Gurnell, A., Tranter, M., Bogen, J., Hagen, J. O. & Clark, M. (1998) Suspended sediment yield and transfer processes in a small High-Arctic glacier basin, Svalbard, *Hydrological Processes,* 12(1), pp.73-86. DOI: 10.1002/(SICI)1099-1085(199801)12:1<73::AID-HYP564>3.0.CO;2-S

Hodson, A., Nowak, A., Hornum, M. T., Senger, K., Redeker, K. R., Christiansen, H. H., Jessen, S., Betlem, P., Thornton, S. F. & Turchyn, A. V. (2020) Open system pingos as hotspots for sub-permafrost methane emission in Svalbard, *Cryosphere Discuss.,* 14(.), pp.3829-3842. DOI: 10.5194/tc-2020-11

Hodson, A., Tranter, M., Dowdeswell, J., Gurnell, A. & Hagen, J. (1997) Glacier thermal regime and suspended-sediment yield: a comparison of two high-Arctic glaciers, *Annals of Glaciology,* 24(-), pp.32-37. DOI: https://doi.org/10.3189/S0260305500011897

Hodson, A. J. & Ferguson, R. I. (1999) Fluvial suspended sediment transport from cold and warm-based glaciers in Svalbard, *Earth Surface Processes and Landforms,* 24(11), pp.957-974. DOI: 10.1002/(SICI)1096-9837(199910)24:11<957::AID-ESP19>3.0.CO;2-J

Hoseth, K. A. & Daae, T. C. (1996) *Longyearbyen - Elvesletta, Vassdragstekniske vurderinger.*(Hydrologi, 08/1996). Norges Vassdrag- og Energidirektorat (NVE). Available at: https://www.lokalstyre.no/fagrapporter.488045.no.html (Accessed: 18.04.2021).

Humlum, O., Christiansen, H. H. & Juliussen, H. (2007) Avalanche-derived rock glaciers in Svalbard, *Permafrost and Periglacial Processes,* 18(1), pp.75-88. DOI: 10.1002/ppp.580

Humlum, O., Elberling, B., Hormes, A., Fjordheim, K., Hansen, O. H. & Heinemeier, J. (2005) Late-Holocene glacier growth in Svalbard, documented by subglacial relict vegetation and living soil microbes, *The Holocene : an interdisciplinary journal focusing on recent environmental change,* 15(3), pp.396-407. DOI: 10.1191/0959683605hl817rp

Humlum, O., Instanes, A. & Sollid, J. L. (2003) Permafrost in Svalbard: a review of research history, climatic background and engineering challenges, *Polar research,* 22(2), pp.191-215. DOI: 10.1111/j.1751-8369.2003.tb00107.x

Instanes, A. & Rongved, J. (2017) *Forventede klimaendringers påvirkning på byggegrunn i Longyearbyen-området. Delrapport 2 i oppdraget «Bygging og forvaltning på Svalbard i et langsiktig Klimaperspektiv».*(Geoteknikk, IAS2171-1). INSTANES AS for Statsbygg. Available at: https://www.lokalstyre.no/fagrapporter.488045.no.html (Accessed: 20.04.2021).

Isaksen, K., Førland, E. J., Dobler, A., Benestad, R., Haugen, J. E. & Mezghani, A. (2017) *Klimascenarioer for Longyearbyen-området, Svalbard - Delrapport 1, Statsbygg oppdrag: "Bygging og forvaltning på Svalbard i et langsiktig klimaperspektiv".*(Meteorologi 15/2017). Norwegian Meteorological Institute (MET) Available at: https://www.lokalstyre.no/fagrapporter.488045.no.html (Accessed: 26.04.2021).

Kay, M. (2008) *Practical hydraulics.* 2nd edn, USA/Canada: Taylor & Francis.
Killingtveit, A. (2004) Water balance studies in two catchments on Spitsbergen, Svalbard.*Northern Research Basins Water Balance, IAHS.* Victoria, Canada. International Association of Hydrological Sciences (IAHS), pp.120-138, available at: https://www.researchgate.net/profile/Anund-Killingtveit/publication/299626446_Water_balance_studies_in_two_catchments_on_Spitsbergen_Svalbard/links/570366e508ae646a9da88793/Water-balance-studies-in-two-catchments-on-Spitsbergen-Svalbard.pdf (Accessed: 20.04.2021).
Kociuba, W. (2014) Bedload transport in a High Arctic gravel-bed river (Scott River, Svalbard SW). *New perspectives to polar research.* Wrocław, Poland: Institute of Geography and Regional Development, University of Wroclaw, pp.231-246. Available from: https://www.researchgate.net/publication/275297395_Bedload_transport_in_a_High_Arctic_gravel-bed_river_Scott_River_Svalbard_SW (Accessed: 20.04.2021)
Kociuba, W., Janicki, G. & Dyer, J. L. (2019) Contemporary changes of the channel pattern and braided gravel-bed floodplain under rapid small valley glacier recession (Scott River catchment, Spitsbergen), *Geomorphology,* 328(-), pp.79-92. DOI: 10.1016/j.geomorph.2018.12.008
Kociuba, W., Janicki, G., Siwek, K. & Gluza, A. (2012) Bedload Transport As An Indicator Of Contemporary Transformations Of Arctic Fluvial Systems, *WIT Transactions on Engineering Sciences, WIT Press,* 73(-), pp.125-135. DOI: 10.2495/DEB120111
Krigström, A. (1962) Geomorphological studies of sandur plains and their braided rivers in Iceland, *Geografiska Annaler,* 44(3-4), pp.328-346. DOI: 10.1080/20014422.1962.11881005
Labus, M. & Labus, K. (2018) Thermal conductivity and diffusivity of fine-grained sedimentary rocks, *Journal of Thermal Analysis and Calorimetry,* 132(3), pp.1669-1676. DOI: 10.1007/s10973-018-7090-5
Landrø, M., Mikkelsen, O. & Jaedicke, C. (2017) *Gjennomgang og evaluering av skredhendelsen i Longyearbyen 21.02. 2017.*(31/2017). Oslo, Norway: Norges Vassdrags- og energidirektorat (NVE). Available at: http://publikasjoner.nve.no/rapport/2017/rapport2017_31.pdf (Accessed: 20.04.2021).
Laronne, J. & Carson, M. (1976) Interrelationships between bed morphology and bed-material transport for a small, gravel-bed channel, *Sedimentology,* 23(1), pp.67-85. DOI: 10.1111/j.1365-3091.1976.tb00039.x
Larsen, J. O. (2016) *Skredsikring og fundamentering i permafrost* (Mulighetsstudie Case 12/2016). Almaviva AS. Available at: https://www.lokalstyre.no/fagrapporter.488045.no.html (Accessed: 20.04.2021).
Lewkowicz, A. G. & Way, R. G. (2019) Extremes of summer climate trigger thousands of thermokarst landslides in a High Arctic environment, *Nature communications,* 10(1), pp.1-11. DOI: 10.1038/s41467-019-09314-7
Lied, K. & Hestnes, E. (1986) *Geomorfologisk kartlegging av overflatestrukturer i Longyearbyen, Svalbard.*(Geoteknikk, 52703-1). Norges Geotekniske Institutt (NGI). Available at: https://www.lokalstyre.no/fagrapporter.488045.no.html (Accessed: 20.04.2021).
LL (2019) *Boligbehovsutredning 2019 - kunnskap, analyse og mulige strategier for Longyearbyen.*(Samfunn, 2017/2331). Longyearbyen Lokalstyre (LL). Available at: https://www.lokalstyre.no/fagrapporter.488045.no.html (Accessed: 20.04.2021).
LNSS (2016) *Fyrhus 3 - H320 Pelelogg.*(Geoteknikk, 1/2010). Leonard Nilsen og Sønner Spitsbergen (LNSS). Available at: https://www.lokalstyre.no/fagrapporter.488045.no.html (Accessed: 20.04.2021).

Longley, P. A., Goodchild, M. F., Maguire, D. J. & Rhind, D. W. (2015) *Geographic information science and systems.* 4th edn, USA: John Wiley & Sons inc.
Major, H. & Nagy, J. (1972) *Geology of the Adventdalen map area, with a geological map.*(Svalbard C9G 1: 100 000, C9G 1: 100 000). Oslo: Norsk Polaristitutt (NP). Available at: https://brage.npolar.no/npolar-xmlui/bitstream/handle/11250/173948/Skrifter138.pdf?sequence=2 (Accessed: 21.04.2021).
MET (2021) Observations and weather statistics,. *Svalbard Lufthavn, stasjon SN99840.* Meteorologisk institutt (MET), Available from: https://seklima.met.no/observations/ (Accessed: 21.04.2021)
Moore, R. (2005) Slug injection using salt in solution, *Streamline Watershed Management Bulletin,* 8(2), pp.1-6. DOI: https://www.uvm.edu/bwrl/lab_docs/protocols/2005_Moore_Slug_salt_dilution_gauging_volumetric_method_Streamline.pdf (Accessed: 21.04.2021)
Müller, R. D. & Spielhagen, R. F. (1990) Evolution of the Central Tertiary Basin of Spitsbergen: towards a synthesis of sediment and plate tectonic history, *Palaeogeography, Palaeoclimatology, Palaeoecology,* 80(2), pp.153-172. DOI: 10.1016/0031-0182(90)90127-S
Møen, K. M., Bogen, J., Zuta, J. F., Ade, P. K. & Esbensen, K. (2010) *Bedload measurement in rivers using passive acoustic sensors.*(U.S. Geological Survey Scientific Investigations Report, 2010-5091). Norwegian Water and Energy Directorate (NVE). Available at: https://www.researchgate.net/profile/Kim-Esbensen/publication/267238644_Bedload_Measurement_in_Rivers_Using_Passive_Acoustic_Sensors/links/544f5d680cf2bca5ce90e73b/Bedload-Measurement-in-Rivers-Using-Passive-Acoustic-Sensors.pdf (Accessed: 21.04.2021).
NCCS (2019) HANSSEN-BAUER, I., FØRLAND, E., HISDAL, H., MAYER, S., SANDØ, A. B. & SORTEBERG, A. *Climate in Svalbard 2100 - a knowledge base for climate adaptation.*(Climate report, 1/2019). The Norwegian Centre for Climate Services (NCCS). Available at: https://www.miljodirektoratet.no/globalassets/publikasjoner/m1242/m1242.pdf (Accessed: 17.04.2021).
Neilson, B. T., Cardenas, M. B., O'Connor, M. T., Rasmussen, M. T., King, T. V. & Kling, G. W. (2018) Groundwater flow and exchange across the land surface explain carbon export patterns in continuous permafrost watersheds, *Geophysical Research Letters,* 45(15), pp.7596-7605. DOI: 10.1029/2018GL078140
NGU (2007) Fact Sheet for Borehole. The Boreholde Database at Norwegian Geological Survey (NGU), Available from: http://geo.ngu.no/kart/permafrost_svalbard_mobil/ (Accessed: 21.04.2021)
Nichols, G. (2009) *Sedimentology and stratigraphy.* 2nd edn: John Wiley & Sons ltd.
Nowak, A., Hodgkins, R., Nikulina, A., Osuch, M., Wawrzyniak, T., Kavan, J., Łepkowska, E., Majerska, M., Romashova, K. & Vasilevich, I. (2021) From land to fjords: The review of Svalbard hydrology from 1970 to 2019 (SvalHydro), *SESS Report 2020,* Chapter(7), pp.176-201. DOI: https://doi.org/10.5281/zenodo.4294063
Nowak, A. & Hodson, A. (2013) Hydrological response of a High-Arctic catchment to changing climate over the past 35 years: a case study of Bayelva watershed, Svalbard, *Polar Research,* 32(1), pp.19691. DOI: 10.3402/polar.v32i0.19691
Nowak, A. & Hodson, A. (2014) Changes in meltwater chemistry over a 20-year period following a thermal regime switch from polythermal to cold-based glaciation at Austre Brøggerbreen, Svalbard, *Polar Research,* 33(1), pp.22779. DOI: 10.3402/polar.v33.22779

Nowak, A. & Rubensdotter, L. (2021) *Hydrology, sediment transport and erosion in Longyeardalen, RIS-ID 11641.* Research In Svalbard Database, Available at: https://www.researchinsvalbard.no/project/9738 (Accessed: 09.05 2021).

NPI (1936) *Gamle flyfoto, ID: S36_3039 - TopoSvalbard* [Digital photography]. Norwegian Polar Institute (NPI), available at: https://toposvalbard.npolar.no/xflyfoto.html?lang=no&id=S36_3039 (Accessed: 21.04.2021).

NPI (2020a) SvalbardKartet - Geokart. *Geologi/Geology.* Norwegian Polar Institute (NPI), Available from: https://geokart.npolar.no/Html5Viewer/index.html?viewer=Svalbardkartet (Accessed: 21.04.2021)

NPI (2020b) TopoSvalbard - Online kart. *Longyearbyen.* Svalbard: Norwegian Polar Institute (NPI), Available from: https://toposvalbard.npolar.no/ (Accessed: 21.04.2021)

Nuth, C., Kohler, J., König, M., Deschwanden, A. v., Hagen, J. O. M., Kääb, A., Moholdt, G. & Pettersson, R. (2013) Decadal changes from a multi-temporal glacier inventory of Svalbard, *The Cryosphere,* 7(5), pp.1603-1621. DOI: 10.5194/tc-7-1603-2013

Nårstad, A., Borge, M. V., Nordhus, Ø. & Martinsen, K. (2018) *Raddison Blu Polar hotell, Longyearbyen. Geotekniske grunnundersøkelser - Datarapport.*(Geoteknikk, 58242001_RIG-R01-A01). Sweco AS. Available at: https://www.lokalstyre.no/fagrapporter.488045.no.html (Accessed: 21.04.2021).

Orwin, J. F., Lamoureux, S. F., Warburton, J. & Beylich, A. (2010) A framework for characterizing fluvial sediment fluxes from source to sink in cold environments, *Geografiska Annaler: Series A, Physical Geography,* 92(2), pp.155-176. DOI: 10.1111/j.1468-0459.2010.00387.x

Pedersen, A. T. & Svalbard Museum (1960) *Dosing i Longyearelva - SVF 07465* [digital photography]. Svalbard Museum available at: https://bildearkiv.svalbardmuseum.no/fotoweb/archives/5000-Historiske-bilder/Indekserte%20bilder/SVF%2007465.tif.info (Accessed: 11.11.2020).

Pedersen, M. B. (2017) *Grunnundersøkelser Longyearbyen - Datarapport (Elvesletta og Melkeveien).*(Geoteknikk, 1350021401-G-rap-001). Longyearbyen: Rambøll AS. Available at: https://www.lokalstyre.no/fagrapporter.488045.no.html (Accessed: 12.04.2021).

Pedersen, M. B. (2018) *Studentboliger Elvesletta, Geoteknisk vurdering.*(Geoteknikk, 1350027997_G-not-001). Rambøll Norge AS. Available at: https://www.lokalstyre.no/fagrapporter.488045.no.html (Accessed: 21.04.2021).

Pitlick, J., Mueller, E. R., Segura, C., Cress, R. & Torizzo, M. (2008) Relation between flow, surface-layer armoring and sediment transport in gravel-bed rivers, *Earth Surface Processes and Landforms: The Journal of the British Geomorphological Research Group,* 33(8), pp.1192-1209. DOI: 10.1002/esp.1607

Reid, D. & Church, M. (2015) Geomorphic and ecological consequences of riprap placement in river systems, *Journal of the American Water Resources Association (JAWRA),* 51(4), pp.1043-1059. DOI: 10.1111/jawr.12279

Riger-Kusk, M. (2006) *Hydrology and hydrochemistry of a High Arctic glacier: Longyearbreen, Svalbard.* Master Thesis, University of Aarhus/University Centre in Svalbard (UNIS) , Aarhus. Available at: https://hvlopen.brage.unit.no/hvlopen-xmlui/handle/11250/277221 (Accessed: 22.04.2021).

Rudberg, S. (1988) High arctic landscapes: comparison and reflexions, *Norsk Geografisk Tidsskrift-Norwegian Journal of Geography,* 42(4), pp.255-264. DOI: https://doi.org/10.1080/00291958808552208

Rød, J. K. (2015) *GIS: verktøy for å forstå verden.* 1st edn, Trondheim: Fagbokforlaget.

Røsvik, H. K. (2016) *Kjærligheten og minnene lever videre.* SvalbardPosten, Available at: https://svalbardposten.no/kjarligheten-og-minnene-lever-videre/19.7966 (Accessed: 22.04.2021).
Self, R. F., Nowell, A. R. & Jumars, P. A. (1989) Factors controlling critical shears for deposition and erosion of individual grains, *Marine Geology,* 86(2-3), pp.181-199. DOI: 10.1016/0025-3227(89)90048-0
SNSK. (2020) *Store Norske - Historie.* Store Norske Spitsbergen Kullkompani (SNSK), Available at: https://www.snsk.no/historie (Accessed: 22.04.2021).
SSB (2016) EEG-HENRIKSEN, F. & SJØMÆLING, E. *Dette er Svalbard.*(ISBN 978-82-537-8997-2). Oslo: Statistisk Sentralbyrå (SSB). Available at: https://www.ssb.no/befolkning/artikler-og-publikasjoner/dette-er-svalbard-2016 (Accessed: 22.04.2021).
SSB. (2020) *Population of Svalbard.* Statistisk Sentralbyrå (SSB), Available at: https://www.ssb.no/en/befolkning/statistikker/befsvalbard (Accessed: 22.04.2021).
St.meld 32 (2015-2016) (2016) *Svalbard.*Oslo: Justis-og Beredskapsdepartementet (Norwegian Ministry of Justice and Public Security), available at: www.publikasjoner.dep.no (Accessed: 11.04.2021).
Statsbygg. (2019) *Svalbard Globale Frøhvelv* Statsbygg, Available at: https://www.statsbygg.no/prosjekter-og-eiendommer/svalbard-globale-frohvelv (Accessed).
Steel, R., Dalland, A., Kalgraff, K. & Larsen, V. (1981) The Central Tertiary Basin of Spitsbergen: sedimentary development of a sheared-margin basin, *Geology of the North Atlantic Borderlands,* Memoir(7), pp.647-664. DOI: http://archives.datapages.com/data/cspg_sp/data/007/007001/pdfs/647.pdf (Accessed: 22.04.2021)
Stenius, S. (2016) *Flomberegning for Longyearelva, Spitsbergen, Svalbard.*(Vassdrag 400, 7/2016). Longyearbyen: Norges Vassdrag og Energidirektorat (NVE). Available at: https://www.lokalstyre.no/fagrapporter.488045.no.html (Accessed: 22.04.2021).
Stott, T. & Mount, N. (2007) Alpine proglacial suspended sediment dynamics in warm and cool ablation seasons: implications for global warming, *Journal of Hydrology,* 332(3-4), pp.259-270. DOI: 10.1016/j.jhydrol.2006.07.001
Sund, M. (2008) *Polar hydrology - Norwegian Water Resources and Energy Directorate's work in Svalbard.*(Polar hydrology, 2/2008). Oslo: Norges Vassdrag og Energidirektorat (NVE) Available at: https://publikasjoner.nve.no/report/2008/report2008_02.pdf (Accessed: 22.04.2021).
Sværd, R. (1996) *Longyearbyen - Elvesletta preliminær flomberegning.*(Hydrologi, 07/1996). Longyearbyen: Norges vassdrag- og energidirektorat (NVE). Available at: https://www.lokalstyre.no/fagrapporter.488045.no.html (Accessed: 23.04.2021).
UNIS. (2020) *About UNIS.* The University Centre in Svalbard (UNIS), Available at: https://www.unis.no/about-unis/ (Accessed: 23.04.2021).
van Pelt, W., Pohjola, V., Pettersson, R., Marchenko, S., Kohler, J., Luks, B., Hagen, J. O., Schuler, T. V., Dunse, T. & Noël, B. (2019) A long-term dataset of climatic mass balance, snow conditions, and runoff in Svalbard (1957–2018), *The Cryosphere,* 13(9), pp.2259-2280. DOI: 10.5194/tc-13-2259-2019
Vogel, S., Eckerstorfer, M. & Christiansen, H. H. (2012) Cornice dynamics and meteorological control at Gruvefjellet, Central Svalbard, *The Cryosphere,* 6(1), pp.157-171. DOI: 10.5194/tc-6-157-2012
Walczowski, W. & Piechura, J. (2011) Influence of the West Spitsbergen Current on the local climate, *International journal of climatology,* 31(7), pp.1088-1093. DOI: doi.org/10.1002/joc.2338

Wawrzyniak, T. & Osuch, M. (2020) A 40-year High Arctic climatological dataset of the Polish Polar Station Hornsund (SW Spitsbergen, Svalbard), *Earth System Science Data,* 12(2), pp.805-815. DOI: 10.5194/essd-12-805-2020

Wentworth, C. K. (1922) A scale of grade and class terms for clastic sediments, *The journal of geology,* 30(5), pp.377-392. DOI: 10.1086/622910

Westoby, M. J., Brasington, J., Glasser, N. F., Hambrey, M. J. & Reynolds, J. M. (2012) 'Structure-from-Motion'photogrammetry: A low-cost, effective tool for geoscience applications, *Geomorphology,* 179(-), pp.300-314. DOI: 10.1016/j.geomorph.2012.08.021

Woo, M.-k. & Xia, Z. (1996) Effects of Hydrology on the Thermal Conditions of the Active Layer: Paper presented at the 10th Northern Res. Basin Symposium (Svalbard, Norway—28 Aug./3 Sept. 1994), *Hydrology Research,* 27(1-2), pp.129-142. DOI: https://doi.org/10.2166/nh.1996.0024

Yde, J. C., Riger-Kusk, M., Christiansen, H. H., Knudsen, N. T. & Humlum, O. (2008) Hydrochemical characteristics of bulk meltwater from an entire ablation season, Longyearbreen, Svalbard, *Journal of Glaciology,* 54(185), pp.259-272. DOI: https://doi.org/10.3189/002214308784886234

Ødegård, R. S., Hamran, S.-E., Bø, P. H., Etzelmuller, B., Vatne, G. & Sollid, J. L. (1992) Thermal regime of a valley glacier, Erikbreen, northern Spitsbergen, *Polar Research,* 11(2), pp.69-79. DOI: 10.3402/polar.v11i2.6718

Østrem, G. (1975) Sediment transport in glacial meltwater streams, *Special Publications of SEPM, Glaciofluvial and Glaciolacustrine Sedimentation,* SP(23), pp.101-122. DOI: Available at: http://archives.datapages.com/data/sepm_sp/SP23/Sediment_Transport_in_Glacial_Meltwater_Streams.htm (Accessed: 23.04.2021)

Øvereng, I. (1989) *Forebygging mot Longyearelva, Spitsbergen, Svalbard.*(Vassdrag nr 400, 8195). Norges Vassdrag- og Energidirektorat (NVE) Available at: Copy of internal NVE-document, courtesy of A. Bjordal(NVE) (Accessed: 23.04.2021).

Martin Andreas Solbakken Løvaas

Management of a High Arctic River

NTNU
Kunnskap for en bedre verden

UNIS
The University Centre in Svalbard